Structure - Function Relationship of the Multidrug Efflux Protein AcrB, a Bacterial Homolog of the Human Niemann-Pick C1 Transporter

Dissertation

zur

Erlangung der naturwissenschaftlichen Doktorwürde

(Dr.sc.nat.)

vorgelegt der

Mathematisch-naturwissenschaftlichen Fakultät

der

Universität Zürich

von

Lorenz Brandstätter

aus

Österreich

Promotionskomitee

Prof. Dr. François Verrey

Prof. Dr. Martin Pos

Prof. Dr. Kay Diederichs

Prof. Dr. Carsten Wagner

Zürich, 2011

Contents

Summary

Resistance of human pathogenic bacteria towards antibiotics is a current and growing threat to public health. Bacteria have developed a plethora of resistance mechanisms of which the elimination of the antibiotics from the inside of the cell by active export is one of the most potent measures.

In facultative pathogenic Gram-negative bacteria, such as *Escherichia coli* and *Pseudomonas aeruginosa*, tripartite efflux complexes provide basal resistance against toxic compounds by lowering the concentration of the antibiotics in the cytoplasm and/or periplasm. These complexes span both the inner and outer membrane and transport antibiotics from the cytoplasm or periplasm of the cell to the outside medium. The AcrAB-TolC complex from *E. coli* is the prototypical example of these export machineries and extrudes not only antibiotics belonging to different classes, but also dyes, bile acids and detergents. The uphill extrusion of antibiotics out of the cell is driven by the proton-motive force across the inner membrane. Despite that AcrA and TolC are mandatory for resistance, AcrB is the sole site for energy conversion and substrate specificity of the entire complex.

AcrB, a member of the three domains of life spanning Resistance Nodulation cell Division superfamily of transporters, has been intensively characterized by functional and structural means. Especially high resolution X-ray crystallography structural data provided a wealth of information. To obtain well diffracting crystals, the use of designed ankyrin repeat proteins (DARPins), which bind specifically and in a defined stoichiometry to AcrB, was found to be beneficial.

The functional unit of AcrB is a homotrimer and the monomers adopt three different conformations designated loose (L), tight (T) and open (O). It is postulated that the AcrB monomers cycle consecutively through these three conformational stages in a concerted fashion, from L to T to O and back to L, much in analogy to the functional rotation observed in the F_1F_O-ATP synthase.

Initial substrate binding occurs in the L monomer, where potential substrate binding sites are located in the transmembrane domain at the periplasmic side of the inner membrane. Upon conformational change to the T monomer, a tunnel inside the periplasmic domain leads to a substrate binding pocket. The binding of drugs to this pocket triggers the proton-motive force dependent conformational change from the T to the O conformation. Central to the energization of this process is a proton binding site made out of titratable residues inside the transmembrane domain of AcrB. Upon proton binding, the free energy is subsequently

converted into mechanical energy through movements of the transmembrane helices towards the periplasmic domain, which results in the closure of the entrance tunnel and the binding pocket initiating substrate release into a newly formed exit tunnel towards TolC. The transient formation and closure of tunnels inside the periplasmic domain is postulated to resemble the mechanism of a peristaltic pump.

The focus of this thesis was on the stoichiometric analysis of different AcrB/DARPin complexes (**Chapter 2**), the crystallization of crosslink variants of AcrB (**Chapter 3**) and initial experiments to functionally reconstitute AcrB (**Chapter 4**).

Chapter 2 describes the analysis of DARPin binding to wildtype AcrB and distinct binding pocket variants of AcrB via densitometry after microchannel electrophoresis, analytical ultracentrifugation and via laser-induced liquid bead ion desorption mass spectrometry (LILBID-MS). Structural analysis of co-crystallized AcrB/DARPins complexes revealed the alternating DARPin binding stoichiometry of the wildtype AcrB compared to the binding pocket AcrB variants. Using LILBID-MS, the gradual disassembly of the AcrB trimer and bound DARPin ligands in dependence on laser intensity was analyzed in solution. At low laser intensity, the release of the detergent micelle from the AcrB/DARPin complex was observed. By increasing laser intensity, dimeric and monomeric AcrB species with bound DARPin molecules were detected showing the high affinity binding of DARPin to monomeric AcrB species. High laser intensity LILBID-MS experiments indicated a spectral shift of the monomeric AcrB peak of 3.1 kDa, representing a low molecular weight ligand in all detergent-solubilized AcrB samples and in the AcrB crystal. The identity of this ligand was further investigated using phospholipid analysis of purified AcrB and AcrB variant samples, and indicated the presence of phosphatidylethanolamine and possibly cardiolipin, both constituents of the *Escherichia coli* membrane.

The structural analysis presented in **Chapter 3**, describes the introduction of pairs of cysteines into a cysteine-free AcrB background resulting in crosslinking and functional impairment of periplasmic AcrB subdomains and leading to inhibition of the AcrAB-TolC transport activity. In this study, high resolution crystal structures of four AcrB variants are presented. One particular cross-linking variant revealed a novel intermediate conformation. This novel conformation indicates an independent rearrangement of the subdomains during conformational change from O to L.

To establish an *in vitro* transport assay for AcrAB-TolC drug efflux, functional reconstitution of the AcrB trimer was pursued (**Chapter 4**). Initial experiments demonstrated AcrB association to liposomes after the reconstitution process and proteoliposomes were shown to stably maintain

a membrane potential. Furthermore, a soluble TolC variant was generated for *in vitro* complex formation with reconstituted AcrB and AcrA. This β-barrel-less TolC variant could be produced in the *E. coli* cytoplasm and was subsequently purified. Size-exclusion chromatography revealed the presence of monomeric TolC variant in contrast to the trimeric wildtype TolC.

Zusammenfassung

Antibiotikaresistenz in humanpathogenen Bakterien stellt eine allgegenwärtige und zunehmende Gefahr für das Gesundheitswesen dar. Bakterien entwickelten eine Vielzahl von Resistenzmechanismen, wobei das Ausschleusen von Antibiotika aus der Zelle durch aktiven Export eine der bedeutendsten Massnahmen darstellt.

In Gram-negativen Bakterien, wie den opportunistischen Krankheitserregern *Escherichia coli* oder *Pseudomonas aeruginosa*, sind dreiteilige Pumpkomplexe für die grundlegenden Resistenzeigenschaften gegen toxische Verbindungen verantwortlich, indem sie deren Konzentration im Zytoplasma und/oder im Periplasma herabsetzen. Diese Komplexe erstrecken sich über die innere und äussere Membran und sind in der Lage Antibiotika direkt vom Zytoplasma oder Periplasma der Zelle nach Aussen zu transportieren. Der Komplex aus AcrA, AcrB und TolC von *E. coli* stellt einen Prototyp dieser Exportmaschinerien dar und schleust nicht nur Antibiotika verschiedener Klassen, sondern auch Farbstoffe, Gallensalze und Detergenzien aus. Der Transport von Antibiotika gegen den Konzentrationsgradienten wird vom elektrochemischen Protonengradienten über die innere Membran angetrieben. Obwohl AcrA und TolC für die Resistenz notwendig sind, ist AcrB allein für die Energieumwandlung und die Substratspezifität des Komplexes verantwortlich.

AcrB, ein Mitglied aus der in allen drei Königreichen des Lebens vertretenen RND (kurz für engl. „Resistance Nodulation cell Division“) Transporter-Superfamilie, wurde strukturell und funktionell detailliert charakterisiert. Vor allem hochauflösende Röntgenstrukturanalyse Daten trugen wertvolle Informationen dazu bei. Der Einsatz von DARPins (kurz für engl. „designed ankyrin repeat proteins“), die spezifisch und in einer bestimmten Stöchiometrie an AcrB binden, war ausschlaggebend für die Gewinnung gut streuender Kristalle.

Die funktionstüchtige Einheit von AcrB stellt das Homotrimer dar und die Monomere nehmen drei verschiedene Konformationen an, die loose (L), tight (T) und open (O) benannt wurden. Es ist postuliert, dass die AcrB Monomere, in Analogie zur funktionellen Rotation der F_1F_O-ATPase, aufeinander abgestimmt die Konformationen L, T, O und wieder zurück zu L durchlaufen.

Erste Substratbindung erfolgt in der L Konformation, in welcher potentielle Substratbindestellen in der Transmembrandomäne an der periplasmatischen Seite der inneren Membrane vorhanden sind. Nach der konformationellen Änderung zu T, führt ein Tunnel in der periplasmatischen Domäne zu einer Substratbindungstasche. Die Bindung von Antibiotika an diese Bindungstasche

löst die konformationelle Änderung von T zu O aus, die vom elektrochemischen Protonengradienten abhängig ist. Eine Protonenbindestelle aus titrierbaren Seitenketten in der Transmembrandomäne von AcrB ist für die Energetisierung dieses Prozesses verantwortlich. Die freie Energie der Protonenbindung wird in mechanische Energie umgewandelt und durch Positionsänderungen von Membranhelices in die periplasmatische Domäne weitergeleitet. Dort bewirkt sie, dass der Eingangstunnel und die Substratbindungstasche kollabieren und das Substrat durch einen neu entstandenen Ausgangstunnel an TolC weitergeleitet wird. Dieses vorübergehende Entstehen und Verschwinden von Tunnels in der periplasmatischen Domäne ähnelt dem Mechanismus einer peristaltischen Pumpe.

Der Fokus dieser Arbeit wurde auf die stöchiometrische Analyse von verschiedenen AcrB/ DARPin Komplexen (**Kapitel 2**), die Kristallisation von „Crosslink"-Varianten (**Kapitel 3**) und erste Versuche AcrB funktionell zu rekonstituieren (**Kapitel 4**) gelegt.

Kapitel 2 beschreibt die Analyse von DARPin-Bindung zum Wildtyp AcrB und verschiedenen Substratbindetaschen Varianten von AcrB mit Hilfe von Densitometrie nach Mikrokanal-Elektrophorese, analytischer Ultrazentrifugation und LILBID (kurz für engl. „laser-induced liquid bead ion desorption") Massenspektrometrie. Strukturanalyse von ko-kristallisierten AcrB/ DARPin Komplexen zeigte unterschiedliche Stöchiometrie von DARPins zum Wildtyp und den Substratbindetaschen Varianten. Mit LILBID-MS wurde der schrittweise Zerfall der AcrB Trimers und der gebundenen DARPin Liganden in Abhängigkeit von der Laserintensität analysiert. Bei niedriger Intensität wurde die Ablösung von Detergenzmizellen beobachtet. Bei steigender Intensität wurden Di- und Monomere AcrB Spezies mit gebundenen DARPins detektiert, die von der hohen Bindungsaffinität der DARPins für monomeres AcrB zeugen. Hohe Laserintensitäten verursachten eine Spektralverschiebung im Bereich des monomeren AcrB um 3,1 kDa, wobei es sich um einen niedrigmolekularen Liganden handelt, der in allen Detergenz-solubilisierten AcrB Proben und in AcrB Kristallen nachgewiesen wurde. Phospholipidanalyse von gereinigtem AcrB und AcrB Varianten weist auf Bindung von den *E. coli* Lipiden Phosphatidylethanolamin und möglicherweise Cardiolipin an solubilisiertem AcrB hin.

Die Strukturanalyse in **Kapitel 3** zeigt das Einfügen von Cysteinpaaren in einer Cystein-freie Variante von AcrB und die daraus resultierenden Vernetzungen (Crosslinks) und funktionellen Beeinträchtigungen in den periplasmatischen Unterdomänen von AcrB, die zur Hemmung der AcrAB-TolC Transportaktivität führen. In dieser Arbeit werden hochauflösende Strukturen von vier Crosslink-Varianten gezeigt. Eine dieser Crosslink-Varianten zeigt eine neuartige Zwischenkonformation. Diese neue Konformation weist auf eine voneinander unabhängige Reorganisation der Unterdomänen während der Konformationsänderung von O nach L hin.

Um einen *in vitro* Transportassay für AcrAB-TolC bedingten Substratefflux zu konzipieren wurde die funktionelle Rekonstitution des AcrB Trimers verfolgt (**Kapitel 4**). Erste Experimente belegten, dass AcrB nach dem Rekonstitutionsprozess mit den Liposomen assoziiert und über die Membran der Proteoliposomen konnte ein stabiles Membranpotential aufgebaut werden. Für die *in vitro* Komplexbildung von rekonstituiertem AcrB und AcrA wurde eine lösliche Variante von TolC konstruiert. Diese β-faltblattlose Variante konnte in *E. coli* produziert und aus dem Zytoplasma aufgereinigt werden. Grössenausschluss-Chromatographie deutete allerdings darauf hin, dass die gereinigte Variante nicht wie im Wildtyp TolC als Trimer, sondern als Monomer vorlag.

1 Introduction

1.1 General introduction

Even diseases have lost their prestige, there aren't so many of them left.
Think it over... no more syphilis, no more clap, no more typhoid...
antibiotics have taken half the tragedy out of medicine.

(Louis Ferdinand Celine, French writer and physician, 1894-1961)

All living organisms are defined by their cellular organization. The cell provides a defined space, separated from the environment by at least one membrane. All cellular membranes are derivatives of a prototypical design – the unit membrane. Biological membranes consist of a lipid bilayer, with the aliphatic tails as a core of a hydrophobic layer, and the hydrophilic headgroups defining the border towards the aqueous phase on both sides of the membrane (Figure 1.1). This setup effectively prevents transition of water-soluble substances across the membrane. To have controlled interchange of substances taken from and expelled to the surrounding environment, cells have membrane embedded proteins. These perform many important tasks like uptake of essential compounds and expel of noxious substances. Others are involved in signal transduction, protein or DNA excretion or membrane protein insertion. Extrusion of toxic compounds has been studied intensively since this phenomenon has been the major culprit in the fight against cancer and has become alarmingly in the limelight due to antibiotic resistance. The catalysts playing a major role are efflux pumps that extrude multiple antibiotics and anticancer drugs out of the cell. Multidrug efflux pumps are often able to transport a great number of chemically unrelated toxic substances.

Since the discovery of antibiotic drugs at the beginning of the twentieth century, the treatment of infectious diseases went through dramatic changes. At first, the availability of antibiotics was seen as a major triumph of modern science over the perpetual thread

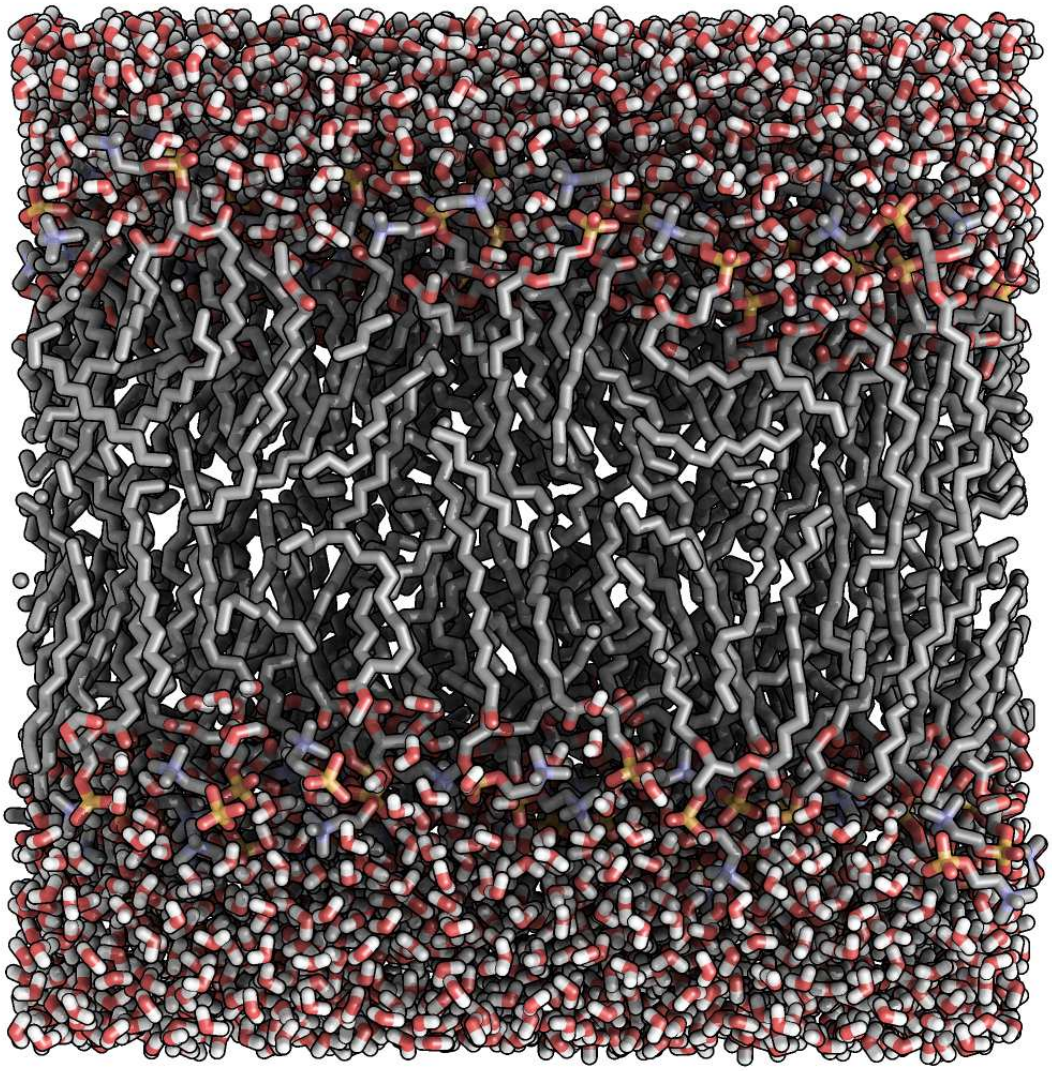

Figure 1.1: Illustration of a dipalmitoylphosphatidylcholine (DPPC) bilayer representing the structural composition of lipid bilayers in biological membranes. The core of the membrane consists of the aliphatic tails (here: palmitic fatty acids) and the borders are defined by the headgroups of the lipids. Water molecules at both sides of the membranes represent the aqueous composition of the intra- and extracellular fluids. In cells, membranes are composed of a set of different lipids (often phospholipids). Colors by element: H white, O red, C gray, P orange, N blue. (DPPC coordinates from http://moose.bio.ucalgary.ca, dppc128.pdb)

of infectious microorganisms. In the beginning the antibiotics seemed convincingly effective against the thread of bacterial borne diseases, however, the mass-application started to take reverse effects relatively soon. The pressure caused by the widely-used drugs brought forward strains of bacteria that were less vulnerable towards antibiotic treatment. Due to this antibiotic resistance, infectious diseases that have been kept in check for decades, are resurgent today. Many diseases that were thought to be eradicated from developed countries, for example tuberculosis, are newly spreading and resistant strains set back therapy to the pre-antibiotic era leaving modern medicine with few options to hold against. Drug resistance in principle can occur in any microbial borne infectious disease treated with antibiotics. Already nowadays the situation is dramatic, since there are Gram-negative bacterial strains reported to show resistance towards almost all of the effective drugs available [1]. Furthermore, many bacteria are able to exchange the genetic elements causing resistance and share them with pathogens that have never been confronted with antimicrobial agents. Nowadays the study on resistance mechanisms is central to understanding the phenomenon of multi-drug resistance. It is hoped for that in due time, new drugs can be found or alternatively inhibitors of resistance catalysts, so that the commonly used antibiotic drugs are gaining their potency against bacterial pathogens.

1.2 Bacterial multidrug resistance pumps

In bacteria, the basis for antibiotic resistance can be associated with four basic mechanisms of resistance [2] (Figure 1.2). Resistant cells can enzymatically inactivate (degrade or modify) antibiotics to render these nonfunctional (i). The best known example is the inactivation by hydrolysis of β-lactam antibiotics catalyzed by β-lactamases. Another strategy is the alteration or modification of the antibiotic target (ii). The introduction of mutations in e. g. topoisomerase IV or DNA gyrase significantly reduces the affinity of quinolones and hence decreases the antibiotic effect [3]. Expression of alternative targets (iii) may give the cell the chance to bypass the inhibitory effect of antibiotics. The alternative target is not affected by the binding of the antibiotic, but effectively reduces the free antibiotic concentration, so that the intended target is not encountered. E. g. in methicillin resistant *Staphylococcus aureus* (MRSA), an alternative binding pro-

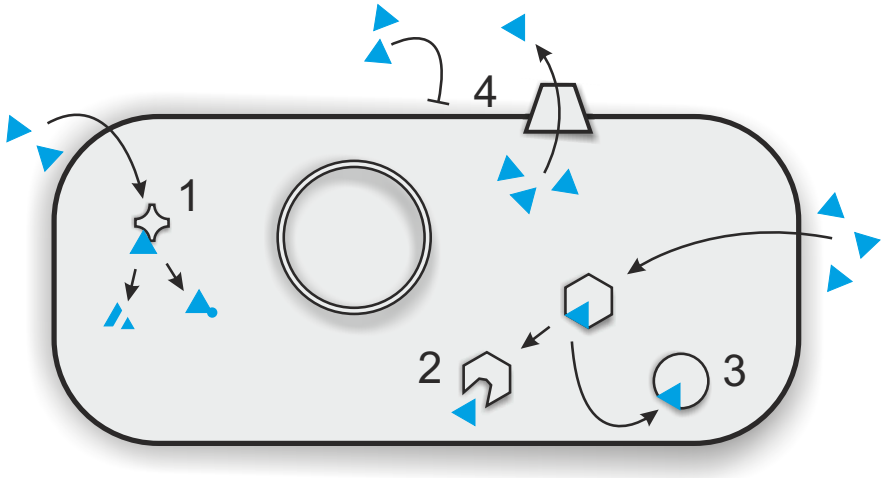

Figure 1.2: Schematic representation of the mechanisms of antibiotic resistance in the bacterial cell. Antibiotic drugs (blue triangles) may enter the cells over the membrane(s) and be modified or enzymatically degraded (1). Drug target (hexagon) alteration (2) or alternative drug target expression (3) may lead to resistance as well. The most potent measure to fight antibiotics is the reduction of permeability for the bacterial membrane(s) and/or expression of drug efflux pumps. Genetic information encoding for degrading enzymes, altered and alternative targets and drug efflux pumps may be present on plasmids and/or the genome (ring).

tein PBP2a is expressed in addition to penicillin binding protein (PBP). In contrast to the original PBP, PBP2a is not inhibited by penicillin antibiotics [4]. Preventing accumulation (iv) of the antibiotic drug inside the cell is probably the first potent measure to confer resistance to a cell. There is no need to enzymatically alter the drug, or to modify the target of the drug. Basically, there are two different mechanisms to prevent drug accumulation. The incorporation of drugs is decreased by reduction of permeability through the bacterial membranes. In Gram-negative bacteria, porins allow the entry of numerous unrelated, water-soluble compounds including antibiotics. The intrinsic resistance of *Pseudomonas aeruginosa* to the hydrophilic β-lactam imipenem, is correlated to the reduced outer membrane permeability [5]. The other strategy is actively pumping the drugs out of the cell. The rate of drugs pumped out of the cell needs to be higher than the rate of entry, to maintain an intracellular sub-toxic concentration. Although many of these efflux pumps are specific for one drug or a related group of drugs, there appear to be numerous efflux pumps transporting a wide variety of very dissimilar chemical compounds [6] commonly referred to as multidrug resistance pumps or multidrug transporters. Inherent to their essential function for every living cell, multidrug efflux pumps are prevalent in all kingdoms of life [7].

A systematic phylogenetic analysis of solute transporters on basis of the available genomic data [8] has led to the transport classification (TC) system [9]. This resulted in a database which provides phylogenetic and associated functional information for over 500 families of transport proteins. Multidrug resistance pumps have been classified into five large superfamilies: the ATP-binding cassette superfamily (ABC), the major facilitator superfamily (MFS), the drug metabolite transporter (DMT), including the small multidrug resistance transporters (SMR), the multidrug/oligosaccharidyl-lipid/polysaccharide flippase superfamily (MOP), including the multidrug and toxic-compound extrusion family (MATE), and the resistance nodulation cell division superfamily (RND) [8, 10].

The ABC superfamily

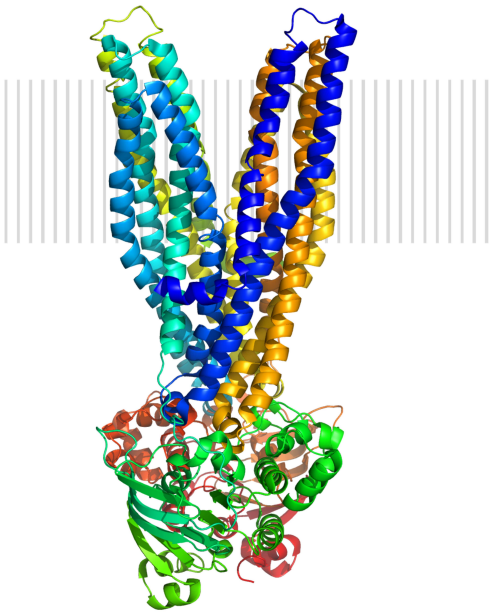

Figure 1.3: Cartoon representation of the ABC -multidrug transporter Sav1866 from *Staphylococcus aureus*. Sav1866 is a homodimer, where each dimer is comprised of a transmembrane domain (top, located in the membrane represented by grey bars) and a nucleotide binding domain (bottom)[11] (pdb ID: 2HYD).

ABC multidrug transporters are primary transporters that couple the substrate transport to ATP hydrolysis. ABC exporters have not only been reported to confer MDR in bacteria, but also in mammalian cells, fungi and parasites and account for e. g. the

omnipresent cancer cell drug resistance due to the action of P-glycoprotein (ABCB1) [12] or herbicidal resistance in plants [13]. ABC transporters are comprised of two trans-membrane domains (TMDs) and two nucleotide binding domains (NBDs). The NBDs contain several highly conserved motifs such as the Walker A and B motifs that are responsible for the binding and hydrolysis of ATP. The TMDs, each usually containing five or six TM helices, span the membranes and facilitate the actual export of the substrates from the cell.

The domain organization of ABC transporters is different in bacteria and eukaryotic cells. In bacteria, ABC transporters are expressed as "half-channels", where one TMD and one NBD are expressed on a single polypeptide. In contrast, many eukaryotic ABC transporters are expressed as a single polypeptide chain, carrying all four domains [14]. The best characterized bacterial ABC multidrug transporter is LmrA from *Lactococcus lactis* [15, 16]. The only crystal structure available so far from a bacterial ABC efflux pump is that of Sav1866 (Figure 1.3) from *Staphylococcus aureus* [11, 17]. Recently, the high resolution structure of mouse P-gp drug efflux pump has been elucidated in apo and drug bound form [18].

Multidrug resistance pumps of the four other superfamilies are secondary antiporters, energized by the proton (or sodium ion) motive force.

The MF superfamily (MFS)

The MFS contains the largest and most diverse set of transporters, mostly containing between 12 and 14 trans-membrane helices (TMH) [8]. MFS multidrug transporters are suggested to function in accordance to the alternating access model, that was postulated by Jardetzky half a century ago and likewise was proposed for the 12 TMH comprising *E. coli* MFS transporters LacY (lactose permease, Figure 1.4) and GlpT (glycerol-3-phosphate transporter) after their structures were solved [20, 21].

Crystal structure determination revealed a pseudo two-fold organization of two 6 TMH containing domains duplicated in a single polypeptide [20, 21]. According to the alternating access model, substrate is bound to the membrane spanning transporter, accessible from one side of the membrane only. In this conformation, an access pathway

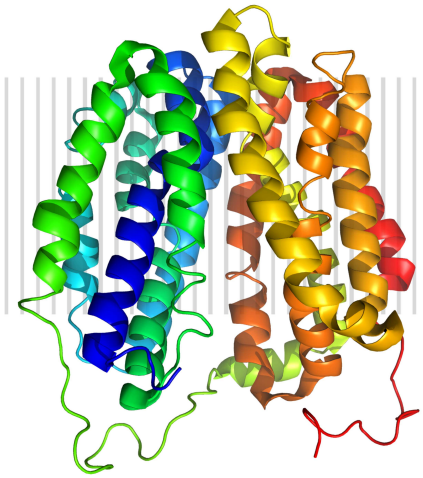

Figure 1.4: Cartoon representation of the lactose permease LacY from *E. coli*. Twelve transmembrane helices form a large hydrophilic cavity that is open to the cytoplasmic side [19] (pdb ID: 2V8N).

is present towards the substrate binding site located at the interior of the membrane embedded protein. Upon binding of substrate, the transporter changes its conformation resulting in the exposure of the substrate binding site to the opposite side of the membrane. In current models an intermediate, 'occluded' state is assumed, where the substrate is trapped in a "sluise-type" conformation [22]. Most bacterial MFS multidrug transporters belong to the three "Drug/H^+ antiporter" (DHA) families. Examples are Bmr of *Bacillus subtilis*, QacA and NorA of *S. aureus*, and EmrD and MdfA from *E. coli* [8, 23].

SMR superfamily

The DMT superfamily contains 14 families of transporters with very diverse substrate specificities in terms of their substrates. Most of these transporters have not been functionally characterized up to now. Within this family, multidrug transport is only reported for proteins of the prokaryotic SMR family. SMR transporters consist of 100–140 amino acid long polypeptides comprising four TMH. SMR transporter substrates are lipophilic or cationic compounds and often quarternary ammonium antibiotics [25, 26].

The best characterized SMR transporter is EmrE of *E. coli* (Figure 1.5). *In vivo* and

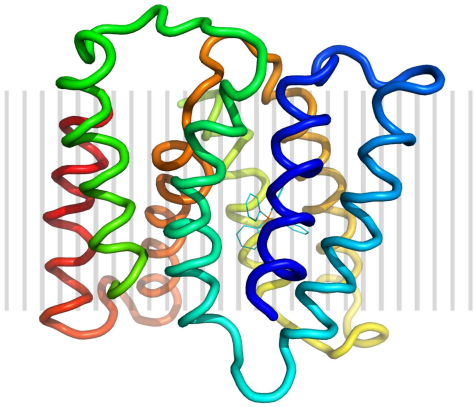

Figure 1.5: Cartoon representation of the Cα atoms of EmrE from *E. coli* with the bound substrate tetraphenylphosphonium (TPP, stick representation) [24] (pdb ID: 3B5D).

in vitro studies have demonstrated that EmrE is functional as a dimer [27]. A major controversy is the orientation of the monomer within the dimeric assembly [28]. Whereas evidence for parallel topology has been found with biochemical experiments [29, 30], there is also evidence for antiparallel topology from structural data [24] and genetic approaches [31, 32].

The MOP superfamily

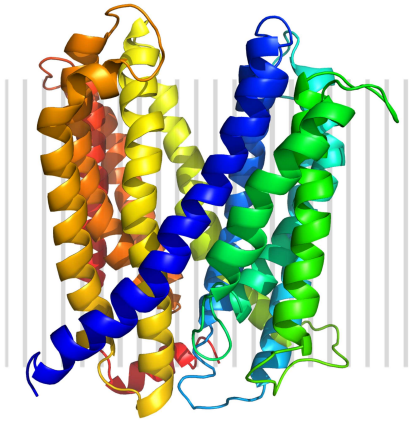

Figure 1.6: Cartoon representation of the sodium/substrate antiporter NorM of *Vibrio parahaemolyticus* in an outward facing conformation [33] (pdb ID: 3MKT).

The MOP exporter superfamily consists of four families. Most proteins within this group are predicted to have 12 TMH. Characterized members of the MATE family drive drug transport on the expense of the electrochemical sodium ion gradient [8, 34]. NorM of *Vibrio parahaemolyticus* (Figure 1.6) was the first multidrug transporter found to utilize

the sodium ion gradient [35, 36]. Other MATE transporters have been shown to facilitate Na^+/substrate antiport as well: VmrA of *Vibrio parahaemolyticus* and VcmA of *Vibrio cholerae* [37, 38]. In *E. coli*, the NorM homolog YdhE confers resistance to a number of antibiotics and dyes [39, 40]. Drug efflux within the MATE family is, however, not exclusively coupled to Na^+ ions, as PmpM of *P. aeruginosa* and AbeM *Acinetobacter baumannii* have been shown to facilitate H^+-coupled drug efflux [41, 42].

RND superfamily

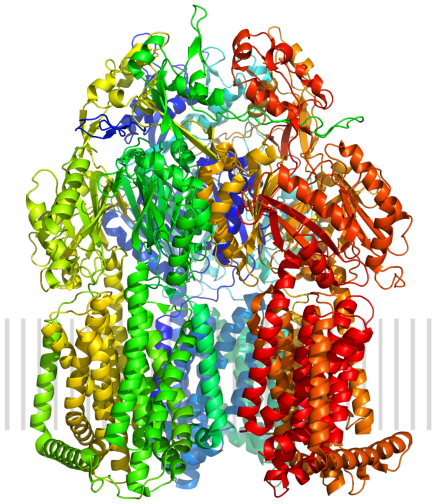

Figure 1.7: Cartoon representation of the AcrB homolog MexB from *Pseudomonas aeruginosa*. The homotrimeric multidrug pump forms an extrusion complex with MexA and OprM [43] (pdb ID: 2V50).

The RND superfamily contains a diverse group of transporters. Found ubiquitously in all phylae of life, RND proteins serve a great number of different tasks, one of those being drug efflux. All members of this superfamily share the same overall architecture, a duplicate of six TMHs with large soluble domains between the first and second and seventh and eighth TMH. Functional oligomerization (trimerization) has been observed in some of the characterized RND transporters and is thought to be a general feature in its quarterary structural organization. The characterized RND transporters operate as H^+ or Na^+/substrate antiporters. Multidrug transport has been shown in two of the nine families within the RND superfamily so far and inferred for two other families (Table 1.1). The heavy metal exporter (HME) family is comprised of proteins that

Table 1.1: Families and example transporters of the RND-superfamily (2.A.6) according to the Transporter Classification Database (www.tcdb.org).

Family	**example**
The Heavy Metal Exporter (HME) Family	CzcA (*Ralstonia* sp.)
The Hydrophobe/Amphiphile Efflux-1 (HAE1) Family (Gram-negative bacteria)	AcrB (*E. coli*)
The Putative Nodulation Factor Exporter (NFE) Family	NolG (*Rhizobium meliloti*)
TheSecDF Family	SecDF (*E. coli*)
The Hydrophobe/Amphiphile Efflux-2 (HAE2) Family (Gram-positive bacteria)	MmpL7 (*Mycobacterium tuberculosis*)
The Eukaryotic Sterol Transporter (EST) Family	NPC1 (*Homo sapiens*)
The Hydrophobe/Amphiphile Efflux-3 (HAE3) Family (Archeal)	gene *MJ1562* (*Methanococcus jannaschii*)
The Brominated, Aryl Polyene Pigment Exporter (APPE) Family	gene *ORF4* (*Xanthomonas oryzae*)
The Dispatched Family	Dispatched (*Drosophila melanogaster*)

are mainly found in Gram-negative bacteria. These provide resistance to toxic divalent (e. g. Co^{2+}, Zn^{2+}, Cd^{2+}) and monovalent cations (Ag^{+}, Cu^{+}). CzcA from *Ralstonia* sp. confers resistance to copper, zinc and cobalt ions. CzcA forms a complex with CzcB and CzcC that functions as a H^{+}/cation antiporter [44]. Recently, the structure of CusA, a copper (Cu^{+}) and silver (Ag^{+}) exporter has recently been elucidated [45]. The homotrimer was crystallized without and with bound copper ions. It was shown that the binding of copper induces a different conformation.

The hydrophobe/amphiphile efflux-1 (HAE1) family is largely restricted to Gram-negative bacteria and most of its members are able to transport a variety of chemically unrelated compounds [8, 46]. AcrB from *E. coli* and MexB from *P. aeruginosa* (Figure 1.7) are considered RND protein paradigms and are structurally as well as functionally the best characterized HAE1 transporters. Homologs are known to exist in many opportunistic and pathogenic bacteria and contribute to their high intrinsic antibiotic resistance.

The putative nodulation factor exporter (NFE) family includes only one characterized example so far. NolG from *Rhizobium meliloti*, a nitrogen-fixing bacterium living in symbiosis with *Medicago sativa*, a plant of the family of *Fabaceae*. Nodulation factors are extracellular lipooligosaccharid signals that are required to infect the root cells of the host plants. The nodulation factor export protein may play a role in nodulation of the host [47].

SecD and SecF are part of the secretory complex in *E. coli*. They form a heterotrimeric complex with YajC and are involved in protein translocation [48]. A member of the HAE2 family is MmpL7 of *Mycobacterium tuberculosis*. This transporter was shown to increase resistance against isoniacid, a first-line antibiotic in tuberculosis therapy [49]. YerP of *Bacillus subtilis* is the first RND transporter characterized in Gram-positive bacteria and was found to confer resistance to surfactin, a strong surfactant [50].

In humans, the NPC1 protein is associated with the distribution of cholesterol in the cell [51]. It belongs to the eukaryotic sterol transporter (EST) family. There are several single amino acid substitutions known in this protein that can cause an inactivation of NPC1, resulting in the accumulation of sterols in lysosomes causing the Niemann-Pick C1 disease [52].

The hydrophobe/amphiphile efflux-3 (HAE3) family contains two hypothetical membrane proteins, MJ1562 and AF1229 from *Methanococcus jannaschii* and *Archaeoglobus fulgidus*, respectively. The function of these proteins is unknown.

The gene *ORF4* from the brominated, aryl polyene pigment exporter (APPE) family codes for a putative membrane protein in *Xanthomonas oryzae*. It is involved in pigment export in this plant-pathogen [53].

In *Drosophila melanogaster*, Dispatched has been found to be required for Hedgehog (Hh) signaling. The Hedgehog signaling family is crucial for embryonal development in vertebrates. Dispatched is responsible for the secretion of Hedgehog from the signaling cells [54]. In the responding cell, the membrane protein Patched (Ptc) is the receptor for Hedgehog [55]. Interestingly, Hh was reported to be posttranslationally modified with cholesterol [56] and both, Dispatched and Patched, were shown to contain sterol sensing domains [57]. Smoothened (Smo), another membrane protein in the Hedgehog

signaling pathway, was reported to form complexes with Patched [55]. Smoothened is required for the Hedgehog signal to be mediated into the cell [58, 59]. Chen and Struhl [59] discussed possible mechanisms of the Smo/Ptc complex. Basically, Patched is inhibiting Smoothened in the absence of Hedgehog. Upon binding of Hedgehog, the inhibitory effect of Patched is suspended, resulting in the activation of Smoothened and causes activation of genes by downstream signaling.

Drug transport complexes in Gram-negative bacteria

The outer membrane of Gram-negative bacteria contributes to intrinsic resistance by providing an additional barrier (in addition to the inner membrane) to antimicrobial agents [60]. Consequently, the expelled drug has to cross both membranes in order to guarantee efficient resistance. Gram-negative bacteria have developed systems to form complex machineries that span both membranes and the periplasm. These drug extrusion complexes have a tripartite setup comprised by a pump, residing in the inner membrane (inner membrane protein, IMP), an outer membrane channel (outer membrane factor, OMF) and a membrane fusion protein (MFP) which is essential for complex formation of the IMP, MFP and OMF. The inner membrane efflux pump and the associated MFP are in general encoded by genes located on the same operon, whereas the OMF is often located elsewhere on the chromosome. In *E. coli*, the MFP AcrA and the IMP AcrB are co-localized within the same operon, whereas the OMF TolC is encoded at a different location on the chromosome. Nevertheless, operon-like structures encoding all three components are also present on the chromosomes of some bacteria like the *cmeABC* of *Campylobacter jejuni* [61] or *adeABC* of *Acinetobacter baumannii* [62]. For some of the IMP it has been shown that they are determinants of substrate specificity and the main site for energy conversion within the complex. Transporters of the ABC, MFS and RND superfamilies have been shown to function as IMPs in such complexes. For example, the *E. coli* ABC transporter MacB requires the MFP MacA and the OMF TolC to confer macrolide resistance [63]. In *E. coli* the MFS transporter EmrB has been identified to cooperate with the MFP EmrA [64] and suggested to dock to the OMF TolC [65] as well. Best characterized transmembrane complexes expelling antibiotics are based on IMPs of the RND superfamily. Complexes based on the HAE1

pumps AcrB and MexB from *E. coli* and *P. aeruginosa*, respectively, are intensively studied. AcrB recruits the MFP AcrA to form such a complex with TolC. In *E. coli* there are several other similar complexes known all of which require the OMF TolC. The situation is slightly different in *P. aeruginosa*, where there are different OMFs available and have been shown to participate in various tripartite complexes [66]. Tripartite multidrug efflux complexes rely on the presence of all three components. With one of the components nonfunctional, drug efflux activity subsides [67, 68].

The physiological role of tripartite efflux systems is still a matter of ongoing research and speculations [66]. In enterobacteria like *E. coli*, efflux pumps may be evolved to clear the cell from harmful bile salts present in the natural environment of the animal gut. Indeed, AcrAB-TolC expels bile salts [69]. However, the natural ability to extrude a plethora of antibiotic compounds next to bile salts is still puzzling.

1.3 The AcrAB-TolC complex of *E. coli*, a prototypical multi-drug efflux machinery

1.3.1 AcrB

AcrB from *E. coli* and MexB from *P. aeruginosa* are the best characterized RND transporters on both structural [43, 70–75] and functional [76–80] level. AcrB was first described and mapped on the genome of *E. coli* as *a*criflavin *r*esistance determining gene *B* in 1978 [81]. AcrB is the energy module and the substrate specificity determinant within the AcrAB-TolC complex. AcrAB-TolC was shown to confer resistance to many toxic compounds of various classes of antibiotics, dyes, bile salts, detergents and organic solvents [82]. Many of the compounds are structurally unrelated and diverse in size and shape. Moreover, the compounds are neutral, cationic or anionic. A commonality of AcrB substrates is their hydrophobicity (pOW[1] greater than -0.3) and limited size (smaller than 1000 Da).

AcrB comprises of 1049 amino acids and its topology contains a RND signature, i. e. the structure of AcrB involves twelve transmembrane helices and two large periplasmic loops

[1] pOW: Octanol-Water partition coefficient

between TM1 and 2 and TM7 and 8. Due to the duplication in the RND signature the α-helices 1–6 and 7–12 are arranged in a pseudo symmetry within one monomer. Helices 4 and 10 are located in the center encircled by the other eight helices (Figure 1.8) [70], with TM1 and TM7 at a more peripheral location. The functional unit of

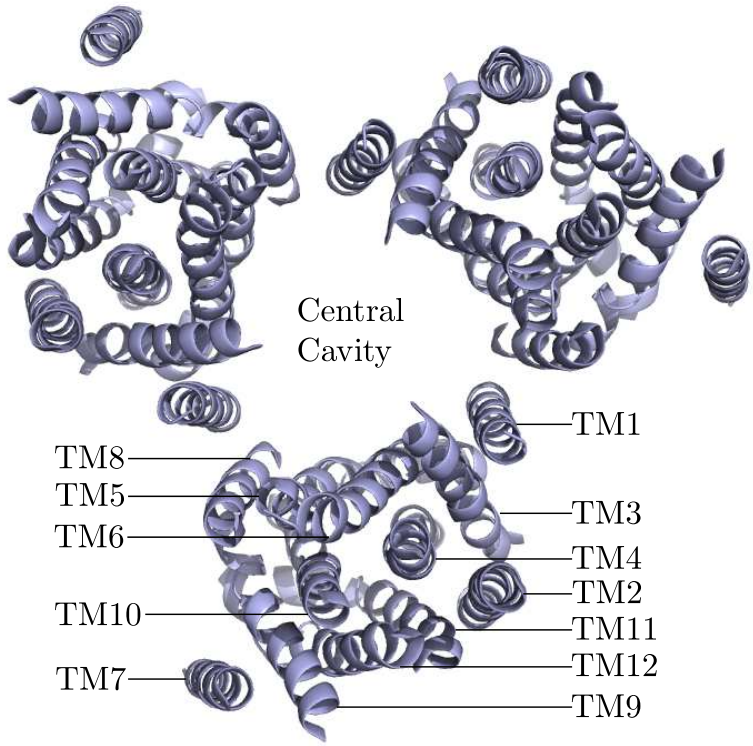

Figure 1.8: Topview on the transmembrane domain of the AcrB trimer. Transmembrane helices (TM1–TM12) of the monomers are arranged around the central cavity (pdb ID: 1IWG).

AcrB is a homotrimer. The first crystal structure revealed a detailed view on the overall architecture of the pump (Figure 1.9). The AcrB trimer can be subdivided into three domains. The (i) transmembrane domain contains twelve transmembrane helices per monomer and are located in the inner membrane of *E. coli* cells. The two periplasmic loops are arranged as large soluble domains protruding into the periplasm. The membrane proximal part is the (ii) porter domain containing subdomains PN1, PN2, PC1 and PC2, and the (iii) TolC docking domain with the subdomains DN and DC is located at the distal end of the trimeric structure. The complex resembles a dome structure and is about 120 Å in total height (Figure 1.9). The monomers are grouped around a 3-fold symmetry axis perpendicular to the membrane plane. Within the membrane, the twelve helices of the monomers encircle a central cavity that is assumed

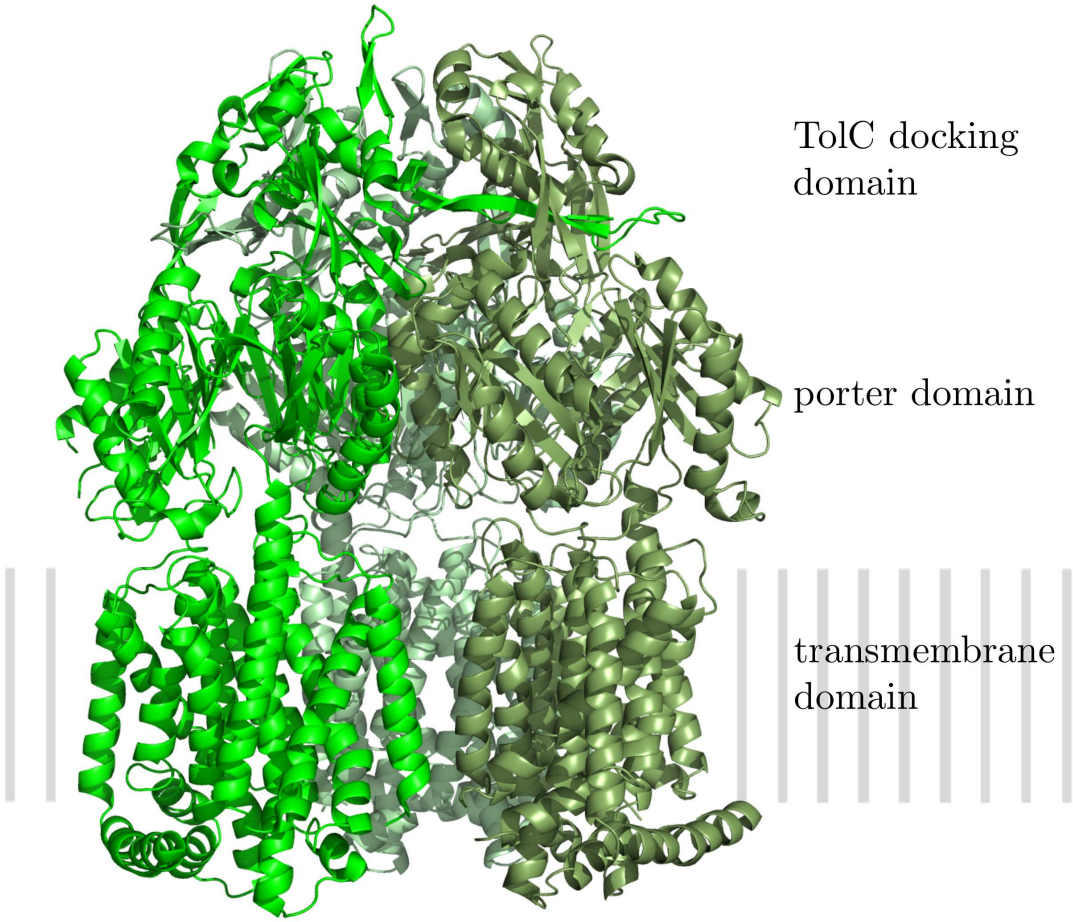

Figure 1.9: Sideview on the AcrB trimer (pdb ID: 1IWG). The three monomers are shown in different shades of green. The pump can be subdivided into three domains: the transmembrane domain, the porter domain and the TolC docking domain. The gray bars indicate the inner membrane of *E. coli*.

to be filled with phospholipids *in vivo*. From the outer leaflet of the inner membrane, the cavity expands into the periplasm and finally tapers into a pore-like structure inside the porter domain. On top of the periplasmic end of the docking domain, a funnel can be observed. The first structural determinations of AcrB showed a symmetrical trimer, where all three monomers were in a single conformation as implied by the 3-fold symmetry [70, 72]. Based on the symmetric structure, a transport mechanism was proposed, where uptake of the substrate was thought to occur from the cytoplasm via the central cavity. From there the drugs have to pass the central pore to enter the funnel and subsequently be extruded through the TolC channel to the external medium. Since the pore consists of three α-helices with close (van der Waals) side chain interaction, conformational changes were suggested to open and close the pore for substrate transit. Because of the vertical transport pathway this mechanism was named the "elevator mechanism" [22, 71].

Recent crystallographic studies on AcrB revealed another, this time asymmetric, conformation of the trimer [73–75]. In the crystal, each monomer within the trimer adopts a different conformation. These conformations were postulated to represent three consecutive steps of a transport cycle, which were designated loose (L), tight (T) and open (O). The denotation is in analogy to the conformational states of the F_1F_O-ATP synthase as originally proposed by Boyer [83]. The monomers in the initial (symmetric) crystal structure [70, 72] resemble the L conformation from the asymmetric structures [73–75] with minor deviations. The supposed functional rotation in the transport cycle of AcrB involves conformational changes of each of the monomers from L to T to O and back to L again. A series of structural differences in the conformations can be observed that affect the organization of the porter domain. The PN1, PN2, PC1 and PC2 subdomains change their relative position considerably during the anticipated conformational cycling. The lateral cleft on the surface of the PC1 and PC2 subdomain confines a tunnel opening which is about 15 Å above the membrane and is leading to the center of the porter domain. In the T monomer, a conformational shift of the PN2 and PC2 subdomains causes formation of a second tunnel starting from the transmembrane domain at the level of the outer leaflet of the inner membrane and is merging with the initial tunnel observed in the loose monomer. Moreover, at the joint of the tunnels in

the T conformation a hydrophobic pocket at the interface of PN2/PC1 becomes apparent. This pocket is lined with a number of hydrophobic residues and is expected to represent a drug binding pocket. In O conformation, reorganization of the porter domain (involving PN1, PN2 and PC2 subdomain movements) and part of the transmembrane domain result in closure of the lateral cleft. The tunnels disappear and the binding pocket collapses. An exit pathway comes up, leading from the former binding pocket to the funnel of the TolC docking domain. Upon conformational change back to the L conformation, the exit pathway recedes. These findings inspired the postulation of pumping transport mechanism by AcrB resembling that of a peristaltic pump. In L and T conformation, substrates can enter from the periplasm and the membrane via the tunnels. In the T conformation the binding pocket is able to accommodate entering substrates. Closing of the lateral tunnels and collapse of the binding pocket in O conformation squeezes substrates into the newly emerging exit pathway. From there substrates are translocated via TolC towards to the outside of the cell. The presence of asymmetric AcrB trimers *in vivo* and the postulated conformational cycling was confirmed by a series of experiments with introduced pairs of cysteines [77, 84]. These residues were strategically located at the surfaces of subdomains that are involved in the structural rearrangements during the conformational cycling. In the oxidative environment of the periplasm, disulfide bridges spontaneously formed, covalently locked the subdomains in a specific conformation and inhibited transport activity of AcrB. This resulted in significant reduction of transport of a fluorescent substrate *in vivo*. Incubation with the reducing agent dithiothreitol (DTT) removed disulfide bridges and restored functionality of AcrB. Furthermore, the functional rotation cycle could be supported by experiments with covalently (genetically) linked trimers that are expressed as a single giant protein. Introducing only one non-functional monomer as part of the covalent trimer basically renders the whole trimeric complex non-functional [80].

In the asymmetric AcrB structure, co-crystallization with 9-bromo-minocyclin and doxorubicin was achieved [73].The binding pocket of AcrB is lined with hydrophobic residues, particular phenylalanine residues, are crucial for substrate binding [73, 78]. Moreover, substrate binding was only observed in the T conformer of the asymmetric AcrB trimer. Furthermore, mutational analysis of various phenylalanines in the binding pocket iden-

tified Phe610 as a key residue in binding of several antibiotic agents. The other phenylalanine residues exhibited a less severe impact on resistance of *E. coli* cells up on substitution by alanine [78]. During conformational cycling the binding pocket undergoes dramatic changes. Only in the T conformation it is forming a hold, voluminous enough to harbor substrates. The structural configuration and spatial restrictions in L and O do not allow molecules being bound within this pocket.

In AcrB and the MexB homolog from *Pseudomonas aeruginosa* four key residues were identified to be crucial for activity. The titratable residues Asp407, Asp408, Lys940 (Lys939 in MexB) and Arg971, located on transmembrane helices (TM) 4, 10 and 11 respectively, were found to be the functional important residues for proton translocation and energy/substrate transport coupling [76, 79, 85]. The orientation of these key residues undergo effective changes in the conformational cycling. Compared to the situation in the L and T monomer, residues Asp407, Asp408, Lys940 and Arg971 in the O monomer are reorientated and presumably differ in their protonation state. This rearrangement, putatively driven by the uptake of (a) proton(s), coincides with a coil to helix transition in TM8. This appears to be the mechanism of energy transduction, driven by proton translocation and coupled to the conformational changes in the porter subdomains, leading to drug extrusion [86].

1.3.2 AcrA

AcrA belongs to the family of membrane fusion proteins (MFPs), a family of auxiliary adaptor proteins in Gram-negative bacteria, connecting transporters in the inner membrane to channels in the outer membrane. The terminology membrane fusion proteins stems from the similarity to the membrane fusion protein (F protein) of paramyxovirus, which is essential for cell penetration and cell fusion [87]. Each adaptor protein functions with a cognate inner membrane transporter. In *E. coli*, AcrA works in conjunction with the multidrug efflux pump AcrB or the homolog AcrD [88] and the outer membrane protein TolC [89]. The homologous MFP MexA of *P. aeruginosa* is part of a very similar transmembrane complex, which is constituted of the inner membrane pump MexB and the outer membrane channel OprM. Protein crystallography revealed high resolution

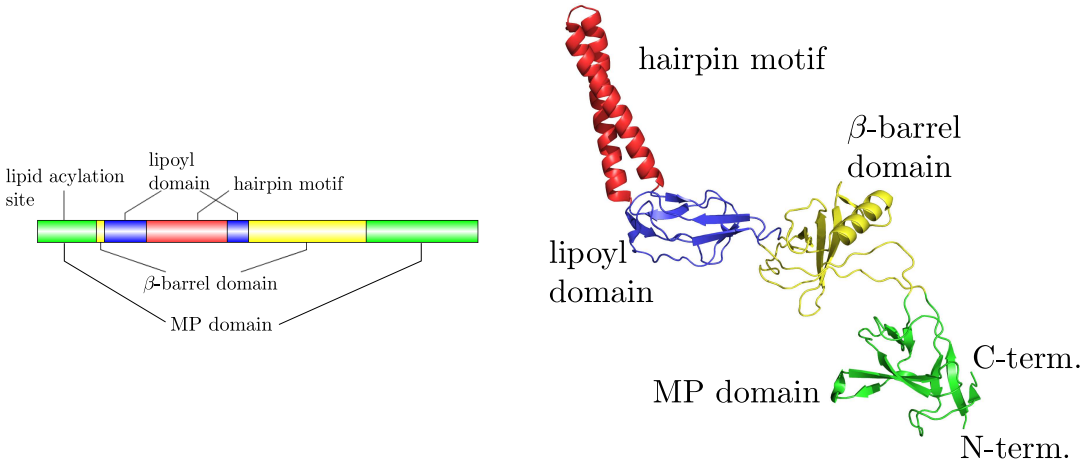

Figure 1.10: Left panel: organization of AcrA domains on the gene *acrA* indicated by colored boxes. Right panel: Cartoon representation of the AcrA homolog MexA crystal structure, with the structural domains represented in the same representative colors. Hairpin motif (red), lipoyl domain (blue), β-barrel domain (yellow), membrane proximal (MP) domain (green) (pdb ID: 2V4D).

structures of AcrA [90] and MexA [91, 92] resolved to 2.7 and 2.4 (and 3.0) Å, respectively. AcrA bears an N-terminal signal sequence (amino acid 1–24), that is cleaved off after translocation to the periplasm to form the processed protein. At the N-terminus, a cysteinyl residue (AA 25) is post-translationally palmitylated, concluding the AcrA maturation. The fatty acid attachment most likely functions as a membrane anchor and attach AcrA to the inner membrane. The lipoyl anchor seems not to be essential for its function, since AcrA without lipid modification showed no difference in function [93]. Mature AcrA is 373 (25–397) amino acids (AA) long. It basically consists of three globular domains, the β-barrel domain, the lipoyl domain, the membrane proximal domain and a hairpin α-helical structure (Figure 1.10). Recent revision of crystal data of MexA revealed a novel defined domain in the area of the disordered terminal stretches [94]. This membrane proximal (MP) domain has not been observed in crystal structures of AcrA before. It stretches from the inner membrane into the periplasm and brings the remaining AcrA domains in range of the TolC docking domain of AcrB. The following β-barrel domain is composed of six β-sheets and arranges spatial proximity of the C-terminal disordered domain to the AcrB-TolC docking interface. The C-terminal domain was found to be essential for the interaction with both AcrB and TolC [95, 96]. The lipoyl domain extends AcrA towards the outer membrane and TolC via a 58 Å long hairpin motif composed of a helix-turn-helix arrangement. The hairpin connects the two

halves of the lipoyl domain (Figure 1.10). Compared to AcrA, MexA is shorter in both sequence and structural length. A missing 7 AA repeat in each of the hairpin forming α-helices is responsible for the shorter overall measure of MexA. The structures of AcrA and MexA show high structural homology given the 62 % identity and 73 % similarity of the adaptor proteins. Nevertheless, they are not able to functionally complement for each other in the according complexes [97].

1.3.3 TolC

The outer membrane protein TolC of *E. coli* and homologous proteins (for example OprM in *P. aeruginosa*) participate in numerous transport complexes in Gram-negative bacteria. Best studied example is the AcrAB-TolC multidrug export complex. Being also part of type I secretion systems, TolC facilitates transport of enzymes and toxins (e. g. colicin V, hemolysin) and thus is considered to be a major factor for both resistance and pathogenicity. This homotrimeric protein is located in the outer membrane, and its soluble domain protrudes into the periplasm. Crystal structure of a C-terminally truncated, but still fully functional TolC is available in high resolution [98]. The three monomers form a 140 Å barrel, comprised of two domains. Anchored in the outer membrane, the β-barrel domain is composed twelve β-sheets arranged in anti-parallel pairs, where four sheets are donated by each of the three monomers. The periplasmic domain is a cylindrical barrel formed by coiled coil α-helices. The β-barrel domain and the helical domain are connected via a short proline-containing hinge-like linkers. The α-helical domain of around 100 Å bridges the periplasm to make contact with the inner membrane pump. Within TolC, short α-helical structures referred to as equatorial domain pack against the barrel forming helices. N- and C-termini are located in this domain. Since truncation of 43 C-terminal amino acid residues for this crystallographic study maintains functional properties of the wild-type, the function of the deleted residues remains unknown. The structure establishes a tunnel connected to the outside of the cell with a cavity surrounded by the α-helices. TolC may structurally resemble a tunnel but the fact that it was crystallized in a closed state it resembles on the functional level a channel. The periplasmic opening of the outer membrane protein was found to be obstructed by three of the α-barrel forming α-helices. In a model, Koronakis *et al.* [98]

postulate an aperture-like twisting opening-closing mechanism of the inner helices. In a later study two TolC structures were published showing the channel in a partially open, asymmetric, state [99]. Furthermore, indications of a putative AcrA-TolC interface in a groove among the barrel forming α-helices were found [99, 100].

1.4 Trimerization of assembled RND pumps

High resolution X-ray data on RND pumps is available for the prototypical RND pump AcrB, the HAE1 family homolog MexB from *Pseudomonas aeruginosa* [43] and CusA from the HME family [45]. Comparative analysis of predicted topologies revealed a fundamental structural organization of RND transporters, the "RND signature" [101]. Remarkably, from the information on the RND pumps up to date, another general feature appears to be the trimeric state of the functionally assembled transporter complexes. For AcrB, MexB, CusA and MdtBC from *E. coli* it has been shown that these proteins form homotrimers, or heterotrimers in the case of the latter. Amino acid sequence similarities and identities are shown in detail in Table 1.2. In AcrB, MexB and

Table 1.2: Amino acid sequence similarity and identity values for MdtB, MdtC, AcrB and CusA.

	MdtB	MdtC	AcrB	CusA
MdtB	—	64.4	43.3	35.9
MdtC	51.6	—	43.7	36.8
AcrB	27.9	28.1	—	36.1
CusA	21.7	21.7	20.0	—

% identity — % simil.

CusA, the trimeric assembly is observed in the crystal structures. There is no structure available that shows any of these examples as a monomer. The trimeric organisation for AcrB, CusA and MdtBC has also been shown using other techniques [80, 102, 103]. The functional rotation hypothesis implies the necessity for oligomers, where conformational changes in one of the monomers trigger structural rearrangements in a neighboring monomer. Beside the structural evidence, strong biochemical evidence has been published that confirms homotrimeric AcrB as the functional unit [80]. Three genetically

linked monomers, that are encoded and translated from a single open reading frame, assemble to fully functional pumps. Inactivation of one of the three linked trimers, leads to the termination of pump activity in the trimeric complex. This finding is in favor of the functional rotation and substantiates the need of trimers for functionality.

CusA is a member of the RND-heavy metal efflux (HME) family in *E. coli*. It is part of the CusCFBA complex that confers resistance to copper (Cu^+) and silver (Ag^+) ions. The composition of the functional complex is believed to be comparable to that of the AcrAB-TolC complex. The inner membrane pump CusA is working in concert with the MFP CusB and the OMF CusC [87, 104]. CusF, a protein that has been located in the periplasm and found to bind copper ions may act in concert with the CusABC metal efflux complex [105]. CusA shares 20 % identical and 36 % similar residues with AcrB. Comparative analysis by analytical ultracentrifugation of AcrB and CusA in DDM solubilized solutions revealed the presence of monomeric and oligomeric states of both proteins. AcrB as well as CusA could be found as mono-, di- and trimers. A small portion was present in undefined oligomeric states bigger than the trimeric forms [102].

The MdtABC-TolC complex of *E. coli* has been identified as a multi-drug export machinery [9, 106]. It confers resistance to cholate and cholate-derivatives, sodium dodecylsulphate (SDS) and novobiocin. In this complex, MdtB and MdtC represent RND proteins belonging to the hydrophobe/amphiphile efflux-1 family (HAE1). The efflux complex involves the promiscuous OMF TolC. In correlation to the AcrAB-TolC system, the MFP MdtA propagates the docking of $MtdB_2C$ to TolC and stabilizes the periplasm spanning complex. Substrate specificity for MdtB and MdtC were found to be different in minimal inhibitory concentration experiments. MdtC expressed together with MdtA (in the absence of MdtB) conferred resistance to bile salts, but not to SDS and novobiocin. These findings suggest that MdtC is able to form a partial functional transporter $MdtC_3$. In contrast, the expression of MdtA and MdtB (in absence of MdtC) did not confer resistance to either of the reported substrates indicating that MdtB alone is not able to form a functional pump. Hence both, MdtB and MdtC are required to form a fully functional transporter, in which MdtB and MdtC seem to be responsible to confer resistance to SDS and novobiocin and bile salts, respectively [107]. These

findings suggest the formation of a heterotrimeric pump composed of MdtB and MdtC, the stoichiometric constitution of the two components was, however, not clear in the first place. Kim *et al.* described the creation of genetically linked trimers to determine stoichiometric composition of the RND pump MdtBC [103]. This approach was similar to the covalently linked trimer experiments of AcrB [80]. It was shown, that a composition of two MdtB and one MdtC ($MtdB_2C$) resembles the wildtype MdtBC activity. Other combinations of covalently linked MdtB and MdtC exhibit considerably lower or no activity. Furthermore, the impact of the two proteins in terms of proton transport on the trimer was investigated. Putative key residues were identified in homology to Asp407 and Asp408 in AcrB. These putatively H^+-conducting residues also exist in MdtB and MdtC. Interestingly, the activity of the complex is diminished upon Asp410 to alanine mutation in any of MdtB, whereas the same mutation in MdtC (Asp401 to alanine) does only moderately affect activity. Individual functions of MdtB and MdtC remain unclear, but the experimental data suggest discrete substrate specificities and unequal participation in energy conversion.

The ability of the RND transporters to form trimers can probably be attributed to the large periplasmic domains rather than the transmembrane domains. The intermonomer loop, a structure within the TolC docking domain, is reaching from one monomer to its neighboring monomer and is supposed to stabilize the trimer [70]. In the DDM solubilized state, it was shown that the oligomeric state of purified AcrB mutant lacking the intermonomer loop sequence (ΔAA212–AA239), is shifted towards the monomeric state compared to wildtype AcrB (Chapter 2). The corresponding loop sequence of CusA is shorter than that of AcrB [102] as shown by comparative analysis of the amino-acid sequence of the loop region of AcrB, CusA, MdtB and MdtC (Figure 1.11).

1.5 Stoichiometry and assembly of the tripartite system AcrAB-TolC

The AcrAB-TolC complex is the major determinant for intrinsic and acquired multidrug resistance in *E. coli*. Its components are constitutively expressed in wild type *E. coli* cells. This complex is remarkable in its way to transport various drugs from the inner membrane or the periplasm to the extracellular environment. AcrB, located in the inner membrane, performs substrate binding and passage to TolC as well as energy coupling

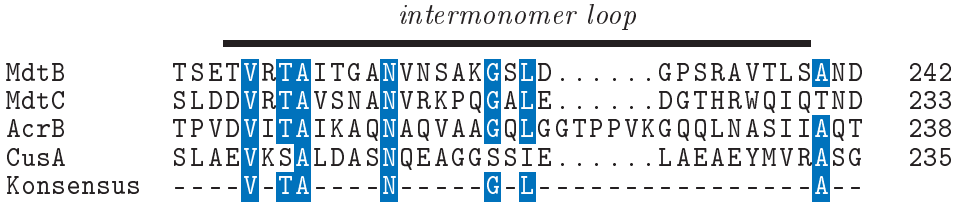

Figure 1.11: Sequence alignment of the intermonomer loop region of MdtB, MdtC, AcrB and CusA. Identical residues are shaded blue, gaps are indicated by dots. The alignment was done using the ClustalW2 program (www.ebi.ac.uk/Tools/clustalw2/index.html).

via the proton motive force. AcrB interacts with TolC via its TolC-docking domain. TolC provides a gateway for the pump assembly through the outer membrane and to the outside of the cell. The periplasmic domains of AcrB and TolC protrude into the periplasm for 70 and 100 Å , respectively, which appears sufficient to span the periplasm. AcrA is suggested to connect AcrB to TolC and might function as an adaptor, stabilizing the complex. Crystal structures of all three individual components are available, but up to date there is no crystallographic structure of the assembled complex.

The stoichiometry of the AcrAB-TolC complex has been handled very controversially in literature. From high resolution data, the trimerity of the functional units of the inner membrane pump AcrB and the outer membrane channel TolC are clear without ambiguity. The accurate number of MFPs within the complex could not be determined from its crystallographic data. The lack of structural data for the entire tripartite complex, led to several alternative suggestions on the number of the adaptor proteins within the assembly. Initial data retrieved from AcrA and MexA protein crystals were deficient in structural information of the N- and C-terminal part of the fusion proteins. In literature this domain was referred to as the disordered domain. This lack of information was obstructive for understanding the assembly of the tripartite complex, because the terminal domains were thought to be involved in the interaction with the inner membrane pump. Studies to understand the assembly of the complex involved several biochemical techniques like cross-linking of the individual components, pull-down assays, and isothermal titration calorimetry. The MexAB-OprM complex of *P. aeruginosa* showed tight complex formation, where all three components MexA, MexB and OprM could be co-purified with tagged MexA, MexB or OprM [108]. In the same study it was shown

that in a system expressing only two of the three components, neither MexA nor OprM were co-purified with His-tagged MexB, whereas OprM could be co-purified with His-tagged MexA. The assembly has also been characterized in cross-link experiments using dithiobissuccinimidyl propionate (DSP) as cross-linking agent [89, 96, 109, 110] and isothermal titration calorimetry (ITC) [96]. These experiments provided information about physical proximity and intersubunit affinity of the components *in vivo*.

In early attempts, the holocomplex was reconstructed based on the crystallographic information derived from each individual component. However, in one study, crystallized MexA was described as an helical assembly of thirteen monomers forming a tunnel like structure [91]. This composition, considered physiologically unlikely and possibly a crystallographic artifact, was not taken into account for complex reconstruction. The idea of the adaptor proteins laterally covering the binding interface of the inner membrane pump and the outer membrane channel led to a first model composed of twelve MexA proteins wrapping around the periplasmic part of AcrB. The adaptor proteins are not arranged equiplanar but at different distances from the reference point of the outer and the inner membrane. This model features a 4:1:1 stoichiometry of MexA:MexB:OprM respectively. Alternatively, a uniplanar model of three dimers of MexA was presented (2:1:1). Both models suggest molecular interactions in a way, that the adaptor protein's helical domain contacts the outer rim of the helical tunnel of OprM. In the hexamer model, the lipoyl- and β-barrel domain of the adaptor make contact with the MexB-OprM interface and MexB, respectively. Another suggestion emphasizes a sheath of nine MexA molecules (3:1:1) [92]. This model is similar to the MexA-hexamer configuration in terms of its sites of interaction. Both, the hexamer and the nonamer models contain a three-fold (pseudo) symmetry which is also true for TolC and AcrB. By using MexA as a homology model for AcrA (at that time no crystal structure of AcrA was available), extensive *in silico* modeling let to yet another interesting trimeric complex assembly [111]. This construction displays a stoichiometric complex of all three protein factors (1:1:1). This model derived from competitive analysis from a number of alternatively generated models. Furthermore, it also takes the experimentally demonstrated AcrB and TolC interaction [110] into account for the overall architecture of the tripartite complex.

Initial experiments showed that AcrA, AcrB and TolC formed a tripartite complex in *E. coli*, similar to that of the toxin exporter HlyBD-TolC [96]. Interactions of all three components were demonstrated by chemical cross-linking and co-purification. Using ITC, it was shown that the pump AcrB and the channel-tunnel TolC exhibit no detectable interaction but AcrA was able to associate with both AcrB and TolC in the absence of crosslinking agents [96]. These findings indicate that AcrB and TolC are either too distant to one another to be cross-linked in the assembled complex or the affinity of these two proteins is too low to form a complex without the support of the adaptor protein. In contrast, AcrA seems to bind to AcrB independently of TolC and vice versa. These findings confirmed that AcrA is essential for complex formation by contact between AcrB and TolC. This study and the identification of specific binding sites of AcrA for TolC and AcrB [95] were basis for successive investigation of the complex assembly.

Direct interactions between AcrA and TolC or AcrB were studied by *in vivo* cross-linking and co-purification [92, 100]. Two hetero bifunctional chemical cross-linkers *N*-succinimidyl 3-(2-pyridylthio)-propionate (SPDP) and sulfosuccinimidyl 6-[3'(2-pyridyldithio)-propionamido] hexanoate (LC-SPDP) with 6.8 Å and 15.6 Å spacers, respectively, were used to establish *in vivo* stable cross-links between accessible lysine side chains within AcrB or TolC and cysteine residues within AcrA. For that, cysteines had to be introduced in the naturally cysteine-free AcrA. Due to the distance restraints given by the chemical cross-linkers, some of the AcrA cysteine-variants allowed cross-linking with lysines of AcrB or TolC. Moreover, twelve cysteines were introduced in TolC, four of which showed binding to lysines of the AcrA wild type protein. The cysteines within TolC were located on the H3, H4, H7 and H8 α-helices, which are involved in AcrA binding. Vice versa, eight single cysteine AcrA variants were found to cross-link to wild type TolC [100]. The same approach was used to investigate the interaction of AcrA and AcrB. Fundamental for the AcrB/AcrA cross-link experiments was the re-evaluation of crystallographic data of the AcrA homolog MexA [92] as in the light of the new data a membrane proximal (MP) domain was defined and suggested to play an important role in interaction between the adaptor protein and AcrB. AcrA residues in the lipoyl-, β-barrel- and MP-domain were substituted by cysteines for subsequent use with chemical cross-linkers. Twelve out of 21 cysteines showed cross-link formation

with wildtype AcrB. In contrast, 16 individual cysteine mutations were introduced in the periplasmic domain of an otherwise cysteine-less AcrB. In seven single cysteine variants, cross-linking to wildtype AcrA could be observed in the presence of the two cross-linkers LC-SPDP and SPDP. Analogous to the AcrA-TolC experiments, the cross-linking data led to an interaction map of AcrA and AcrB [94]. These two studies presented *in vivo* cross-linking assays to map AcrA-TolC and AcrA-AcrB interactions. Docking studies utilizing the acquired data as distance constraints lead to a detailed experimental based tripartite AcrAB-TolC model (Figure 1.12). The assembly revealed a stoichiometric setup and illustrated the efflux machinery connecting inner and outer membranes as a 270 Å stretching complex. Notably, all these models integrated the TolC in an open state conformation and a symmetric AcrB trimer.

This cross-linking method revealed interaction of one of the AcrA α-helices of the hairpin motif to be involved in the interaction of AcrA and TolC. Several residues located on the helix α1 were identified in TolC binding, whereas none of the introduced cysteines in the helix α2 was able to cross-link (Figure 1.13). Considering the distance restraints from the different length of spacers of the cross-linkers, a molecular docking study led to a single AcrA-TolC model matching the experimental data [94]. This model supports the interaction of a single AcrA monomer per TolC monomer. The loop of the AcrA hairpin motif is located just below the equatorial domain of TolC. The α1 helix of AcrA is embedded in a groove formed by the periplasmic TolC helices H3, H7 and H8. Coiled-coil interactions seem to be the profound interaction mechanism found in this association. The AcrA helix extends from the equatorial domain to the periplasmic opening of the TolC channel in parallel to the TolC helices.

The acquired data from the cross-link experiments was consistent with the former findings of a 1:1:1 stoichiometry within the complex. In the most recent model [94] one AcrA monomer binds to one AcrB monomer, in favor for the 1:1:1 complex stoichiometry hypothesis. The lipoyl-domain of AcrA was found to contact the AcrB DN subdomain of the TolC docking domain. The β-barrel-domain and the MP-domain interact with the PN2 subdomain. In this way, the AcrA monomer seems to attach to AcrB, snugly fitting to the periplasmic domain. The globular domains of AcrA seem to clamp each AcrB monomer, forming a lateral bracket stretching from the AcrB-TolC interface to

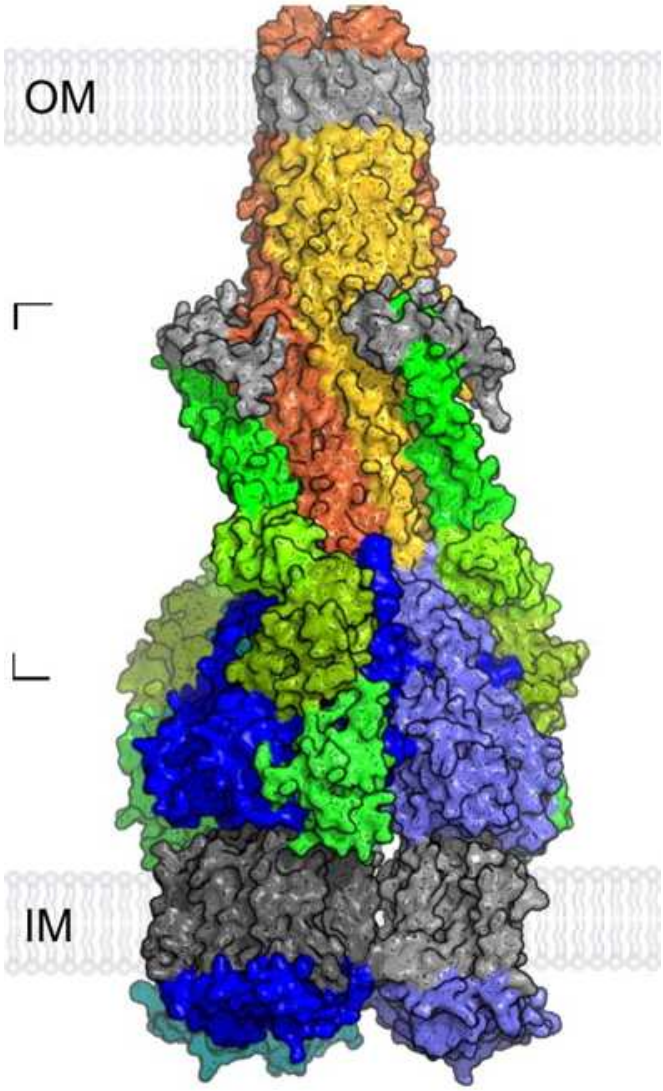

Figure 1.12: Schematic illustration of the AcrAB-TolC assembly in *E. coli*. The RND pump AcrB (blue, membrane regions gray) is inserted in the inner bacterial membrane (IM). The outer membrane factor (OMF) TolC (yellow/orange, equatorial domains and membrane regions gray) resides in the outer membrane (OM) and docks to AcrB in the periplasm. The complex is stabilized by the membrane fusion protein (MFP) AcrA (green), forming a clamp around AcrB-TolC interaction site. (This representation is Figure 5A from [94].)

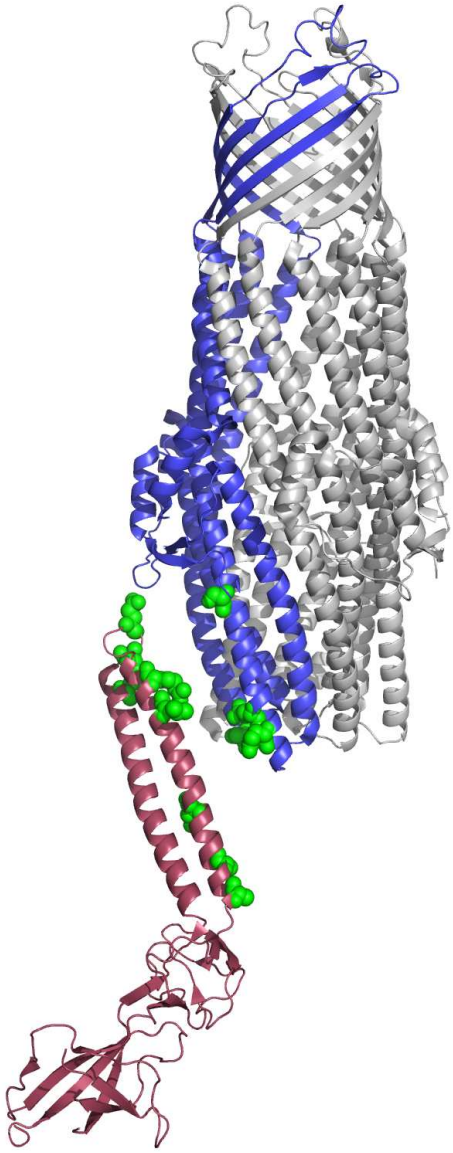

Figure 1.13: Interaction sites of AcrA and TolC. Eight cysteine residues, introduced to AcrA helix α1 and the hairpin loop, could be cross-linked to TolC residues using chemical bi-functional cross-linkers. Likewise, in TolC, four introduced cysteines on helices H3 and H7 could be cross-linked to AcrA [100]. AcrA wildtype is shown in red. TolC wildtype trimer is shown in grey, one monomer is highlighted blue. Positions of introduced cysteines are shown as green spheres. (pdb IDs: 1EK9 and 2F1M).

the inner membrane.

The latter model ([94], Figure 1.12) envisions a situation in which AcrA clings together the inner pump AcrB and the outer channel TolC. Interaction between AcrB and TolC, if any, is very weak and AcrA is necessary for complex formation. This seems to be in accordance with the necessity for AcrA to have a functional pump. The authors assume that within the complex, binding of AcrA may favor and stabilize the open state of the TolC channel. Moreover, AcrA may act as a flexible connector between AcrB and TolC, leveraging conformational changes from one protein to the other. Furthermore, the model suggests that binding of inhibitory designed ankyrin repeat proteins (DARPins) onto AcrB within the tripartite complex is possible. These DARPins bind to the periplasmic domain and were co-crystallized with AcrB [75]. The attachment sites of the DARPins were found to be different compared to that of AcrA and not overlapping (Figure 1.14). This might imply that the inhibitory function of the DARPin is

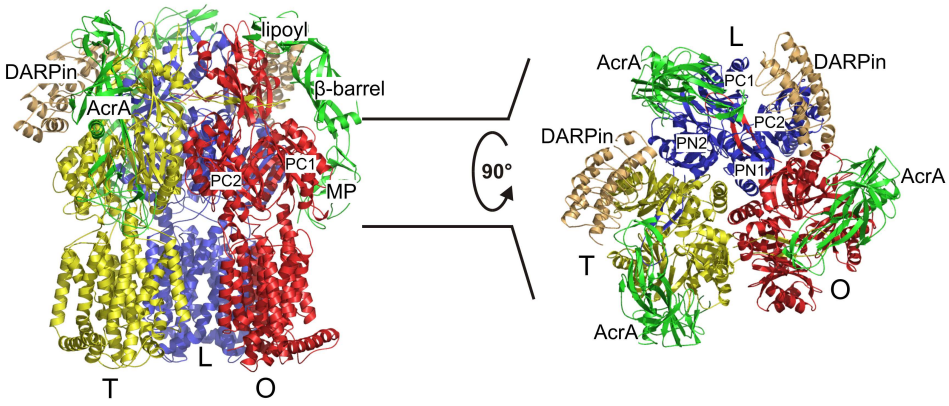

Figure 1.14: Side view (left) and top view (right) of the asymmetric AcrB with interacting DARPins (gold) and lipoyl-, β-barrel- and membrane proximal (MP) domains of AcrA (green) based on the docking model of Symmons *et al.* [94]. DARPins only bind to the loose (L, blue) and tight (T, yellow), but not to the open (O, red) conformer of AcrB. There is no sterical clash between the bound AcrA and DARPin molecules (From Pos with permissions [112]).

based on the inhibition of AcrB itself rather than on the inhibition of the assembly of the tripartite complex [112]. The complex composition of this assembly and the intrinsic difficulties of purifying and crystallizing membrane proteins render the crystallization of the entire complex a very delicate matter. The current data-driven model, however, represents the state-of-the-art archetypal of a multi-protein assembled multi-drug efflux machinery.

1.6 Cross-linking as technique

High-resolution structures of the asymmetric AcrB revealed three conformational states in a way that every monomer displays a different conformation [73–75]. The differences between the conformations are most pronounced in the relative location of subdomains of the periplasmic porter domain and reorganization in the transmembrane domain. Like snapshots of a continuous movement, the structures provide a basis for the hypothesis that the three conformations from the crystal structure represent certain states of a consecutive transport cycle in AcrB. However, crystal structures often display one of the possible local energy minima and the asymmetric conformation might represent one of those. To confirm the presence of the different conformations *in vivo*, a cross-link technique was used that allowed to trace conformational cycling *in vivo* [77, 84, 113].

In a cysteine-less background (AcrB_cl), numerous variants containing pairs of introduced cysteines were generated. In the oxidative environment of the periplasm, the sulfhydryl groups (Sγ) of two cysteines residues can form disulfide bridges (cross-links). A general assumption for two Sγ atoms to react to a disulfide bond is the proximity of less than 6.4 Å [77]. Furthermore, geometrical restraints of the involved cysteine residues have to be in favor for the cross-link formation. The proposed cycling of the monomers through the conformations L, T and O, causes rigid body movements of the specific subdomains. The rationale of this experiment was that strategically introduced cysteines located on the surfaces of adjacent subdomains, can form disulfide cross-links when within an appropriate distance of each other. Guided by the high resolution structure of the asymmetric AcrB crystal, cysteine residues were introduced that would report the proximity in only one of the conformations L, T or O. Cysteine locations included the four subdomains of the periplasmic porter domain (PN1, PN2, PC1, PC2), the docking domain (DC), the intermonomerical loop (Loop) and transmembrane helices 1 and 7 (TM1, TM7). According to the proposed conformational cycling of the monomers, formation of cross-links in one of the conformations was anticipated to lock the involved domains, thus arresting the monomer in a single conformation. Restriction of one of the monomers was expected to render the trimeric complex nonfunctional. This study's set of cross-link constructs included mutants that were expected to be able to form a disulfide bridge in either one of the conformations L, T and O. Controls

that were expected to show cross-links in all or cross-links in none of the conformations were included as controls. Cross-link variants in this study featured both, intra- and intermolecular cross-links.

Drug transport capabilities of the cross-link mutants was investigated using conventional minimal inhibitory concentration (MIC) and fluorescence dye (*N*-phenylnaphthylamine, NPN) based transport assays with *E. coli* cells. Additionally, the extent of disulfide cross-linking was quantitatively determined by mass spectrometry. In MIC experiments, AcrB variants containing cysteine pairs causing arrest of the continuous change of conformations within monomers in general significantly reduced drug resistance of the recombinant cells, whereas introduction of single cysteines exhibited negligible or minor effects on resistance towards various substrates of AcrB. Controls (constructs with up to 80 % cross-links) did not show substantial reduced drug transport. The effect of cross-linking was further characterized using NPN-fluorescence spectrometry. NPN, administered to de-energized bacterial cells, partitions into the inner membrane. NPN, an AcrB substrate, shows a strong fluorescent signal when located in the hydrophobic environment of the bacterial inner membrane, whereas removal of this compound after re-energization of the cells and due to the pumping action of AcrB to the aqueous outside of the cell causes a quenching of the signal. The fluorescence profile of NPN is a direct indication of the bacteria's ability to export the drug. Disulfide bridge formation inside AcrB inhibiting the conformational cycling resulted in accumulation of NPN in the membranes due to diminished transport activity of AcrB. AcrB activity and hence fluorescence quenching could be in part reversed by administration of dithiothreitol (DTT). Reduction of the disulfide bridges within AcrB restored export of NPN and decreased the fluorescence signal.The cross-link experiments support the proposed conformational cycling hypothesis derived from high resolution X-ray structures of AcrB. It elegantly demonstrates the existence of all three conformations (L, T and O) *in vivo*.

1.7 Goal of the Thesis

ArcB crystal structures have been obtained by X-ray diffraction data up to 2.5 Å resolution [73–75]. The high resolution data not only allow detailed structural insight to the protein's architecture, but also allow interpretation on the actual transport mechanism in which the three observed conformations may represent isolated snapshots of the complete conformational cycling.

To address this monomer cycling hypothesis, the functional crosslink data [77] was investigated on a structural level. Double cysteine AcrB variants were crystallized, diffraction data collected and the structures solved. In one case, an intermediate state was visualized, which provides substantial insights into the cycling events during catalysis. High resolution data structures of AcrB crosslink variants were obtained as co-crystal structures with designed ankyrin repeat proteins (DARPins) [75].

With different AcrB mutants, we observed different AcrB:DARPin stoichiometries. In this thesis, the stoichiometries of detergent-solubilized AcrB:DARPin complexes were investigated using LILBID MS, analytical ultracentrifugation, gel filtration chromatography and capillary electrophoresis assays.

To establish an *in vitro* transport assay for AcrAB-TolC drug efflux, functional reconstitution of the AcrB trimer was pursued. Initial reconstitution experiments in proteoliposomes were performed and a soluble TolC variant was generated for *in vitro* complex formation with reconstituted AcrB and AcrA.

2 Manuscript: Analysis of AcrB/DARPin Ligand Complexes by LILBID MS

This chapter contains a manuscript describing the experiments results and interpretations of the analysis of AcrB/DARPin complexes.

My contribution to this work was the overexpression purification and crystallization of the AcrB (wt and AcrB_V612F)/DARPin complexes. Furthermore, I conducted the capillary electrophoresis and the phospholipid analysis via thin-layer chromatography.

Lucie Sokolova and Mihaela Cernescu performed the LILBID MS experiments.

Dr. Thomas Eicher constructed the AcrB_V612F variant and performed and evaluated the analytical ultracentrifugation experiments with the help of Dr. Christophe Briand.

Dr. Markus Seeger constructed, overexpressed and purified the AcrB_dl and conducted the size-exclusion chromatography.

Hi-Jea Cha constructed, overexpressed and purified the AcrB_G616N for the LILBID MS analysis.

Analysis of AcrB/DARPin Ligand Complexes by LILBID MS

Lorenz Brandstätter, Lucie Sokolova, Thomas Eicher, Markus A. Seeger, Christophe Briand, Hi-jea Cha, Mihaela Cernescu, Jürgen Bohnert, Winfried V. Kern, Bernd Brutschy and Klaas M. Pos

2.1 Abstract

The AcrA/AcrB/TolC complex is responsible for intrinsic multidrug resistance (MDR) in *Escherichia coli*. Together with the periplasmic adaptor protein AcrA and the outer membrane channel TolC, the inner membrane component AcrB forms an efflux complex that spans both the inner and outer membrane and bridges the periplasm of the Gram-negative cell. Within the entire tripartite complex, homotrimeric AcrB plays a central role in energy transduction and substrate selection. *In vitro* selected designed ankyrin repeat proteins (DARPin) that specifically bind to the periplasmic domain of AcrB were shown to ameliorate diffraction resolution of AcrB/DARPin protein co-crystals [75]. Structural analysis revealed that the specific stoichiometry between trimeric AcrB wildtype protein to DARPins of 0.5 was shifted to 1 upon interaction of the DARPins with a V612F and G616N AcrB variant. These specific stoichiometric differences were analyzed in solution via densitometry after microchannel electrophoresis, analytical ultracentrifugation and via laser-induced liquid bead ion desorption mass spectrometry (LILBID MS). Using the latter technology, we investigated the gradual disassembly of the AcrB trimer and bound DARPin ligands in dependence on laser intensity in solution. At low laser intensity, the release of the detergent micelle from the AcrB/-DARPin complex was observed. By increasing laser intensity, dimeric and monomeric AcrB species with bound DARPin molecules were detected showing the high affinity binding of DARPin to monomeric AcrB species. High laser intensity LILBID MS experiments indicated a spectral shift of the monomeric AcrB peak of 3.1 kDa, representing a low molecular weight ligand in all detergent-solubilized AcrB samples and in the AcrB crystal. The identity of this ligand was further investigated using phospholipid analysis of purified AcrB and AcrB variant samples, and indicated the presence of phosphatidylethanolamine and possibly cardiolipin, both constituents of the *Escherichia coli*

membrane.

2.2 Introduction

Tripartite complexes are important toxic compound resistance determinants in Gram-negative bacteria. These complexes are composed of an energy transducing pump, residing in the inner membrane, a channel in the outer membrane and a periplasmic adapter protein that establishes a stable connection between the inner-membrane pump and the outer-membrane channel. In opportunistic pathogens like *Escherichia coli* and *Pseudomonas aeruginosa*, the multidrug resistance (MDR) pumps AcrAB-TolC and MexAB-OprM, respectively, are responsible for resistance phenotypes against a great variety of different antimicrobial agents. AcrB and MexB represent the inner-membrane located pump in these complexes and belong to the large superfamily of Resistance Nodulation and cell Division (RND) transport proteins. These homologous proteins have been studied in detail on the functional [76–79, 86, 114] and structural level [43, 73–75]. AcrA and MexA act as adapter proteins and stabilize binding of AcrB and MexB to TolC and OprM, respectively [115].

Initial crystallographic data from AcrB protein crystals provided substantial structural insights and presented the protein as a homotrimer [70], in which all of the monomers adopt the same conformation. Later, trimerization was postulated to be the physical basis for a conformational cycling mechanism for drug efflux, on basis of recent crystal structures of asymmetric AcrB, which suggested that each monomer can adopt different conformational states loose (L), tight (T) and open (O) [73–75, 86]. Moreover, trimerization was also observed in the crystal structure of the AcrB homolog MexB from *P. aeruginosa* [43] and the CusA silver and copper ion RND efflux protein [45]. Biochemical experiments with covalently linked AcrB monomers indicated that trimerization of AcrB is essential for its function and that inactivation of one monomer is sufficient to block the activity of the entire AcrAB-TolC complex [80]. Analytical ultracentrifugation provided evidence that AcrB is most likely trimeric in its detergent solubilized state as well [75, 102]. Thus, trimerization is believed a general feature of proteins of the RND superfamily.

Designed ankyrin repeat proteins (DARPins) represent a novel antibody-like scaffold that is based on a consensus design of the ankyrin repeat motif [116]. In nature, the fundamental function of ankyrin repeat proteins is the establishment of specific protein-protein interactions [117]. Highly specific DARPins have been raised against a number of target protein using *in vitro* selection methods such as ribosome display [118] and phage display [119]. Selected high affinity binders have been used in co-crystallization experiments [120] and with AcrB, the first example of crystals for a membrane protein in complex with DARPins was obtained [75]. In the AcrB/DARPin co-crystal structure, two DARPins are bound to the periplasmic domain of the AcrB trimer. A single DARPin molecule binds to the surface of the loose (L) and tight (T) conformers each, but not to the open (O) conformer.

Laser-induced liquid bead ion desorption mass spectrometry (LILBID-MS) is a novel technique, that allows detection of membrane protein complexes in a detergent-solubilized state. Depending on the laser intensity, entire protein complexes or contributing subunits can be observed [121–124]. Here, we analyze three different AcrB variants in detergent-solubilized and crystalline state, with and without bound DARPin molecules.

2.3 Material and Methods

Construction of the AcrB mutants AcrB_dl, AcrB_V612F and AcrB_G616N

AcrB variants (AcrB_dl, AcrB_V612F and AcrB_G616N) were constructed by site-directed mutagenesis using the Quikchange protocol from Stratagene. In the AcrB_dl (deleted loop) mutant amino acids 218–239 (QLGGTPPVKGQQLNASIIAQTR) were removed. Amino acid substitution and region deletion were achieved with 5' phosphorylated primers. Cloning procedures were performed on the pET24 vector carrying the wildtype acrB gene as template (pET24acrB$_{His}$, [125]). The final constructs were verified by sequencing (Microsynth, Switzerland).

Drug susceptibility assay

E. coli BW25113 Δ*acrB* carrying pET24acrB$_{His}$ (AcrB wt), pET24acrB_dl$_{His}$ (AcrB_dl) and pET24 (vector) were used for minimal inhibitory concentration (MIC) experiments as described earlier [77].

Protein expression and purification

Overexpression and membrane preparation of AcrB wt, AcrB_V612F, AcrB_dl and AcrB_G616N was carried out as previously described [74] with modifications. During solubilization and purification only the detergent n-dodecyl-β-maltoside (DDM, GLYCON Biochemicals GmbH, Luckenwalde, Germany) was used throughout the procedure. Membranes were solubilized in 20 mM Tris/Cl, 150 mM NaCl, 10 mM imidazole, 10 % glycerol and 2 % DDM, pH 7.5 (15–20 ml total volume). The detergent-solubilized fraction was separated from insoluble material by centrifugation at 145000×g at 4 °C for 1 h and was subsequently applied to a Ni^{2+}-nitrilotriacetic acid (NTA)-agarose column (2 ml bed volume, Qiagen) pre-equilibrated with 20 column volumes (CV) of buffer 1 (20 mM Tris/Cl, 150 mM NaCl, 10 mM imidazole, 10 % glycerol and 0.03 % DDM, pH 7.5). The column was washed with 45 CV buffer 1 and subsequently washed with 30 CV buffer 2 (20 mM Tris/Cl, 150 mM NaCl, 50 mM imidazole, 10 % glycerol and 0.03 % DDM, pH 7.5). AcrB was eluted in 6 ml of buffer 3 (20 mM Tris/Cl, 150 mM NaCl, 200 mM imidazole, 10 % glycerol and 0.03 % DDM, pH 7.5). Purified DARPins (inhibitor 1108_19 [75]) were added to the purified AcrB in a two-fold molar excess (to AcrB monomer). After concentration in centrifugal filter devices with a cutoff size of 100 kDa (Amicon Ultra, Millipore), AcrB/DARPin protein mixture (0.7 ml) was subjected to size exclusion chromatography in buffer 4 (20 mM Tris/Cl, 150 mM NaCl, 0.03 % DDM, pH 7.5) using a GE Superdex 200 10/300GL column connected to a GE Healthcare ÄKTAprime system. Peak fractions corresponding to AcrB(trimer)/DARPin complexes were collected and concentrated in centrifugal filter devices with a cutoff size of 100 kDa (Amicon Ultra, Millipore) to 10 mg·ml^{-1}. For the gel filtration run shown in Fig. 2.2, AcrB and AcrB_dl were purified as above, but with 0.05 % cyclohexyl-hexylmaltoside as detergent. Subsequent size-exclusion chromatography was performed using a GE HiLoad

16/60 Superdex 200 (120 ml pack size) with 10 mM Na-HEPES, pH 7.0, 200 mM NaCl, and 0.05 % cyclohexyl-hexylmaltoside as running buffer at 0.4 ml·min^{-1}. Apparent molecular weight values were calculated on basis of a run under identical conditions with 4 marker proteins (Ferritin (440 kDa), Albumin (67 kDa), Ovalbumin (43 kDa), Ribonuclease A (13.7 kDa)). Protein concentration was determined using the absorption at 280 nm (Nanodrop ND-1000 spectrophotometer) or using the colorimetric BCA protein determination method (Pierce).

LILBID MS

Before subjecting the samples to LILBID MS, a buffer exchange on Wizard desalting columns (Promega) was carried out on purified AcrB wt, AcrB variants and the AcrB/DARPin complexes into 30 mM NH_4HCO_3, pH 7, 0.05 % DDM. AcrB/DARPin co-crystals were dissolved in 20 mM Tris/Cl, pH 7.5 containing 0.05 % DDM. Insoluble particles were removed by filtration through a Millex-GV syringe-driven filter unit (0.22 µm, Millipore). The final protein concentration was 10 µM with respect to the AcrB monomer.

Details of the experimental set-up for LILBID have been published previously [126]. Micro-droplets of sample solution (diameter: 50 µm) are produced at 10 Hz by a Piezo-driven droplet generator and introduced into vacuum via differential pumping stages. There the droplets are irradiated one by one by synchronized high-power mid-infrared laser pulses. These are generated in a home-built optical parametric oscillator using $LiNbO_3$ crystals and a neodymium-doped yttrium aluminium garnet; Nd:$Y_3Al_5O_{12}$ laser as pump. The wavelength of the optical parametric oscillator radiation is tuned to the absorption maximum of water at around 3 µm corresponding to an excitation of the stretching vibrations of water. At threshold intensity the droplet explodes resulting in the emission of ions from liquid into gas phase. There the ions are mass analyzed in a time-of-flight reflectron mass spectrometer. To detect very large biomolecules, a Daly-type ion detector is used, working up to an m/z range in the low MDa region. At low laser intensity, LILBID desorbs ions out of the liquid very gently (ultrasoft mode) enabling detection of the non-covalently assembled protein complexes. At higher laser intensity (soft mode) the strong interactions are still kept, the weak ones are broken. At

the highest laser intensities the complex is thermolyzed into its covalent subunits (harsh mode). The signals from the detector are recorded by a transient recorder. For data acquisition and analysis a user-written labview program is used. The signal to noise ratio is improved by subtracting an unstructured background, caused by metastable loss of water and buffer molecules, from the original ion spectra. These difference spectra are smoothed by averaging the signal over a pre-set number of channels of the transient recorder.

Capillary electrophoresis

Protein samples (AcrB wt and AcrB_V612F) co-purified with DARPins via SEC were analyzed on a 2100 Bioanalyzer (Agilent Technologies Inc.) using the Agilent Protein 230 chips. Samples (approx. 10 $mg \cdot ml^{-1}$, 4 µl) were prepared according to the manual with omission of the sample heating step. Relative concentrations of AcrB and DARPin fractions were calculated from the integrals of the eluted protein peak areas in the recorded electropherograms by the software 2100 Expert (Agilent Technologies Inc.).

Phospholipid analysis via thin-layer chromatography

Phospholipid analysis of AcrB wt and AcrB_V612F samples was done by thin-layer chromatography. Reference phospholipids (*E. coli* polar lipids, 1,2-dioleoyl-*sn*-glycero-3-phosphocholine (DOPC), 1,2-dioleoyl-*sn*-glycero-3-phosphate (DOPA), 1,2-dioleoyl-*sn*-glycero-3-phosphoethanolamine (DOPE), cardiolipin, (Avanti Polar Lipids, Inc.) at 10–20 µg in $CHCl_3$), DDM solution (1 %), buffer (20 mM Tris, 150 mM NaCl, 0.03 % DDM, pH 7.5) and purified protein (applied at 5×1 µl steps, 8.5 µg) in buffer were spotted onto a HPTC silica-gel 60 plate (Merck), which was pre-washed by migration with acetone in a chromatography tank and air-dried in a fume hood for several hours. The plate was subsequently air-dried and the chromatography step was performed in a chromatography tank with a mixture of $CHCl_3$/MeOH/H_2O (65:25:4, v/v). Subsequently, the plate was dried for 30 min and phospholipids were stained with iodine (sublimating iodine in a chromatography tank at room temperature). For subsequent

molybdate staining, the plate was initially heat dried at 160 °C to completely evaporate the iodine and sprayed with molybdatophosphoric acid solution (Carl Roth) with subsequent development at 160 °C.

Analytical ultracentrifugation

The molecular weight of AcrB wt and AcrB_V612F proteins in complex with bound DARPins was estimated by sedimentation velocity experiments. 400 µl of purified protein complexes (in 20 mM Tris/Cl, 150 mM NaCl, 0.03 % DDM, pH 7.5) with an OD_{280} of 0.7 were applied to an An50-Ti analytical rotor (Beckman Coulter) in a Beckman Proteome Lab XL-I centrifuge. Buffer was used as a reference in sedimentation velocity experiments. Data were collected at 280 nm. Ultracentrifugation was performed at 40000 rpm at 4 °C. Sedimentation velocities were analyzed with the software SEDFIT [127].

2.4 Results and Discussion

Oligomeric state of wt AcrB

Crystallographic and biochemical studies provided substantial evidence for the characterized members of the RND superfamily to be functional as a homotrimer [43, 45, 70, 73–75, 80, 103]. The state of these proteins in solution has recently been analyzed by analytical ultracentrifugation [102] and suggests equilibrium between monomeric, dimeric, trimeric and higher oligomerization states of the AcrB and CusA proteins. We selected the highly sensitive LILBID MS as method of choice to determine the oligomeric state of AcrB (theoretical M_W of His-tagged monomer: 114.6 kDa) in detergent solution (Fig. 2.1). Under ultrasoft laser condition, the AcrB trimer is observed together with the detergent micelle as a broad peak ranging from 190 kDa to 260 kDa with a maximum at 425 kDa (Fig. 2.1E). With increasing laser intensity, the distribution shifted to detergent-free trimeric AcrB (apparent M_W: 355 kDa)(Fig. 2.1B-D). The estimated detergent micelle from these experiments would be 70 kDa, close to the size of a dodecylmaltoside detergent micelle in solution [128]. At the highest laser intensity used,

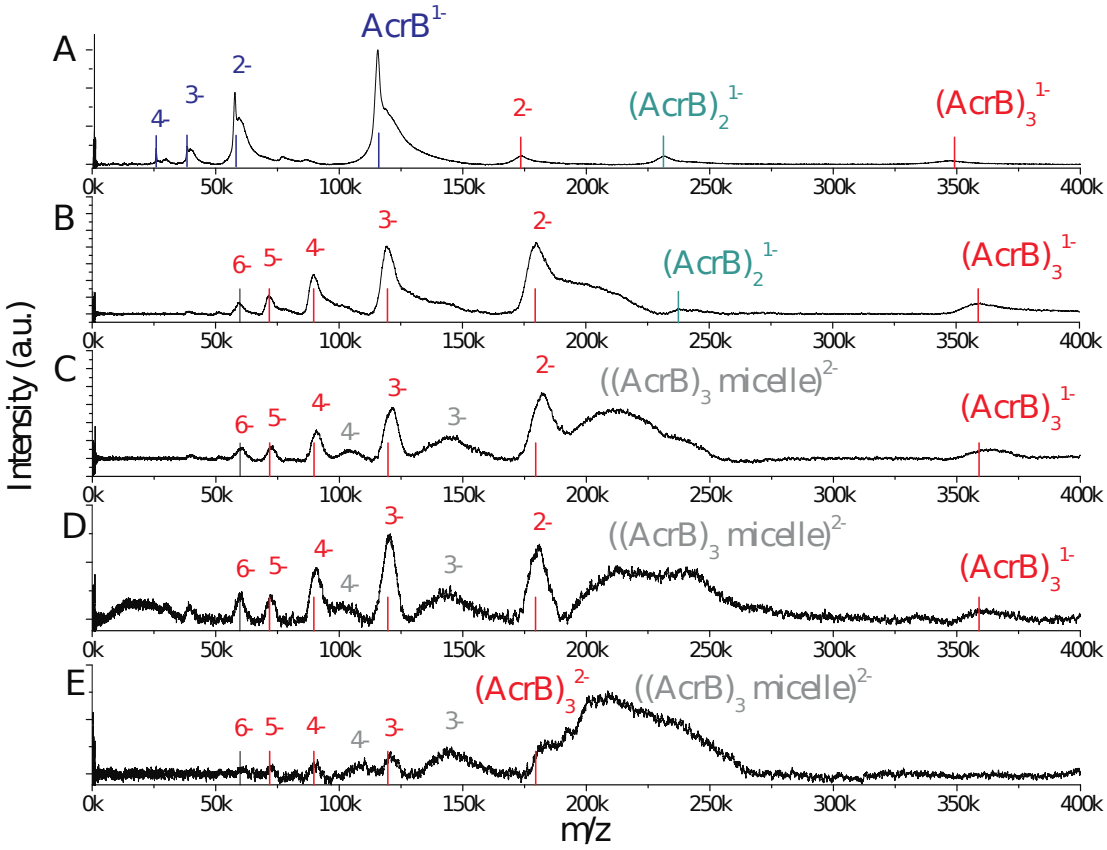

Figure 2.1: Anion LILBID MS spectra of $AcrB_{His}$ in detergent solution. The laser intensity decreases from the spectrum A (harsh) to the spectrum E (ultrasoft). At harsh laser intensity (A), the charge distribution of the monomer (blue bars) is detected as the major species in the spectrum but also a dimeric species (green bar) is observed. At soft laser intensity (B and C), mainly AcrB trimers (red bars) are observed. At even softer laser intensity conditions (C to E), the trimeric species is shifting its mass distribution (((AcrB)$_3$ micelle), grey), most likely due to the presence of a detergent micelle on the $AcrB_{His}$ trimer and displays a peak maxima corresponding to a charge distribution of a mass of 425 kDa.

mainly monomeric AcrB (apparent M_W: 116 kDa) was observed, but still a detectable amount of di- and possibly trimeric AcrB were present in the sample (Fig. 2.1A). This extraordinary stability appears to be quite unique compared with other membrane protein complexes tested with LILBID MS [121–123]. The AcrB trimer contains an intermonomeric loop structure, protruding from one monomer to the neighboring monomer, which might be the determinant for the observed stability of the trimeric complex. Indeed, deletion of the loop resulted in the formation of mainly monomeric AcrB (apparent M_W: 116 kDa compared to calculated M_W: 114.6 kDa) in detergent solution (Fig. 2.2) and *Escherichia coli* harboring the deleted loop gene mutant of

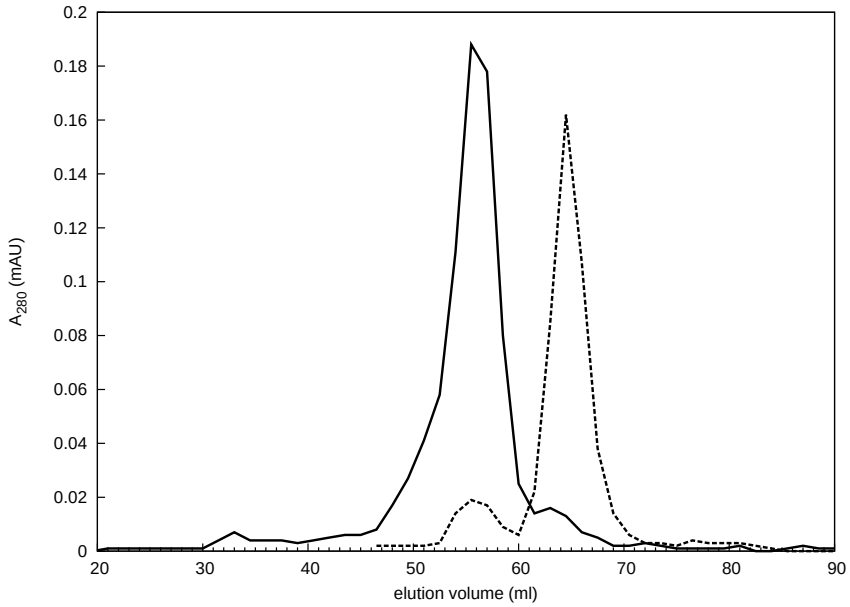

Figure 2.2: Size-exclusion chromatography elution profiles of purified wildtype AcrB (solid line) and the deleted loop AcrB variant (AcrB_dl, dashed line) on a GE Superdex 200 10/300GL column coupled to a GE Healthcare ÄKTAprime FPLC system. The main peak of the wildtype AcrB corresponds to AcrB trimers. In contrast, only a small fraction of AcrB_dl elutes at comparable elution volume, whereas the majority of the protein sample elutes later, indicating the presence of AcrB_dl monomers.

AcrB (AcrB_dl) in a Δ*acrB* background led to an increased sensitivity towards drugs (Table 2.1). Notably, activity was not reduced completely, indicating that the role of the loop region could be an exclusive structural one. Since the deleted loop variant of AcrB is still able to form trimeric assemblies (Fig. 2.2, apparent M_W: 267 kDa compared to calculated M_W: 343.8 kDa), it appears that trimerization is mandatory for the activity of AcrB, as has been postulated based on biochemical and structural

Table 2.1: Drug susceptibility of *E. coli* BW25113 Δ*acrB* expressing wt and mutant AcrB[a]

	Ery	**Oxa**	**TPP$^+$**	**Novo**	**Cipro**
AcrB wt	32–64	64	200–400	16–32	0.004–0.008
No AcrB	2	4	6.25	4	0.002
AcrB_dl	4	4	50	8	0.002

[a]Abbreviations: Ery=Erythromycin, Oxa=Oxacillin, TPP$^+$=Tetraphenylphosphonium, Novo=Novobiocin, Cipro=Ciprofloxacin, AcrB wt=AcrB wildtype (pET24acrB$_{His}$), No AcrB=pET24 vector, AcrB_dl=AcrB with deleted loop (pET24acrB_dl$_{His}$)

data [73, 74, 80, 86].

DARPin binding to AcrB and AcrB variants

AcrB-specific DARPins were selected *in vitro* using ribosome display, which facilitated the formation of well-diffracting (to 2.5 Å) crystals of AcrB [75]. One AcrB trimer, containing two bound DARPin molecules, was present in the asymmetric unit. This 3:2 (AcrB monomer to DARPin) ratio was also found in detergent solution using analytical ultracentrifugation [75].

Initial crystallographic studies of AcrB variants, which have substitutions near the drug binding pocket located in the porter domain of the periplasmic part of AcrB (i. e. V612F and G616N), revealed cubic crystal forms (I23) with one AcrB monomer and one DARPin molecule in the asymmetric unit (Eicher, Cha *et al.* , unpublished). A symmetric setup would imply that DARPin/AcrB trimer stoichiometry would have been shifted from 2 in the case of wildtype AcrB to 3 in the case of the AcrB variants. To distinguish if the different stoichiometries are only observed in crystalline state or can also be detected in solution, we analyzed the samples using LILBID-MS, capillary electrophoresis and analytical ultracentrifugation.

LILBID-MS of AcrB/DARPin complexes

For the AcrB wt/DARPin complex and the V612F/DARPin complex, similar spectra were obtained under high intensity laser conditions (Fig. 2.3) indicating that 2 or more DARPin molecules bind to the AcrB trimer. For the AcrB_G616N variant,

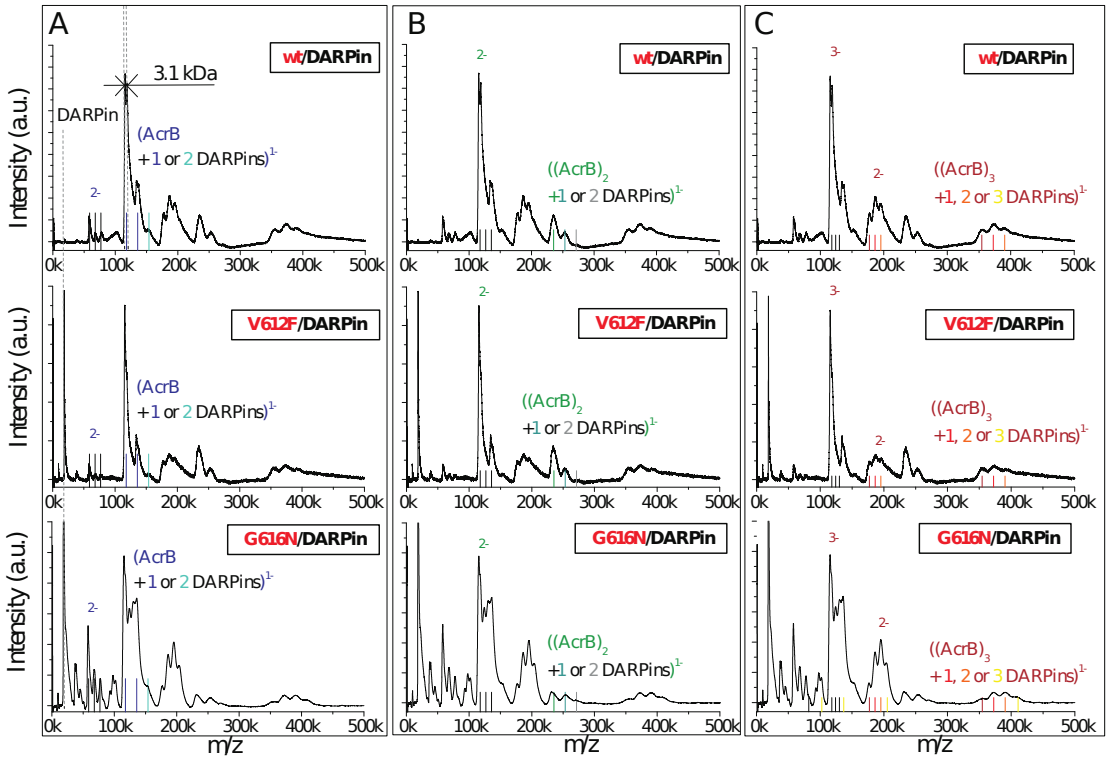

Figure 2.3: Anion LILBID spectra of AcrB wt, AcrB_V612F variant and AcrB_G616N variant at harsh laser intensity. The panels A-C display indentical spectra. The bars in the different blue colors (panel A) represent charge distributions of the AcrB monomer with none (dark blue), one (violet) or two (turquoise) DARPins bound, the bars colored in the green range (panel B) represent charge distribution of AcrB dimers with none (dark green), one (blue-green) or two (grey-green) DARPins bound and the bars in the red colored spectrum (panel C) represent charge distributions of the AcrB trimers with none (dark red), one (red), two (orange) or three (yellow) DARPins bound.

the AcrB monomer to DARPin stoichiometry was determined to be 3 (Fig. 2.3), indicating a symmetric AcrB:DARPin structural complex commensurate to the threefold symmetry found in the AcrB_G616N crystals. The spectra of the all three AcrB variants also revealed a broad peak which might represent an AcrB monomer containing 2 bound DARPin molecules, in contrast to what has been found in the crystal structure [75]. This observation can be best explained by the formation of DARPin dimers via a DARPin/DARPin interface and under ultrasoft laser intensities 4 DARPin molecules

are attached to both the AcrB wt and V612F variant (Fig. 2.4A and B). When using

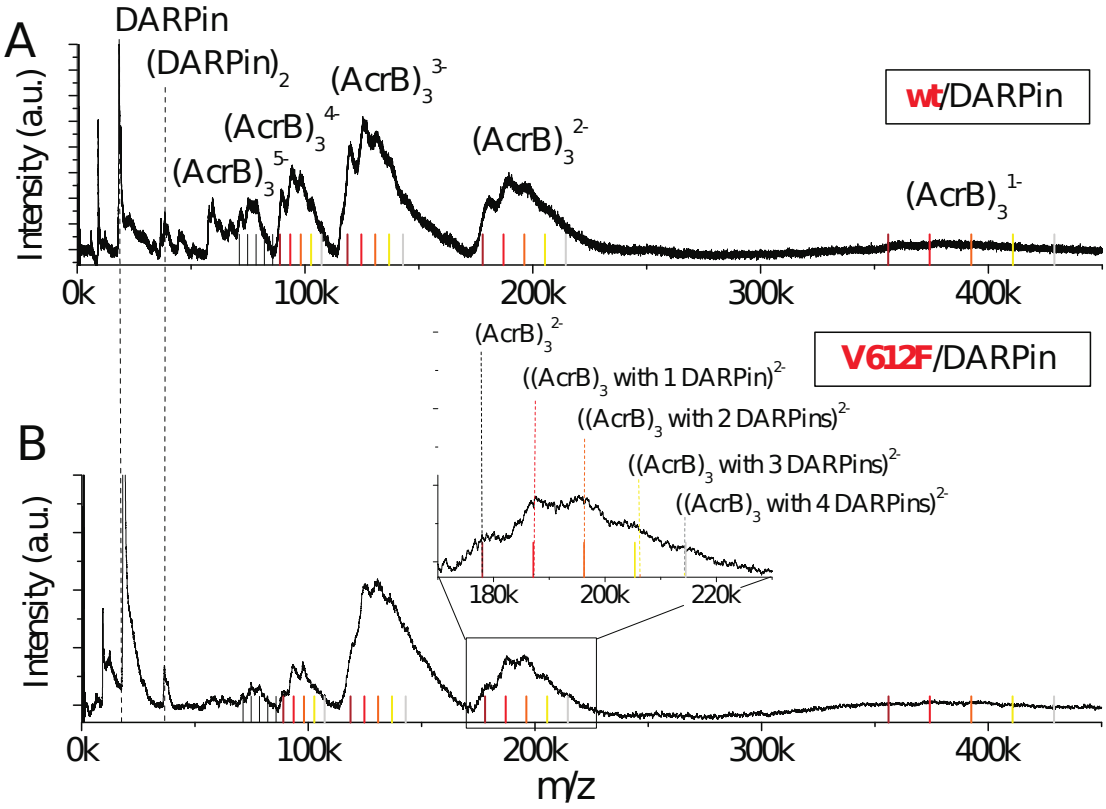

Figure 2.4: Anion LILBID spectra of AcrB wt (A) and AcrB_V612F variant (B) at ultrasoft laser intensity. The bars represent charge distribution of the AcrB trimer with no (brown), 1 (red), 2 (orange), 3 (yellow) or 4 (grey) DARPins bound. In panel B, the inset displays a magnification of the boxed area.

dissolved AcrB/DARPin crystals (space group $P2_12_12_1$) for measurement with LILBID-MS (Fig. 2.5), the only stoichiometry which could be detected was the one observed in the crystal structure i. e. two DARPins bound per AcrB wt trimer. Under ultrasoft laser intensities, the LILBID MS spectrum of the AcrB masses shifted to higher molecular weight species of 460 kDa, representing the AcrB/DARPin complex of 380 kDa (2 DARPins per AcrB trimer) and a detergent micelle of almost 80 kDa, comparable to the difference in molecular weight found in the soluble AcrB preparation (Fig. 2.1).

DARPins stoichiometry from capillary electrophoresis

Complex formation between AcrB wt and AcrB_V612F with DARPin molecules was analyzed via co-elution using size-exclusion chromatography and further investigation on

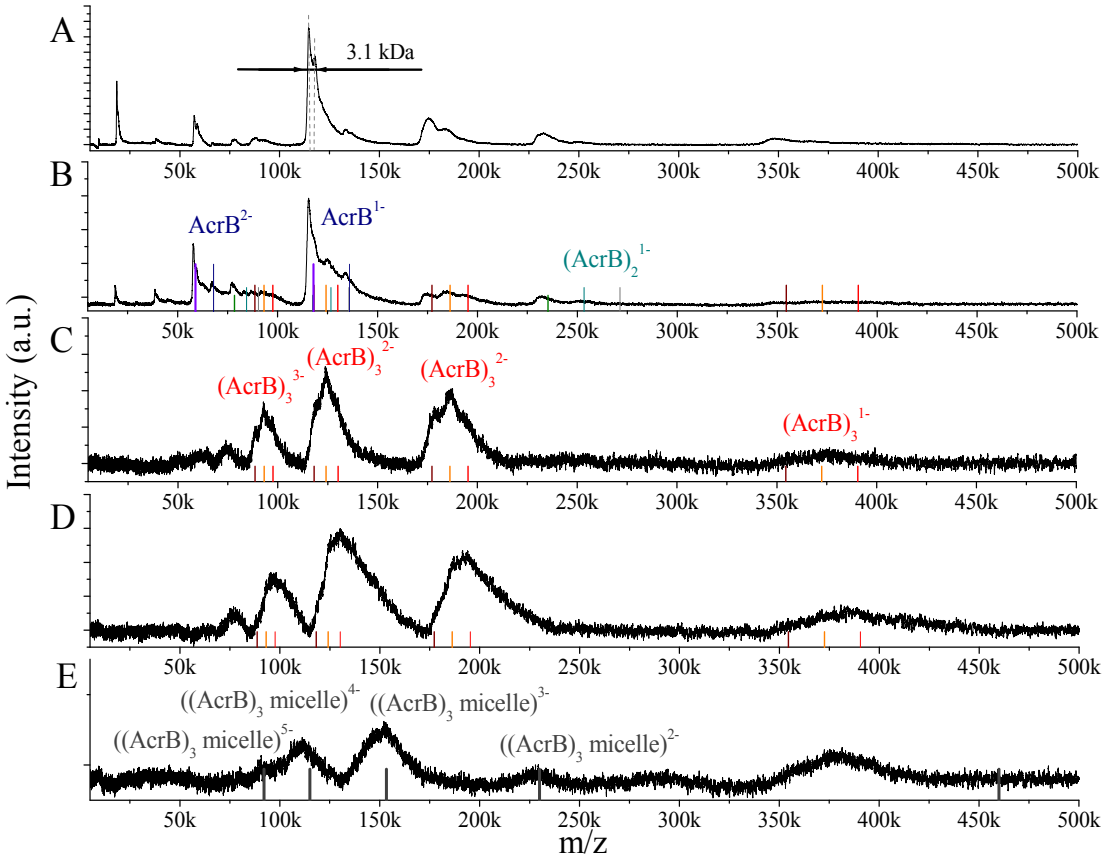

Figure 2.5: Anion LILBID spectra of AcrB/DARPin complex from dissolved orthorhombic crystals. The laser intensity decreases from the spectrum A (harsh) to the spectrum E (ultra-soft). The bars colored in the blue range (spectrum B) represent charge distributions of the AcrB monomer with none or one DARPin bound, the bars in the green range (spectrum B) represent charge distribution of AcrB dimers with none, one or two DARPins bound and the red-colored bars (spectra B-D) represent charge distributions of the AcrB trimers with none, one, or two DARPins bound. The grey bars in spectrum E represent a charge distribution of the trimer with detergent (micelle), the peak maxima correspond to a mass of 460 kDa.

AcrB/DARPin stoichiometry of the peak fractions via an Agilent Lab-on-a-Chip capillary electrophoresis system 2100 Bioanalyzer. Electropherograms of AcrB/DARPin complexes were used for the determination of the concentrations of AcrB and DARPins by integration of the elution peak areas. Combined data from independent experiments (n=5 and n=6 for AcrB wt and AcrB_V612F, respectively) clearly show a significant stoichiometric difference in DARPin binding between the AcrB wt and the AcrB_V612F variant, indicating binding of 2 DARPins to the AcrB wt trimer and binding of 3 DARPins in the case of AcrB_V612F (Fig. 2.6). Whereas this data is in

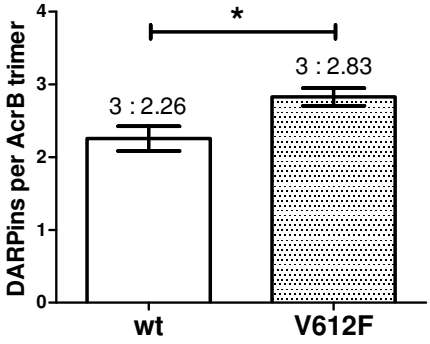

Figure 2.6: The molar ratio of DARPins per AcrB trimer (ordinate) is plotted for wildtype AcrB and AcrB_V612F (indicated on the abscissa). The mean ratios are 2.26 (white bar) and 2.83 (dotted bar) DARPins per AcrB wt and AcrB_V612F variant, respectively. Errors (indicated on top of the bars) are calculated as standard error of the mean (SEM). Unpaired t-test resulted in a P value of 0.022, thus imply a significant difference of relative amount of DARPins bound to AcrB wt and AcrB_V612F.

accordance to the observations in the crystalline assembly of the AcrB wt/DARPins and AcrB_V612F/DARPin complexes, it deviates from the LILBID measurements where higher stoichiometries of AcrB/DARPin formations were observed. However, the samples subjected to capillary electrophoresis where used directly after elution from the gel filtration column, compared to the samples used for LILBID MS which were subjected to buffer exchange and a concentration step, possibly favoring DARPin-DARPin interaction.

Analytical UC of AcrB_V612F/DARPin complex

Solubilized AcrB_V612F (trimer fraction after SEC) and AcrB_V612F/DARPin (after SEC) complexes were subjected to analytical ultracentrifugation and sedimentation velocity analysis. A distinct sedimentation velocity behavior between AcrB_V612F with and without DARPins could be observed (Fig. 2.7). The calculated difference in molecular weight of AcrB_V612F (373 kDa) and AcrB_V612F/DARPin complex (427 kDa) could be attributed to the mass of three DARPin molecules (theoretical molecular weight: 18.3 kDa). The difference in molecular weight between AcrB wt without (374 kDa) and DARPins bound complex (408 kDa) was explained by the binding of two DARPin molecules per AcrB wt trimer [75].

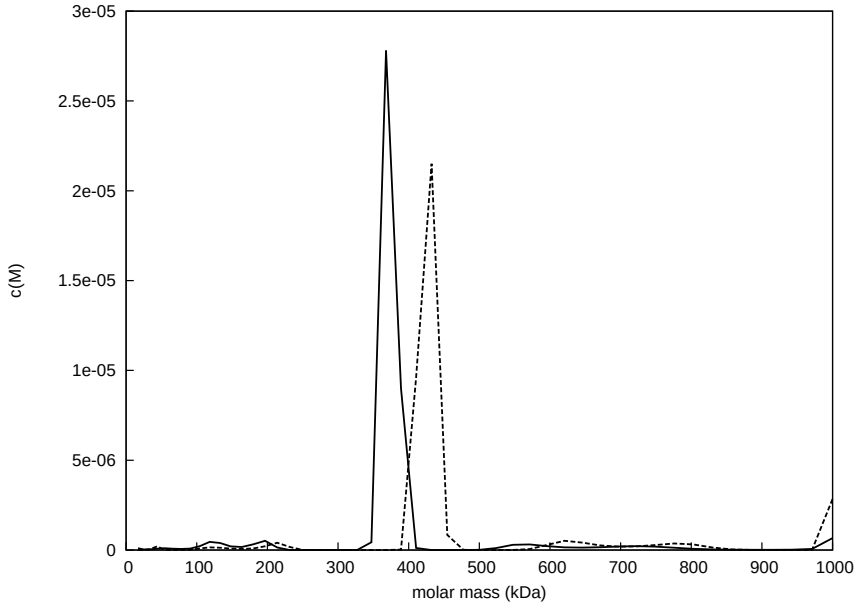

Figure 2.7: Sedimentation velocity experiments with AcrB_V612F with and without bound DARPins after SEC. The calculated mass difference between AcrB_V612F trimers with (dotted line, 426.6 ± 1.9 kDa) and without DARPins (solid line, 373.1 ± 1.7 kDa) corresponds to the mass of three DARPin molecules.

Small molecule ligand and phospholipid analysis

The consistent observation of a double peak in all of the LILBID MS spectra taken in the harsh mode (Fig. 2.3A and 2.5A) representing masses 115.6 kDa and 118.7 kDa was interpreted as a result of a stripping off (a) small molecule(s) with a (total) mass of

3.1 kDa from the AcrB monomer. This additional mass was also observed in the spectra of dissolved AcrB crystals, but has not been observed in the electron density derived from any of the wildtype or variant AcrB crystal. However, AcrB wt, AcrB_V612F and their DARPin complexes crystallize in the presence of DDM (M_W 511 Da). In the AcrB wt/DARPin co-crystal structure, 10 molecules of dodecyl-β-D-maltoside and 1 molecule of dodecyl-α-D-maltoside bound to the trimer are reported [75]. The spectral shift is observed on the AcrB monomers, suggesting that binding of the molecule(s) representing this 3.1 kDa mass is much stronger than the already strong binding of the individual monomers constituting the AcrB trimer. Although a sum of 6 molecules of DDM per monomer would account for the observed mass, the observed "all or nothing" shift of 3.1 kDa mass on the monomer peaks would represent similar affinities for all six DDM molecules to AcrB, which appears unlikely. Moreover, the binding of molecule(s) representing this spectral shift are clearly distinct from the initial stripping of the detergent micelle, which occurs at very low laser intensities and before the release of AcrB monomers from the trimeric assembly. The unsatisfactory explanation concerning the identity of the 3.1 kDa spectral shift triggered the analysis of the presence of phospholipids in our AcrB samples. During the purification process, AcrB is gradually removed from the bacterial membrane and its hydrophobic domains are integrated into detergent/lipid micelles. Phospholipids originating from bacterial membranes have often been reported to be co-purified with integral membrane proteins [129, 130].

We initiated thin-layer chromatography (TLC) analysis with purified samples of AcrB wt and AcrB_V612F to qualitatively identify lipids which might have been co-purified. A number of phospholipid standards, phospholipid mixtures, DDM solution and sample buffer were run in parallel to the protein samples. The chromatography plates then were stained by iodine (Fig. 2.8) and molybdatophosphoric acid solution (not shown). The chromatography pattern of the two protein samples (AcrB wt and AcrB_V612F) were basically identical (Fig. 2.8, lanes 8 and 9). Two distinct spots are visible that may represent phospholipids. The signal with the lower retention factor corresponds with the migration pattern of DDM or cardiolipin, the latter being an *E. coli* lipid component. The high retention factor signal observed in the lanes containing protein samples (Fig. 2.8, lanes 8 and 9) may represent phosphatidylethanolamine (PE),

commensurate to the samples in lane 1 (polar lipid extract of *E. coli*) and lane 4 (dioleoyl-phosphatidylethanolamine, DOPE). Considering the mass of each of the potential ligands which could give rise to the signal, several combinations of each of the detected molecules could explain the spectral shift of 3.1 kDa e. g. 6 molecules of DDM (M_W 511 Da), or a combination of cardiolipin (1435.9 Da), PE (743.5 Da) and DDM. The exact combination and ligand identities remain, however, elusive.

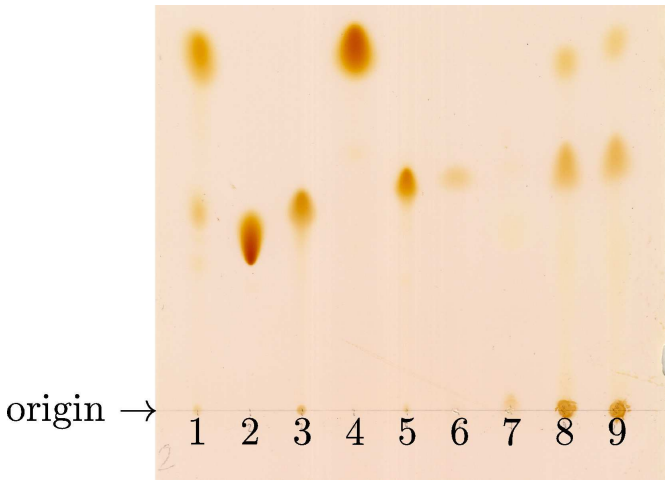

Figure 2.8: Identification of phospholipids by thin-layer chromatography (TLC) in purified AcrB samples. *E. coli* polar lipids (lane 1), DOPC (lane 2), DOPA (lane 3), DOPE (lane 4), cardiolipin (lane 5), 1 % DDM (lane 6), sample buffer (lane 7), AcrB wt (lane 8) and AcrB_V612F (lane9). Samples were dissolved in buffers as described in the materials and methods section. TLC was performed using the eluent system $CHCl_3$/MeOH/H_2O (65:25:4, v/v). The TLC plates were stained with iodine to visualize the lipid and detergent components.

2.5 Conclusions

We analyzed three different AcrB variants in detergent-solubilized and crystalline state, with and without bound DARPin molecules. The AcrB/DARPin complex stoichiometry differs depending on the AcrB variant used, consistent with preliminary crystallographic data on AcrB variant/DARPin co-crystals. Moreover, AcrB trimerization is due to strong binding of the monomers, most likely via the periplasmic loop (amino acids 218–239) protruding from one AcrB monomer into the neighboring monomer. DARPin binding appears to be even stronger than the interaction between the AcrB monomers, since interaction of DARPins is observed to trimeric, dimeric and monomeric AcrB. We also observed the consistent release of a 3.1 kDa mass after high intensity laser exposure,

which might represent very strong binding of detergent and/or lipids.

3 Manuscript: Crystal Structures of AcrB Crosslink Variants

This chapter contains a manuscript describing the experiments, results and interpretation of the crystallization data from five different crosslink variants of AcrB.

My contribution to this work was the overexpression, purification, crystallization and collection of crystallographic data of the AcrB variants.

The processing and refinement of the data was performed by me with substantial support by Prof. Dr. Klaas Martinus Pos.

Dr. Markus Seeger did the MALDI-TOF analysis, the MIC and the NPN efflux experiment.

Crystal Structures of AcrB Crosslink Variants

Lorenz Brandstätter, Markus Seeger, François Verrey, Kay Diederichs and Klaas M. Pos

3.1 Abstract

The AcrA/AcrB/TolC multidrug efflux protein complex is the main determinant for multidrug resistance in *Escherichia coli*. Within this complex, the inner membrane component AcrB acts as a proton/substrate antiporter, responsible for substrate specificity and energy transduction. In the periplasm, the membrane fusion protein AcrA promotes the coupling of AcrB to the outer membrane channel/tunnel TolC. Substrates are exported from the periplasm directly to the outside of the cell. The AcrA/AcrB/-TolC complex was shown to confer resistance to a great number of structurally different toxic compounds. Whereas first crystal structures indicated a symmetric state of the homotrimeric pump component AcrB, latest structures represent asymmetric trimers where the monomers adopt three different conformations. A conformational cycling of the monomers was proposed as the transport mechanism of AcrB. Recent crosslink experiments were compliant with the presence of all three conformations *in vivo*. Pairs of cysteines were introduced into a cysteine-free AcrB background to crosslink and arrest periplasmic subdomains in particular conformations. It was shown, that crosslinks can arrest one or more monomers within the AcrB trimer to inhibit transport activity. In this study, we present crystallization trials and crystal structures of a set of crosslink variants of AcrB. One particular cross-linking variant revealed a novel intermediate conformation.

3.2 Introduction

Multiple drug resistance (MDR) in human pathogenic bacteria is nowadays an emerging and serious thread inside the hospital setting. The cause for MDR phenotypes is often correlated with the overproduction of drug efflux systems. These efflux pumps

represent a potent measure of generating antibiotic resistance by virtue of removing cytotoxic compounds from the cell. In the opportunistic Gram-negative human pathogens *Escherichia coli* and *Pseudomonas aeruginosa*, the tripartite efflux systems AcrA/AcrB/TolC and MexA/MexB/OprM, respectively, have been shown to be responsible for a majority of multiple drug resistance phenotypes [131].

AcrB is a homotrimeric protein that resides in the inner membrane of the Gram-negative *E. coli* and belongs to the Resistance Nodulation and (cell) Division (RND) transporter superfamily. It forms an assembly with the membrane fusion protein AcrA and the outer membrane factor TolC. The homotrimeric tunnel/channel TolC is inserted in the outer membrane protruding into the periplasm, docking onto the docking domain of AcrB. AcrA binds laterally to the AcrB/TolC docking site, putatively acting as an adaptor stabilizing the tripartite assembly. The AcrA/AcrB/TolC complex spans the periplasm and facilitates efflux of noxious substances from the inner membrane or the periplasm directly over the outer membrane to the outside of the cell. Within this complex, AcrB is the substrate specificity determinant and energy conversion module. Substrates of the AcrA/AcrB/TolC complex are structurally very diverse [82] and includes various classes of antibiotics, dyes, detergents and bile salts.

Initial crystal structures of AcrB envisage a trimer, in which every monomer adopts the same conformation [70–72, 125]. More recently obtained crystal structures, however, showed an asymmetric AcrB trimer [73–75]. In these structures, every monomer within the trimer adopts a different conformation. Due to the apparent analogy to the F_1F_O-ATP synthase, the three conformations found in AcrB were designated loose (L), tight (T) and open (O). The model for AcrB anticipates a conformational cycling of the monomers, in a way that they sequentially adopt the conformations L, T, O (and L again to enter a new cycle). Structural rearrangements in the subdomains of the periplasmic domain of AcrB during conformational cycling establish the basis for a transport process that resembles the function of a peristaltic pump. In the L monomer, a tunnel leading from the surface of AcrB (15 Å above the inner membrane) into the periplasmic domain emerges. This tunnel is prolonged in the T conformation and opens up to a hydrophobic pocket in the center of the periplasmic domain, the putative substrate binding pocket. Furthermore, a second tunnel emerges, connecting the AcrB surface within the inner

membrane to the hydrophobic pocket. These tunnels are hypothetical access routes for AcrB's substrates to the binding site. In the O conformation, the lateral tunnels disappear, the hydrophobic pocket collapses and a new passage from the center of the periplasmic domain leading to the TolC docking domain arises. This tunnel provides the substrates access to TolC, from where these are expelled to the outside of the cell.

In a following study, we found support for the occurrence of the three conformations *in vivo*, by applying cysteine crosslinking [77]. Cysteine pairs were introduced to surfaces of moving subdomains of a fully functional cysteine free variant of AcrB (AcrB_cl = AcrB_C493A_C887A) by site-directed mutagenesis. The locations were strategically selected with regard to the movements of these subdomains in the course of the proposed conformational cycling. Some of the cysteine variants spontaneously formed crosslinks in the oxidative environment of the periplasm when the thiol groups came within a critical range of about 6.4 Å. The rate of crosslinking was quantitatively determined by mass spectrometry and for any of the three conformations at least one AcrB crosslink variant was shown to establish a disulfide bridge, resulting in the arrest of the drug efflux cycling as indicated by minimal inhibitory concentration assays and *N*-phenylnaphthylamine (NPN) efflux. In a functional control, pairs of cysteines were introduced at the interface of the intermonomeric loop (Loop) and the TolC docking subdomain DC. This region appeared invarious between the three conformational states within the asymmetric AcrB structure. In all three conformations, the introduced cysteines are within the critical range for disulfide bridge formation. The extent of cross-linking was determined to be 80 % by MALDI-TOF analysis, but did, however, not significantly undermine AcrB activity using minimal inhibitory concentration (MIC) and *in vivo* NPN efflux experiments.

In this study, we present crystal structures of previously selected crosslink variants [77] as well as new crosslink variants. The established disulfide bridges are visualized in the crystal structures and give insight into the proposed functional rotation by acquisition of new conformational states.

3.3 Results

Here we present the results of crystallization of five different crosslink variants of AcrB. Throughout this work, the AcrB variants were co-crystallized with DARPin molecules as described [75] unless indicated otherwise. One of the variants (AcrB_cl_Q229C_E585C, loop-PC1 subdomain, Table 3.1) resulted in non-diffracting microcrystals, whereas diffraction data could be obtained for the other variants: three high resolution datasets (up to 2.3 Å) and one dataset to a resolution of 7.0 Å were obtained (Table 3.1). To compare the structural deviation of these cross-linked variants with the asymmetric wildtype AcrB structure, superimposition of the trimers was carried out (Table 3.2).

Table 3.1: Overview of the AcrB variants (derivatives of cysteine less AcrB_cl) used in this study. Listed are the crystallized crosslink variants, their crosslink rates, space group and resolution of measured protein crystals.

	Q229C_ E585C	**S562C_ T837C**	**S132C_ A294C**	**S233C_ Q726C**	**V225C_ A777C**
subdomains	Loop-PC1	PC2-TM7	PN1-PN2	Loop-DC	Loop-DC
crosslink rate (%)	40.0[a]	15.4[b]	41.6[b]	17.0[b]	80.2[b]
space group	n.d.[c]	$P2_12_12_1$	$P2_12_12_1$	$P2_12_12_1$	I23
resolution (Å)	n.d.[c]	2.5	2.5	2.3	7.0
figure	3.1	3.3, 3.2	3.4	3.5	-

[a]: this work; [b]: from Seeger *et al.* [77]; [c]: crystals did not diffract.

AcrB_cl_Q229C_E585C, crosslink between Loop and PC1 subdomain

Based on the high resolution crystal structure of asymmetric AcrB, the distances of cysteine substitutions at position Q229 and E585 were considered too distant to allow disulfide bridge formation in any of the three conformations L, T or O (Figure 3.1, left). Surprisingly, quantification of crosslink formation by matrix assisted laser desorption ionization-time of flight (MALDI-TOF) revealed a crosslink rate of about 40 %. In minimal inhibitory concentration (MIC) experiments with five different AcrB substrates, the substitution with one cysteine (E585C in this study, Q229C in

Table 3.2: Superimposition of the 3D high resolution AcrB variant structures from this study (2–4) with wildtype AcrB (1, pdb ID: 2GIF). RMSD (Root Mean Square Deviation) values of Cα alignment are given in Å. Superimposition was done with structures devoid of ligands (DARPins, substrates, waters). Superimposition was performed with the program "superpose" from the CCP4 program suite [132].

structure		1	2	3	4
AcrB wt (pdb ID: 2GIF)	**1**	-	1.165	0.928	0.812
PC2-TM7 (S562C_T837C)	**2**	1.165	-	1.159	1.026
PN1-PN2 (S132C_A294C)	**3**	0.928	1.159	-	0.483
Loop-DC (S233C_Q726C	**4**	0.812	1.026	0.483	-

[77]) showed moderate inhibiting effects, whereas the introduction of both of the cysteines (Q229C_E585C) significantly impairs AcrB's drug transport abilities (Table 3.3). Affinity purified Q229C_E585C AcrB displayed a heterogeneous size-exclusion chromatography profile indicating high susceptibility towards aggregation with and without supplemented DARPins. Fractions corresponding to non aggregated AcrB trimers were collected and used for protein crystallization. Crystallization screens with and without DARPin binders [75] and in the presence of substrates (minocycline and erythromycin) resulted in a set of crystals with a cubic habitus under various conditions. Crystals grew within a two-week period and did not exceed side lengths of 100 µm (Figure 3.1, right). In X-ray diffraction experiments with more than 20 of these crystals, no diffraction could be observed thus far. Initial experiments of several crystal seeding experiments did not improve size and quality of the crystals.

AcrB_cl_S562C_T837C, crosslink between PC2 subdomain and TM7

The S562C_T837C variant was designed to form a crosslink between the PC2 subdomain and TM7 in the O monomer. Only in the O conformation, TM7 approaches the PN2 subdomain at a distance below the threshold for disulfide bridge formation [77]. Protein crystals could be obtained from the AcrB_cl_S562C_T837C variant with DARPins and diffraction experiments resulted in a high resolution dataset of 2.5 Å. Phases were solved by molecular replacement using a high resolution structure of the

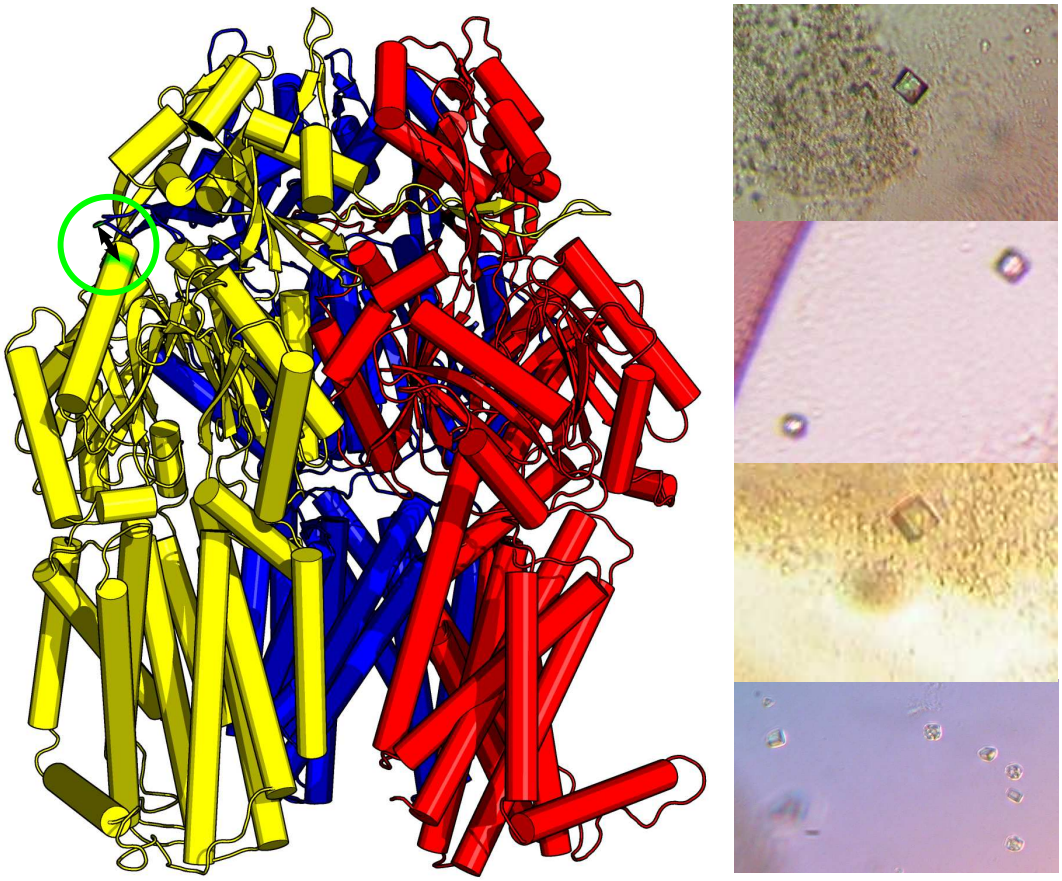

Figure 3.1: Left: Localization of the engineered disulfide bridge in the variant AcrB_cl_Q229C_E585C (arrow) based on the high resolution model of the AcrB wt (pdb ID: 2GIF). The cysteine residues are located on the intermonomeric loop and the PC1 subdomain (green circle: Loop of the L monomer (blue) and PC1 domain of the T monomer (yellow)). Right: Non-diffracting micro-crystals (20–100 µm diameter) of AcrB_cl_Q229C_E585C displaying a cubic habitus could be grown under different conditions (Table 3.4). Images of crystals are displayed at different magnifications.

Table 3.3: Minimal inhibitory concentration (MIC) experiments with five AcrB substrates using *E. coli* BW25113Δ*acrB* harboring the empty vector (pET24a) or synthesizing the cysteine-less AcrB variant AcrB_cl, the single cysteine variants AcrB_cl_E585C and AcrB_cl_Q229C, the crosslink variant AcrB_cl_Q229C_E585C or the negative control AcrB_D407N_D408N.

	MIC ($\mu g \cdot ml^{-1}$)				
constructs	**TPP^+**	**R6G**	**Berberine**	**Erythromycin**	**Oxacillin**
pET24a	**12.5**	**4**	**64**	**< 2**	**4**
acrB_cl	800	128	1024	64	128
D407N_D408N	n.d.	**8**[a]	**64**	**< 2**	**< 4**
Q229C[b]	400	128	1024	64	128
E585C	400	128	1024	64	128
Q229C_E585C	**200**	**16**	512	**16**	**16**

abbreviations: MIC, minimal inhibitory concentration; pET24, empty vector; acrB_cl, cysteine less acrB; D407N_D408N, non-functional acrB; E585C, acrb_E585C; Q229C_E585C, acrb_Q229C_E585C; TPP^+, tetraphenylphosphonium; R6G, rhodamine 6G; n.d. not determined [a]: Thomas Eicher, Thesis; [b]: Seeger *et al.* [77]

wildtype AcrB (Eicher, PhD thesis). In the acquired structural model of this crosslink variant, two of the monomers closely resemble the monomers in T and O conformation in the asymmetric wildtype AcrB [74]. In the O conformation, electron densities provide indication for partial crosslinking, revealing densities for crosslinked as well as reduced cysteines (Figure 3.2). The two reduced cysteines (blue) are represented as sticks and their 2Fo-Fc electron density is drawn at 1σ as a blue mesh. Clearly, electron density supported the existence of non-linked cysteines pointing with suboptimal geometries for cysteine-disulfide bridge formation. Additionally, difference (Fo-Fc) electron densities (green mesh) at 3σ indicate the presence of covalently linked cysteine residues (green sticks) in an alternative conformation. The global conformation of the O monomer appears not to be affected by the absence or presence of the disulfide crosslink.

The third monomer within the AcrB_S562C_T837C has a similar conformation as observed in the L monomer of the AcrB wildtype structure. However, electron density is clearly supportive of crosslinking within this monomer and apparently influences the

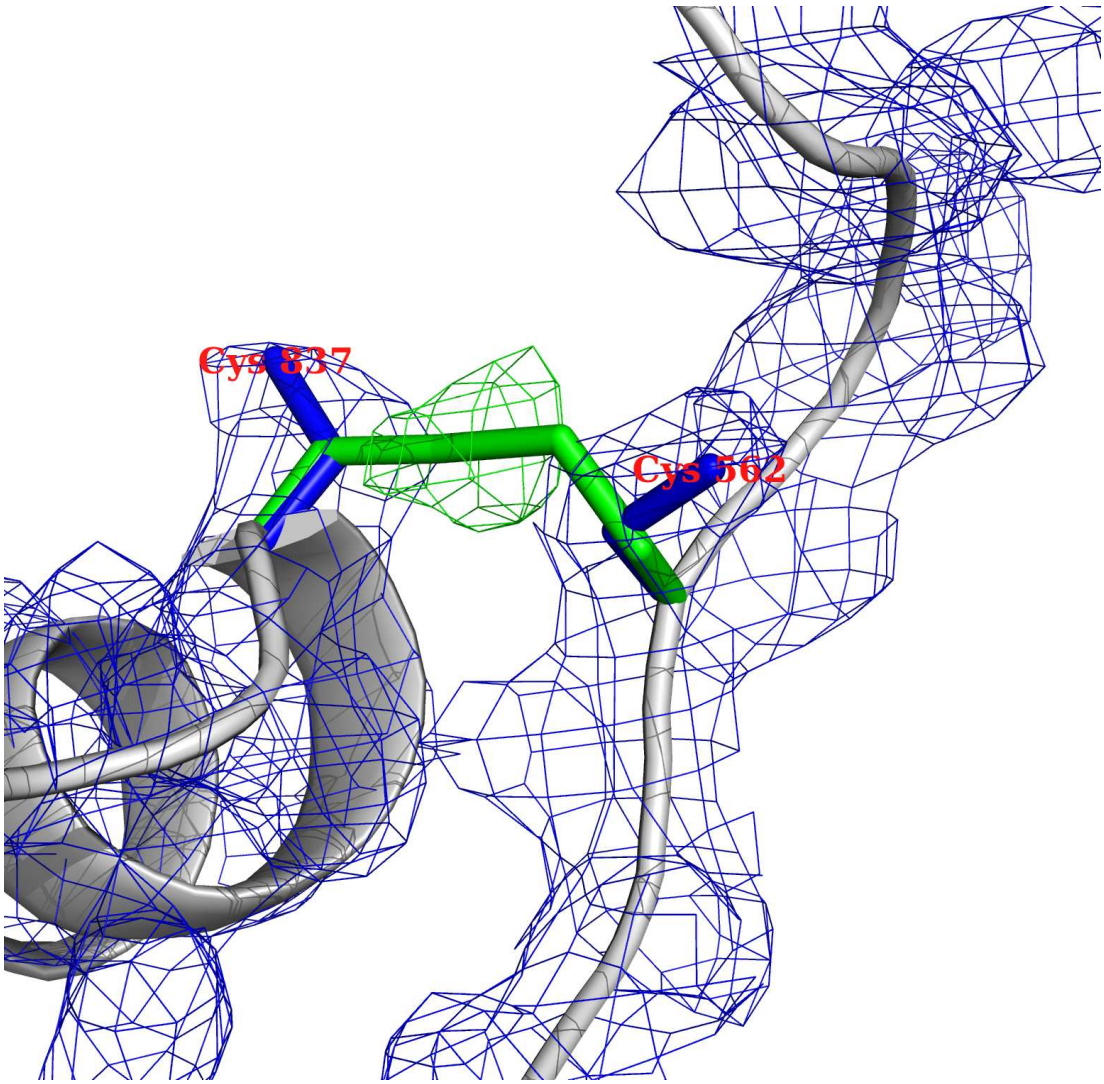

Figure 3.2: Close-up view of the PC2-TM7 interface of the O monomer of the AcrB crosslink variant S562C-T837C. The introduced cysteines residues are shown in stick representation. The corresponding electron density (2Fo-Fc) at 2.5Å resolution is pictured as blue mesh (at 1σ). Difference electron densities (Fo-Fc) (at 3σ) in green are indicative of an alternative conformation and partial crosslink of the cysteines in the O monomer.

conformational state of PC2 subdomain within the porter domain. (Figure 3.3).

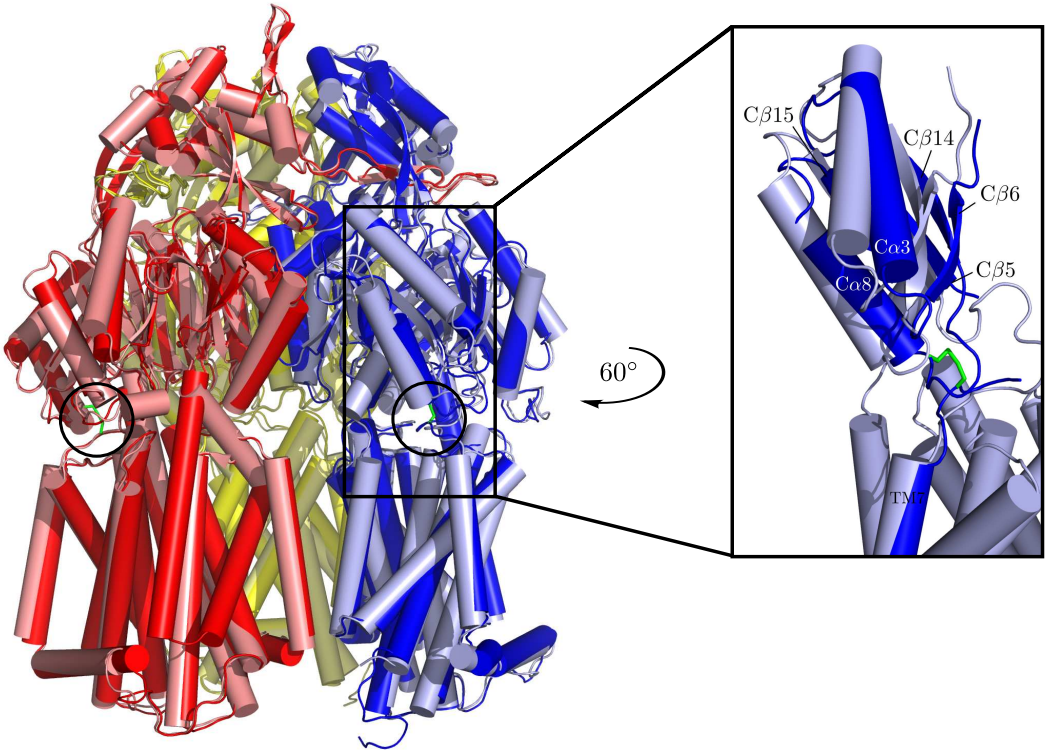

Figure 3.3: Superimposition of AcrB_cl_S562C_T837C (cartoon representation; L, blue; T, yellow; O, red) on the asymmetric wildtype AcrB (pdb ID: 2GIF; light colors). Disulfide bridges (stick representation in green, encircled) can be observed in the L (blue) and O (red) monomers: the L and the O conformer. Co-crystallized DARPin molecules are omitted for clarity. Inset: Superimposition of the L monomer of the wildtype AcrB (pdb ID: 2GIF; light blue) and crosslink variant S562C_T837C (blue) in the PC2 subdomain and TM7 region. Disulfide bridges of the variant are shown in green (stick representation). The crosslink clearly affects the conformation of the PC2 subdomain in the L monomer of the crosslink variant and reveals substantial deviation compared to the wildtype L monomer conformation. Other porter subdomains are omitted for clarity.

AcrB_cl_S132C_A294C, crosslink between PN1 and PN2 subdomains

The AcrB_cl_S132C_A294C was shown to form a disulfide bridge between the PN1 and the PN2 subdomain in the L monomer (at a quantity of about 41 % crosslinking) [77]. This variant was co-crystallized with DARPin binders and a dataset to a resolution of 2.5 Å has been obtained. The space group was determined $P2_12_12_1$ and cell parameters were found 148.27 Å, 162.98 Å and 248.05 Å for a, b and c. The phase problem was solved by molecular replacement with a high resolution model of the wild-

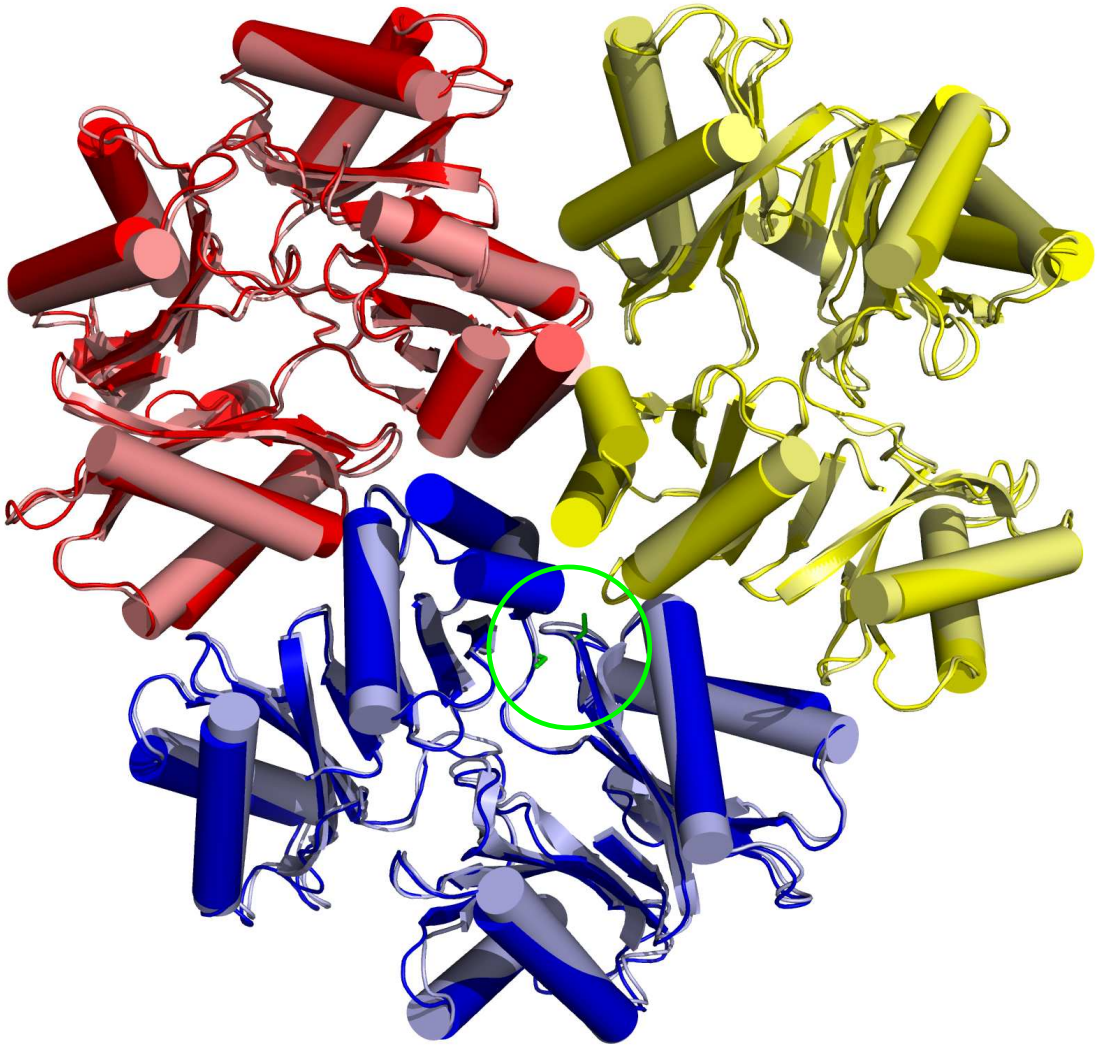

Figure 3.4: Superimposition of the porter domains of AcrB_cl_S132C_A294C (blue: L, yellow: T, red: O monomer) and the asymmetric structure of wildtype AcrB (pdb ID: 2GIF; light colors). A disulfide bridge could not be observed in the structure. In the L monomer, where crosslinking of the cysteines (green, stick representation) was anticipated, the distance between the Sγ atoms of C132 and C294 was 7.64 Å, which is suboptimal to support disulfide bridge formation.

type AcrB (Eicher, PhD thesis). Electron densities derived from the structure factors of the S132_A294C variant were not indicative of disulfide bridges. In the L monomer, the distance between the sulfhydryl groups of the cysteine residues (Sγ) was 7.64 Å, a distance too long for crosslinks to be established and deviating from the original estimations by *in silico* mutagenesis (Figure 3.4). However, a crosslinking percentage of 41 % was observed by Seeger *et al.* [77] in membrane localized AcrB_cl_S132C_A294C by MALDI-TOF analysis. It appeares, therefore, that the population of cross-linked variants might not have been incorporated into crystals.

The structure of AcrB_cl_S132C_A294C (PN1-PN2 cross-link variant) was superimposed onto the asymmetric structure of the wildtype AcrB (pdb ID: 2GIF) considering the backbone atoms of both structures. The RMSD of the superimposition was found 0.928 Å (Cα atoms). Hence, only minor deviations between the structure of AcrB_cl_S132C_A294C and the wildtype are apparent.

AcrB_cl_S233C_Q726C, a crosslink variant with disulfide bridge between Loop and DC subdomain

AcrB_cl_S233C_Q726C (Loop-DC cross-link variant, Figure 3.5) was constructed with the expectation to form crosslinks in all three monomers. The distances between the sulfhydryl groups in the introduced cysteine residues varied from 5.2 to 6.3 Å, as referred from the high resolution data of wildtype AcrB [77]. The amount of cross-link was determined to be 17 % [77]. In the *N*-phenylnaphthylamine (NPN) efflux assay (Figure 3.5, inset), this variant showed a slightly affected transport activity compared to AcrB_cl (as a positive control). Addition of DTT, resulting in the reduction of the disulfide bridges, had almost no effect on the NPN efflux. MIC determination by Seeger *et al.* [77] demonstrated that the drug transport activity of this variant corresponds to that of the control (AcrB_cl). AcrB_cl_S233C_Q726C was co-crystallized with DARPins and the AcrB substrate minocycline. From a high resolution dataset at 2.3 Å, a structure was determined via molecular replacement using wildtype AcrB (Eicher, PhD thesis) as template. In the difference electron densities (Fo-Fc), at any sigma level, there was no indication of crosslinks in any of the monomers. The distances of the Sγ in the variant were 4.8, 4.8 and 5.3 Å, thus favourable for disulfide bridge formation.

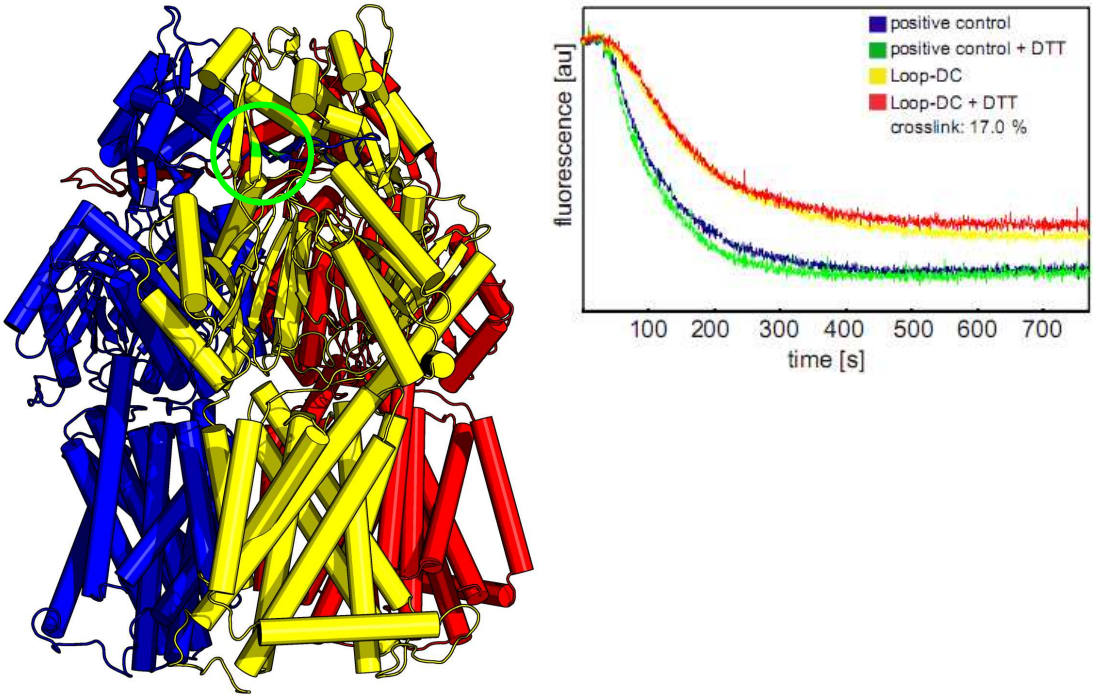

Figure 3.5: Left: Localization of the engineered disulfide bridge in the variant AcrB_cl_S233C_Q726C based on the high resolution structure of the AcrB wt (pdb ID: 2GIF). The cysteine residues are on the Loop and the DC subdomain (green circle: Loop of the L monomer (blue) and DC domain of the T monomer (yellow)). Right: *N*-phenylnaphthylamine (NPN) efflux by *E. coli* BW25113Δ*acrB* synthesizing AcrB_cl (positive control) or AcrB_cl_S233C_Q726C (Loop-DC). The NPN efflux activity of the Loop-DC subdomain crosslinked variant was only slightly affected and addition of DTT was without effect. MIC determinations confirmed these results [77].

Inspection of the cysteine chains revealed a parallel rather than an approaching orientation. Located on β-sheets, both residues may be affected by geometrical constraints of these secondary structures and therefore show a minimal tendency to crosslink. This finding is consistent with the low crosslinking efficiency as shown by MALDI-TOF MS [77]. Furthermore, there may be preferential crystallization of the crosslink free AcrB/-DARPin protein pool within the sample. Superimposition of the S233C_Q726C variant structure to the wildtype (pdb ID: 2GIF) showed no significant deviation (RMSD = 0.812 Å, Table 3.2).

AcrB_cl_V225C_A777C, crosslink between Loop and DC subdomain

In AcrB_cl_V225C_A777C, disulfide bridges were expected to form between the Loop and the DC domain. The relative geometry of the cysteine side chains allows crosslinking in all three conformations. In MALDI-TOF experiments crosslink rate was determined more than 80 % and it has been shown in MIC as well as in NPN efflux experiments, that this variant is fully functional [77]. This variant was successfully crystallized as AcrB/DARPin complex and formed cubic crystals. A dataset to a resolution of 7.0 Å could be recorded and revealed the I23 (cubic) space group. Unit cell contains one AcrB monomer with a bound DARPin molecule and coordinates could be determined to be a=b=c=233.75 Å (Table 3.5). Phases were solved by molecular replacement using a high resolution structure of a binding pocket variant of AcrB that as well could be crystallized in the I23 space group (Eicher, PhD thesis). Interestingly, this space group could only be observed in two individual AcrB binding pocket variants so far (Eicher *et al.* , unpublished, Cha *et al.* , unpublished; see Chapter 5).

3.4 Discussion

During the process of purification of the various crosslink variants, a particular tendency to form protein aggregations could be observed in the size-exclusion chromatography profiles of the AcrB variants containing inter- and intramolecular disulfide bridges (not shown). On the one hand, crosslink variants may be considered to be prone to aggregate due to intermolecular disulfide bridge formation, on the other hand introduction

of crosslinking cysteines may induce alternative conformations that adversely affect solubility and lead to aggregation of the protein variants.

The AcrB_cl_Q229C_E585C variant (Loop-PC1 subdomain cross-link) (Figure 3.1) was found to show unexpected high crosslinking rate in quantitative MALDI-TOF analysis (40 %, Table 3.1) despite of suboptimal side chain orientations and distance of the two cysteines judging from the *in silico* mutagenesis on basis of the high resolution structure of the wildtype AcrB. Therefore, crystallization and high resolution structure determination of this variant was pursued to understand the structural cause for this unexpected crosslinking rate. However, efforts to produce well-diffracting crystals did not succeed so far. Loss of purified protein by precipitation and aggregation during purification and preparation of crystallization indicate heterogeneity of this variant in detergent solubilized form. The lack of a high resolution structure, visualizing the disulfide bridge and the actual structural properties of the AcrB_cl_Q229C_E585C variant, leaves us with speculation about the structural bases of the high crosslink rate. One possibility for this finding is the structure of the (intermonomeric) loop, which may be flexible enough to allow deviances from the structure observed in the high resolution map of the wildtype. This may reduce the distance between the two cysteine residues, and a twist of the loop may also promote a favorable direction of the cysteine side chain. The loop structure may be responsible for the trimerization of AcrB (section 2), but direct involvement in the substrate transport process has not been anticipated thus far. Compared to the wildtype, MIC data of the AcrB_cl_Q229C_E585C indicate restriction in substrate efflux, indicating a minor loss of functionality (Table 3.3). One possibility might be the reduced synthesis of this variants in the *E. coli* cell leading to reduced resistance. Moreover, the crosslink might lead to a restriction of the flexibility in the PC1 subdomain, resulting in the observed phenotype.

The crosslink variant AcrB_cl_V225C_A777C was designed to form disulfide bridges between the Loop structure and the DC domain in all three conformations [77]. The crosslink rate was determined about 80 % by MALDI-TOF MS. This crosslink, apparently did not significantly reduce AcrB activity as shown in MIC and NPN efflux experiments [77]. This variant supported the notion that the Loop-DC subdomain region was devoid of substantial rigid body movement (as opposed to the subdomains of

the porter domain). However, the crystal structure of this Loop-DC crosslink variant revealed some remarkable properties that have not been seen with fully functional AcrB hitherto. Crystals grew in the space group I23, which has not been observed with the wildtype AcrB crystals [73–75]. Interestingly, two binding pocket variants of AcrB that were crystallized in complex with DARPin binders in our group (Eicher *et al.* , unpublished; Cha *et al.* , unpublished) showed very similar structural characteristics. The high resolution structures of these binding pocket variants exhibited an all T state (in which all three monomers within the AcrB trimer adopted the tight conformation). In contrast to the previously described AcrB/DARPin complex [75], this binding pocket variant bound three DARPins per AcrB trimer (see Chapter 2). Preliminary analysis of the low resolution diffraction data and subsequent molecular replacement indicated the presence of one AcrB monomer with one bound DARPin within the asymmetric unit (data not shown). These findings suggest that this variant binds three DARPins per AcrB trimer, just like the binding pocket variant. More detailed structural analysis of this variant is not possible due to the poor resolution, but a putative 1:1 (AcrB:DARPin) stoichiometry might indicate a similar "all-tight" conformation as observed in the binding pocket variants (Chapter 2).

In contrast to the structures of the S562C_T837C (PC2-TM7) variant, disulfide bridges could not be observed in the AcrB_cl_S132C_A294C (Figure 3.4) and AcrB_cl_S233C_Q726C (Figure 3.5) variants. In quantitative MALDI-TOF experiments a crosslinking rate of 41 % was measured for AcrB_cl_S132C_A294C and *in vivo* MIC and NPN efflux experiments clearly showed the impact of the formed crosslink on drug efflux [77]. In the obtained structure of this variant, the distance between the Sγ atoms of the cysteine residues in the L monomer was 7.64 Å, a distance expected to be too large for disulfide formation. Furthermore, the cysteine side chains are oriented away from each other, a condition which would be disadvantageous for disulfide bridge formation. A certain flexibility of the backbone in these regions can be assumed (e. g. during conformational change from one state to the other) to allow the little distortion that may allow the cysteines to reorientate for disulfide formation. A possible explanation for the absence of disulfide bridges in the crystal structure may be that only the non-crosslinked fraction of AcrB formed protein crystals.

AcrB_cl_S233C_Q726C (Loop-DC subdomain cross-link variant) (Figure 3.5) was designed as a functional control. In this variant, crosslinks between the loop and the DC subdomain would form and persist in all three monomers telling from the distances between the cysteine residues. In contrast to the expected high crosslink rate, the actual crosslinking was rather moderate. MALDI-TOF quantification revealed disulfide bridges in 17 % of the monomers [77]. Additionally, this variant had slightly affected NPN efflux activity in vivo, compared to AcrB_cl, the positive control in these experiments. However, the addition of DTT, a reducing agent, had no significant effect on the activity of this variant (Figure 3.5, right). These data may indicate that the somewhat reduced efflux activity of the crosslink variant is not due to the established disulfide bridges, but rather due to the cysteine substitutions. However, the results obtained from MIC experiments with other substrates of AcrB, indicated that this variant exhibits wildtype (i. e. AcrB_cl) activity. In the high resolution data from crystals AcrB_cl_S233C_Q726C, disulfide bridges cannot be seen in any of the monomers. One explanation might be that the lack of visible disulfide bridges is due to the low cross-linking rate. Alternatively, cross-link variants may selectively be excluded from the crystal growth process. The crystal structure obtained from the variant AcrB_cl_S562C_T837C (PC2-TM7 cross-link variant) (Figure 3.3) was the most revealing in this study. The introduced cysteines are located at the surface of the PC2 subdomain and the periplasmic end of the transmembrane helix TM7. In the O conformation, the substituted residues approach each other to 3.3 Å distance [77]. Interestingly, in the crystal structure, electron densities for both reduced cysteines as well as disulfide bridge forming cysteines can be observed (Figure 3.2). In the O conformation, this partial crosslink seems not to have an influence on the global conformation of the monomer. Like the T monomer, the O monomer in this structure is identical to the one in the asymmetric wildtype AcrB structure. In contrast, the monomer that adopts the L conformation, shows considerable structural deviations caused by the crosslink. Alignment of this conformation with the L conformation of the wildtype structure (pdb ID: 2GIF) suggests that it constitutes an intermediate (I) conformation between the O and the L conformation (Figure 3.3). Despite the new conformation, observed in the PC2 subdomain of the L conformer of AcrB_cl_S562C_T837C, DARPin binding was not affected.

The PC2 subdomain is comprised of two α-helices (Cα3 and Cα8) and two pairs of antiparallel β-sheets (Cβ6 and Cβ14, Cβ5 and Cβ15) (Figure 3.3, right). In the context of the conformational changes during the transport cycle, subdomains of AcrB are considered as rigid body entities that undergo spatial rearrangements. The crosslink in the L monomer of AcrB_cl_S562C_T837C seems to arrest the PC2 subdomain before it can adopt the position observed in the L monomer of the wildtype. The change from the O to the L conformation features a tilting of the PN1 and PC2 subdomains towards the PN1-PN2 interface of the O monomer. In the new conformation of the crosslink variant, the PN1 subdomain already adopted the O monomer position, whereas the PC2 subdomain is constrained by the disulfide bridge and got halted during the reorientation. This finding gives rise to new insights into the rearrangement of the PN1 and PC2 porter subdomains during the conformational cycling. It is conceivable, that these two subdomains are largely independent of each other in their conformational rearrangement. Furthermore, it seems reasonable to think of a serially concerted movement. PN1 may initially move to adopt its new location, to make subsequently way for the reorientation of the PC2 subdomain. The tilting of the PN1 subdomain is one of the prominent subdomain features during the conversion from T to O and from O to L. The PN1 subdomain tilting was suggested to be a measure to occlude the exit path of the neighboring T conformer where substrate has bound in the binding pocket [73]. The concomitant movement of the PC2 subdomain, as implied for wildtype AcrB conformational cycling, results in the closure of the lateral cleft and appears to prevent extrusion of the substrate laterally via the tunnel towards the periplasm. In the PC2-TM7 crosslink variant, the latter conformational change is prohibited and might stall the effective efflux of substrates towards TolC. Whether the movement of PN1 and PC2 is sequential i. e. whether the movement of the PN1 precedes that of the PC2 subdomain appears likely, but cannot be postulated with absolute certainty. Moreover, this intermediate conformation still cannot give exclusive information on the direction of cycling, e. g. from L to T to O and back to L.

In summary, the presented data shows substantial new information based on the structures of one AcrB crosslink variant, demonstrating an intermediate conformation of the porter subdomain PC2 possibly representing a cycling intermediate state and another

structure which might represent a fully functional cross-linked AcrB in a symmetric intermediate state.

3.5 Material and Methods

Bacterial strains and plasmids and growth conditions

Cloning procedures were done in the *E. coli* strain DH5α [133] using LB medium [134] supplemented with corresponding selective antibiotics. The pET24 plasmid was used as backbone in cloning, mutagenesis and expression of AcrB. All AcrB variants were expressed in *E. coli* C43 (DE3) [135] using phosphate buffered TB medium. The *E. coli* strain BW25113Δ*acrB* [77] was used for the NPN efflux assay and drug susceptibility tests.

Site-directed mutagenesis

All constructs are based on a cysteine free variant of AcrB (C493A_C887A, AcrB_cl) [77]. Cloning procedures were performed on the pET24_AcrB_cl$_{\mathrm{His}}$ plasmid, a variant of the pET24_AcrB$_{\mathrm{His}}$ [125] carrying the AcrB_cl. The cysteine pairs were consecutively introduced by site-directed mutagenesis using the Quikchange protocol from Stratagene. All constructs were verified by sequencing at Microsynth Laboratory (Balgach, Switzerland).

N-Phenylnaphthylamine (NPN) efflux assay

The NPN efflux experiments were performed as previously described [77]. Cultures of *E. coli* BW25113Δ*acrB* harbouring pET24 carrying the AcrB variants were grown in LB medium supplemented with 50 $\mu g \cdot ml^{-1}$ kanamycin at 37 °C and 280 $rev \cdot min^{-1}$ to an OD_{600} of 0.8–0.9, cells were harvested and resuspended in 4 ml buffer (50 mM KP_i pH 7, 1 mM $MgSO_4$) and de-engergized by addition of 200 μM carbonyl cyanide m-chlorophenylhydrazone (CCCP) for 10 min on ice. Cells were washed three times with 4 ml buffer to remove CCCP. Fluorescence traces were recorded on a Varian Cary Eclipse fluorescence photospectrometer at RT. Excitation and emission wavelengths

were 355 and 420 nm, respectively and sensitivity was set to 700 V. Measurements were conducted in 2 ml buffer, cell densities were adjusted to an OD_{600} of 0.2 and NPN (10 µM) (and DTT (10 mM), where required) were added. After NPN fluorescence was followed to saturation, glucose (0.2 % w/v) was added and traces were recorded.

Drug susceptibility test

Determination of minimal inhibitory concentration (MIC) was carried out as previously described [77]. Basically, *E. coli* BW25113Δ*acrB* harbouring pET24 carrying the AcrB variants were pre-grown to an OD_{600} of 0.6–0.8 in LB medium supplemented with kanamycin (50 $\mu g \cdot ml^{-1}$). These cultures were used to inoculate (1:100) 96-well microtiter plates containing 150 µl LB with kanamycin and the indicated drug. Cells were grown for 22 hours at 37 °C and 160 $rev \cdot min^{-1}$. OD_{600} was measured before and after growth period and the lowest antibiotic concentration where cultures displayed an OD_{600} less than 0.2 was defined as the minimal inhibitory concentration.

Purification and crystallization of AcrB crosslink variants

Overexpression and membrane preparation of AcrB was carried out as previously described [74] with modifications. DARPins (inhibitor 1108_19 [75]) were purified according to [136]. During solubilization and purification n-dodecyl-β-maltoside (DDM, GLYCON Biochemicals GmbH, Luckenwalde, Germany) was exclusively used as detergent. Membranes were solubilized in 20 mM Tris, 150 mM NaCl, 10 mM imidazole, 10 % glycerol and 2 % DDM, pH 7.5. The soluble fraction was applied to a Ni^{2+}-NTA affinity column (Ni-NTA Agarose Quiagen, 2 ml bed volume) pre-equilibrated in buffer1 (20 mM Tris, 150 mM NaCl, 10 mM imidazole, 10 % glycerol, pH 7.5). The column was washed with 45×column volume (CV) buffer1 and subsequently washed with 30xCV buffer2 (20 mM Tris, 150 mM NaCl, 50 mM imidazole, 10 % glycerol, pH 7.5). AcrB was eluted in buffer3 (20 mM Tris, 150 mM NaCl, 200 mM imidazole, 10 % glycerol, pH 7.5). DARPins were added to the purified AcrB in a two-fold molar excess. Concentrated samples were subjected to size-exclusion chromatography (20 mM Tris, 150 mM NaCl, 0.03 % DDM, pH 7.5) using a GE Superdex 200 10/300GL column coupled to a

GE Healthcare ÄKTAprime system (at 0.5 ml·min^{-1} flow rate). Peak fractions corresponding to the AcrB/DARPin complex were collected and concentrated. Concentration steps were performed in centrifugal filter devices with a cutoff size of 100 kDa (Amicon Ultra, Millipore). During concentration, buffer exchange to HEPES buffer (10 mM Na-HEPES, 50 mM NaCl, 0.03 % DDM, pH 7.5) was performed.

Table 3.4: Crystallization conditions and co-crystallized substrates of AcrB crosslink crystals obtained in this study. All crystals grew in co-crystallization setups with specific DARPin binders.

crystal	**cryst. condition**	**substrate**
AcrB_cl_Q229C_E585C	various conditions (100 mM Na-HEPES pH 7.5, 200 mM $CaCl_2$, 36–56 % PEG400)	-
AcrB_cl_S562C_T837C	0.05 M ADA[a] pH 6.4, 0.2 M NH_4SO_4, 9 % PEG4000, 4 % glycerol	-
AcrB_cl_S132C_A294C	0.05 M ADA pH 6.5, 0.2 M NH_4SO_4, 8 % PEG4000	-
AcrB_cl_S233C_Q726C	0.05 M ADA pH 6.5, 0.2 M NH_4SO_4, 7 % PEG4000, 3.4 % glycerol	2 mM minocycline (from 50.61 mM stock in water)
AcrB_cl_V225C_A777C	25 % PEG400, 0.05 M Na-acetate pH 4.5, 15 % glycerol	-

[a]: *N*-(2-Acetamido)iminodiacetic acid

Crystals were grown in hanging drop vapor diffusion setups at 17 °C. Crystallization conditions and substrate supplementation are listed in Table 3.4. Protein sample and crystallization conditions were mixed in equal amounts for the hanging drop. Before freezing in liquid nitrogen, crystals were cryoprotected by stepwise soaking the crystals for 3 minutes with increasing (5 % steps) glycerol concentrations up to 30 %. Cryoprotection was omitted when crystallization solutions were considered to provide suffcient cryoprotection (e. g. $\geq$ 25 % PEG400).

X-ray diffraction dataset analysis and refinement procedure

Dataset were collected at the beamline X06SA of the Swiss Light Source (SLS) at the Paul Scherrer Institut, Villigen, Switzerland at a wavelength of 1 Å. Data reduction was done with the XDS package [137]. The structures were determined by molecular replacement using MOLREP [138]. Refinement was done with PHENIX [139] and REFMAC 5 [140] using rigid body refinement and restrained refinement with TLS restraints. Models were built in COOT [141]. Figures were composed using PyMOL 1.2 (The PyMOL Molecular Graphics System, Schrödinger, LLC.).

Table 3.5: Crystallographic and refinement data of AcrB crosslink variants.

	AcrB_cl_			
	S562C_T837C	**S132C_A294C**	**S233C_Q726C**	**V225C_A777C**
Ligands	DARPin	DARPin	DARPin, minocyclin	DARPin
Data collection				
Space group	$P2_12_12_1$	$P2_12_12_1$	$P2_12_12_1$	I23
Cell dimensions				
a (Å)	145.78	148.27	146.06	233.75
b (Å)	163.51	162.98	163.42	233.75
c (Å)	245.11	248.05	246.35	233.75
$\alpha=\beta=\gamma$ (°)	90	90	90	90
Resolution (Å)	2.5 (2.63–2.48)	2.5 (2.64–2.49)	2.3 (2.43–2.30)	6.9 (7.29–6.89)
R_{meas} (%)	11.6 (137.9)	18.9 (70.2)	15.3 (65.5)	7.1 (181.7)
I/σ_I	9.54 (1.70)	8.97 (2.33)	10.24 (2.06)	25.1 (1.80)
Completeness (%)	99.3 (96.0)	99.3 (96.5)	92.8 (77.4)	98.0 (89.6)
Redundancy	7.3 (6.3)	6.7 (6.6)	4.9 (4.1)	19.5 (18.0)
Refinement	AcrB wt	AcrB wt	AcrB wt	AcrB_V612F
trimer model		Eicher PhD Thesis		
Program	PHENIX & REFMAC	PHENIX & REFMAC	PHENIX & REFMAC	PHENIX & REFMAC
Resolution (Å)	49.0–2.5	30.1–2.5	29.8–2.3	29.9–7.0
No. of reflections	201942	206415	242662	3017
R_{work}	19.61	20.28	21.73	26.51
R_{free}	24.47	25.71	26.43	46.81
N. atoms				
macromolecule residues	27537	27147	27604	9115
solvent residues	1300	640	1034	-
B-factors				
macromolecule	47.24	57.60	56.47	-
solvent	41.80	47.72	45.17	-
overall	46.97	57.33	56.06	81.94
RMS deviations				
bond length (Å)	0.008	0.008	0.008	0.015
bond angles (°)	1.145	1.215	1.166	1.943

4 Supplementary Experiments

4.1 TolC: β-barrel deletion variant

The AcrAB-TolC drug efflux system from *E. coli* is mutally dependent on the presence of all its components [142]. Chromosomal deletion of one of the genes coding for any of the three components causes a complete loss of drug resistance in *E. coli*. Since the active tripartite system exports drugs from the periplasm over the outer membrane, lack of any of the three components will exhibit the same phenotype yet for different reasons. E. g. deletion or fatal mutation of the *acrA* gene might hamper pump assembly, yet the AcrB component might still be able to pump drugs. In this case, the drugs (e. g. β-lactams) might be pumped in a futile cycle from the outer leaflet of the inner membrane to the periplasm, having no net effect on the concentration of the drugs inside the periplasm. Alternatively, one can assume that only the assembled tripartite AcrAB-TolC complex is mechanistically capable to work as an active transporter. To test the latter hypothesis, the aim was to reconstitute an *in vitro* tripartite setup without the imperative for having two membranes, as present in the natural situation in the Gram-negative cell. Therefore, the transmembrane β-barrel domain of TolC was deleted to produce a soluble TolC channel, still capable to bind to AcrB, which would resemble the native complex without the need of a second membrane. The β-barrel is formed by three TolC monomers, each contributing two loops that consist of two β-strands and a connecting turn. Such a soluble, β-barrel-less TolC variant lacking the membrane-embedded domain was generated. Residues constituting the two β-barrel loops, designated loop1 and loop2, were identified using the 3-D structural pdb file 1EK9 (www.pdb.org) from Koronakis *et al.* [98]. Proline residues were chosen beginning and end of the β-strands. A TolC trimer is shown in Figure 4.1 in cartoon representation. One monomer is highlighted in green color. The deleted range of residues on the corresponding loop1 and loop2 are shown in cyan and magenta, respectively. To remove the β-barrel membrane domain, the loops were deleted by site-directed mutagenesis and concomitantly replaced by polyglycine linkers to connect the periplasmic domains in the variant soluble protein. Plasmid pBR*tolC* (pBR322 with *tolC* gene, courtesy of J. Fralick) was used as template to perform site-directed mutagenesis according to

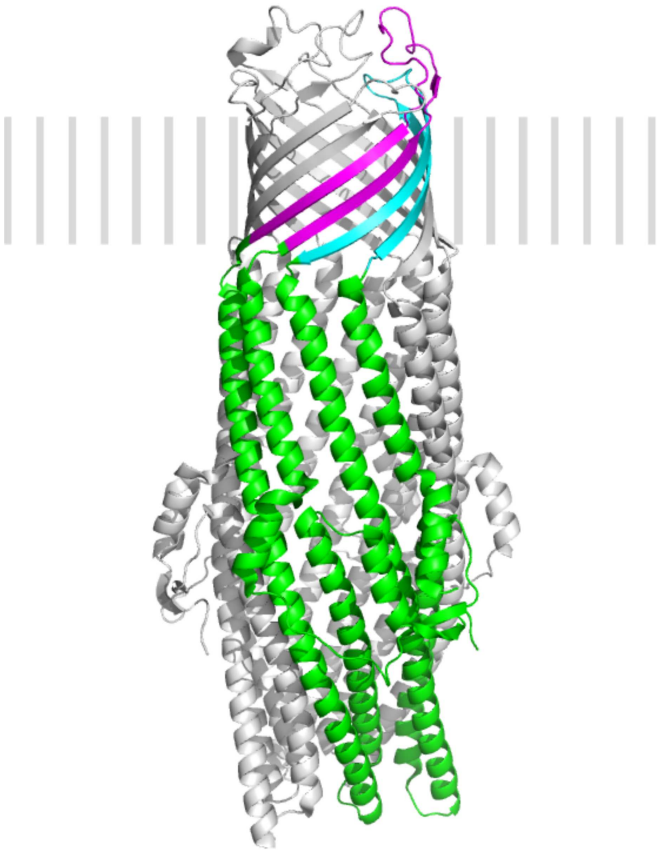

Figure 4.1: Visualization of the TolC trimer in cartoon representation. One monomer is highlighted in different colors. The β-barrel embedded in the outer membrane is composed of two loops (consisting of two antiparallel β-sheets) from each of the three monomers. Deleted residues of loop1 and loop2 are shown in cyan and magenta, respectively (pdb ID: 1EK9). The gray bars indicate the outer membrane of *E. coli* (about 25 Å thick).

the Quikchange protocol (Stratagene) in two consecutive steps. The primers used for these deletions are shown in Table 4.1. The codons encoding for inserted glycine link-

Table 4.1: Primers used for site-directed mutagenesis for the creation of the deleted loop TolC variant. Glycine (codon: GGC) linkers that replace the loops are underlined (loop1: 4x Gly; loop2: 2x Gly).

Name	Sequence
tolC_dl1_for	5'-AAG CGC GCA GTC CAT TAC TGC CAG GCG GCG GCG GCT TTG ATA TGT CGA AAT GGC GT-3'
tolC_dl1_rev	5'-ACG CCA TTT CGA CAT ATC AAA GCC GCC GCC GCC TGG CAG TAA TGG ACT GCG CGC TT-3'
tolC_dl2_for	5'-CAG GAT GGT CAC TTA CCG ACT GGC GGC CCG ATT TAT CAG GGC GGA ATG GTT-3'
tolC_dl2_rev	5'-AAC CAT TCC GCC CTG ATA AAT CGG GCC GCC AGT CGG TAA GTG ACC ATC CTG-3'

ers, four in place of loop1 and two in place of loop2, are underlined. The length of the linkers were chosen based on the distance between the loop-flanking residues in the crystal structure [143]. Site-directed mutagenesis products were verified by sequencing. The gene coding for TolC β-barrel less variant, designated *tolC_bl* was cloned into the pET24 vector (Novagen) for expression studies. Expression from the pET24 vector resulted in a β-barrel less TolC including a histidine-tag at the C-terminal end of the construct. In *E. coli* BL21 (DE3), expression could be detected by subjecting whole cell lysates to SDS-PAGE analysis (Figure 4.2, left panel). The construct resulted in the synthesis of a protein of about 50 kDa (calculated protein mass: 46.05 kDa). To investigate the localization of the construct within the cell, periplasmic protein extraction was performed [144]. The protein could be detected in whole cell lysates (Figure 4.2, left panel); the periplasmic fraction contained only trace amounts (not shown), indicating poor export of the variant to the periplasm despite the signal sequence at the N-terminus. In a next step, *E. coli* BL21(DE3) cells overproducing TolC_bl from pET24 were disrupted in the Emulsiflex cell disruptor and the low-spin supernatant was loaded on a Ni^{2+}-NTA purification column. Small amounts of purified protein could be eluted from the column (Figure 4.2, left panel) which was prone to precipitation upon concentration. Size-exclusion chromatography revealed that the retention time of the

protein peak of purified TolC_bl corresponded to about 40–50 kDa, indicating that the purified construct was existent as a monomer (Figure 4.2, right panel).

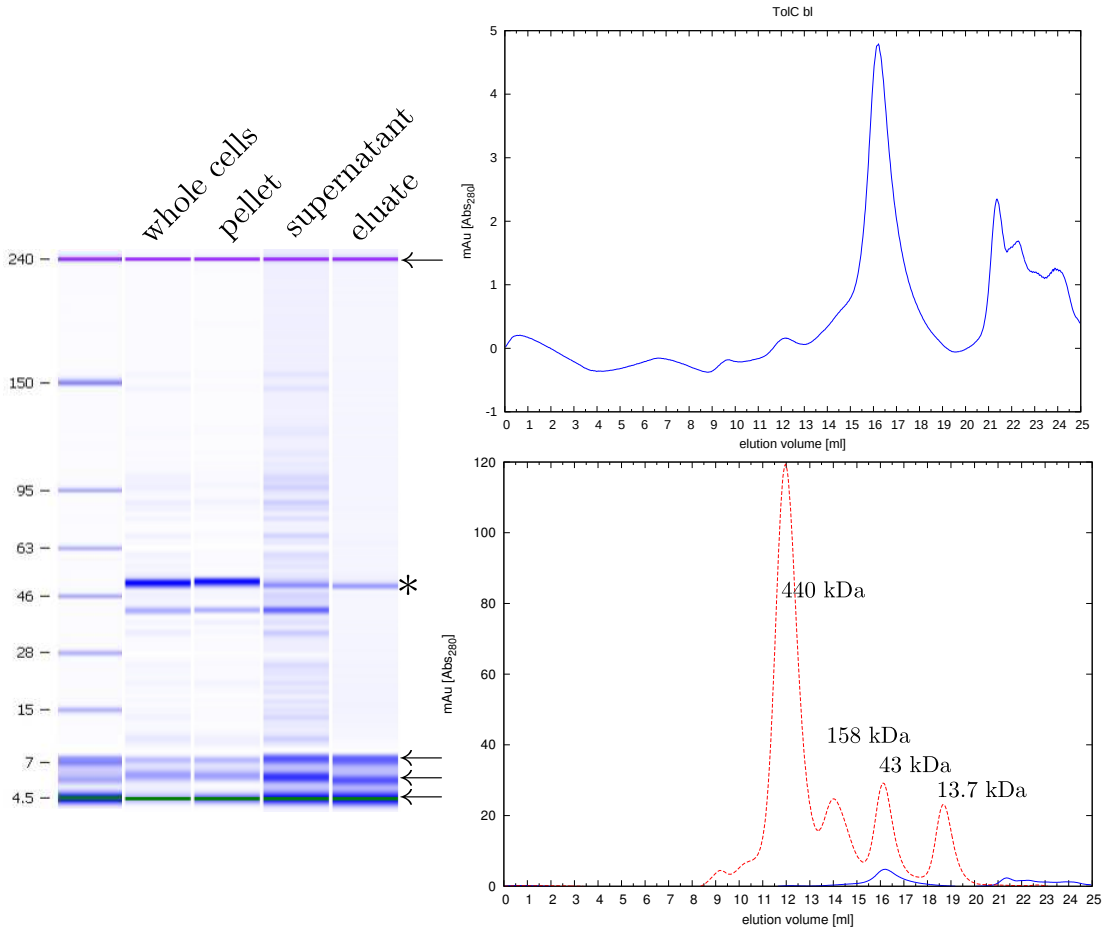

Figure 4.2: Left panel: SDS-PAGE gel like representation (Agilent protein 230 chip, Agilent Bioanalyzer 2100). Lanes: 1 protein ladder, 2 whole cell lysate, 3 pellet and 4 supernatant from low spin centrifugation after cell disruption, 5 eluate from Ni^{2+}-NTA column. TolC_bl (*) displays an electrophoretic mobility of about 50 kDa. Bands at 240 and 4.5 to 7 kDa (arrows) correspond to system signals and do not represent protein. Right panel, top: Size-exclusion profile of purified TolC_bl. Peak at 16 ml elution volume corresponds to monomeric TolC_bl. Peaks at 21 ml and later may represent degradation product or buffer additives. Right panel, bottom: Superimposition of size-exclusion profiles of purified TolC_bl (blue) and a calibration solution (red). The main peak of the purified TolC_bl corresponds with the 43 kDa peak of the calibration. Size exclusion chromatography was performed using a GE Superdex 200 10/300GL column coupled to a GE Äkta Prime FPLC at a flow rate of 0.5 ml·min^{-1}.

In 2008, Kim *et al.* used a similar approach to also synthetize the periplasmic domain (β-barrel less) of TdeA of *Actinobacillus actinomycetemcomitans*, a member of the TolC family [145]. The construct from Kim *et al.* contained a three residue smaller loop1 and a 6 residue smaller loop2 compared to our TolC construct. Moreover, the introduced

linkers differ as well and are SGSGS and SGSGSG replacing loop1 and loop2, respectively. In Figure 4.3 an alignment of the loop regions of wildtype TolC, TolC_bl of this study and the TdeA variant (TdeA_bl) from Kim's study is shown. Identical residues

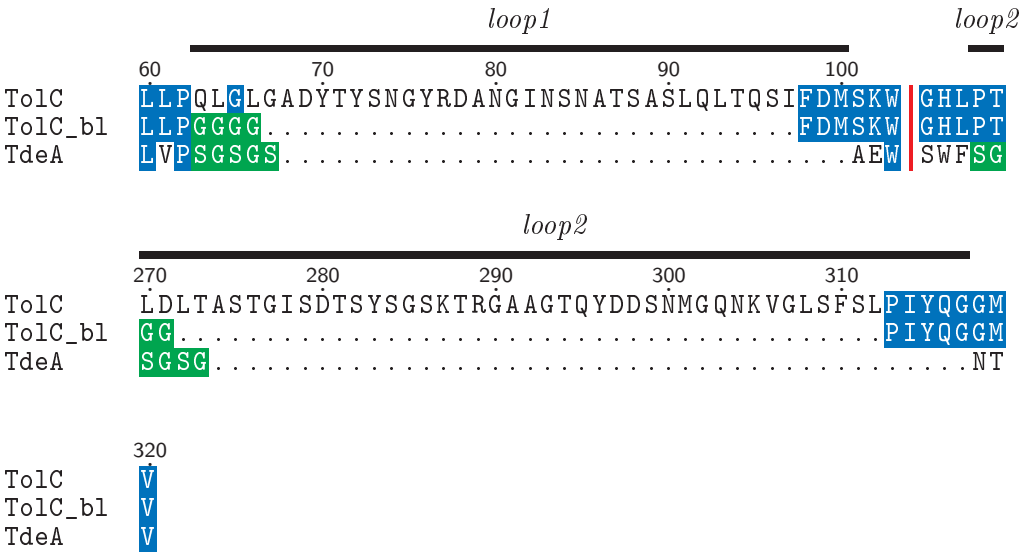

Figure 4.3: Alignment of the loop regions of TolC of *E. coli*, TolC_bl from this work and TdeA_bl from Kim *et al.* [145]. The range of the two β-barrel loops are indicated. Identical residues are shown blue; the red bar represents the gap of intervening sequence (AA 104–264). The introduced linker sequences are shaded green. Alignment was performed with the ClustalW2 program (www.ebi.ac.uk/Tools/clustalw2/index.html).

are shaded blue. Loop regions designated in Kim's study are indicated and introduced linker sequences are shaded green. Kim *et al.* [145] succeeded in the synthesis and purification of the soluble β-barrel less TdeA variant. Electron microscopy showed that the α-helical part of the protein was correctly folded despite the lack of the membrane domain.

4.2 Reconstitution experiments and experiments with inverted vesicles from *E. coli*

Despite detailed structural insights, functional data on binding affinities of substrates and kinetic parameters on drug transport by AcrB are sparse. The main bottleneck here is the lack of suitable *in vitro* binding and transport assays. There are several approaches to study the transport activity of transporters in membranes and membrane-like struc-

tures: e. g. experiments using vesicles, proteoliposomes containing reconstituted experiments and electrophysiology. Initial experiments to investigate drug transport by AcrB *in vitro*, using inverted bacterial vesicles and liposomes containing reconstituted AcrB, have been done and are presented in the following sections.

Experiments with inverted vesicles from *E. coli*

Inverted vesicles (IV) were generated from *E. coli* cells using the French pressure cell at 18,000 psi. During preparation, the orientation of the membrane components is inverted compared to the situation *in vivo*. This method was shown to result in an inside-out situation in 95 % of the generated vesicles [146]. These IVs still contained all constituents of the native bacterial membrane but outward facing proteins were turned against the inside lumen of the vesicles. IVs generated from cells containing AcrB were used to study transport of AcrB substrates. Energy was provided by ATP, which was consequently used by the intrinsic F_1F_O-ATPase to generate a proton motive force that, theoretically, is able to drive transport of drugs by AcrB (Figure 4.4, left panel).

Inverted vesicles were generated from *E. coli* BW25113Δ*acrB* (DE3) overexpressing AcrB from the plasmid pET24_AcrB. The ability of vesicles to generate a transmembrane proton gradient from primary source (ATP) and tightness to keep up the gradient was tested with the fluorescent dye 9-amino-2-chloro-6-methoxy acridine (ACMA). ACMA fluorescence quenching is a method to sense ΔpH over bacterial membranes [147]. ACMA fluorescence in vesicles was quenched when a proton gradient is formed over the membrane (inside acidic) and is re-established as soon as the proton gradient dissipates. Upon ATP addition to suspended vesicles, quenching of ACMA could be observed (Figure 4.4, right panel). This quenching indicated the activity of bacterial F_1F_O-ATPase and confirms the membrane integrity able to sustain a ΔpH gradient. When carbonylcyanide-m-chlorophenylhydrazon (CCCP) was added to the vesicles, a decrease in the quenching, hence increase of fluorescent signal could be observed. CCCP, an uncoupling agent, dissipates the electrochemical proton gradient in membrane vesicles. Further addition of ammonium chloride totally collapsed the remaining ΔpH by acidifying the outside of the vesicles (and consuming internal protons). The fluorescence signal was almost restored to the level before ATP addition.

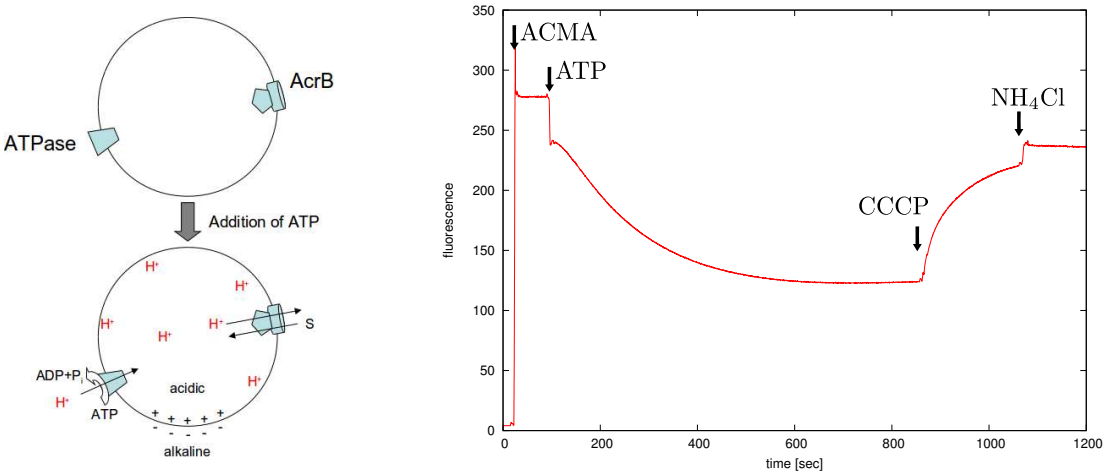

Figure 4.4: Left panel: Working hypothesis with inverted vesicles. In inverted vesicles membrane proteins are reversely oriented compared to the physiological situation. Addition of ATP to the outside activates the bacterial F_1F_O-ATPase generating an electrochemical proton gradient (ΔpH and $\Delta\Psi$) over the membrane vesicles, resulting in the accumulation of protons at the inside of the vesicles. AcrB in turn would theoretically be able to consume these protons while transporting substrates, according to the current hypothesis, from the inner leaflet of the inside vesicles to the vesicle lumen. Alternatively and currently not experimentally excluded, substrate might be transported from the outside to the interior of the inside-out vesicles. Right panel: ACMA fluorescence signal in inverted membrane vesicles obtained from *E. coli* BW25113Δ*acrB* (DE3) overexpressing AcrB. ACMA is a fluorescent dye that distributes into the different compartments of the assay system (outside, membrane and inside) and its fluorescent signal is quenched as a result of proton accumulation inside the vesicles due to the action of the F_1F_O ATPase in the presence of ATP. Both carbonylcyanide-m-chlorophenylhydrazon (CCCP) and ammonium chloride dissipate the established proton gradient resulting in a restored fluorescent signal.

The electrochemical proton gradient generated by the F_1F_O-ATPase theoretically provides energy for AcrB transport activity. Experiments were performed to trace the transport of AcrB substrates either via fluorescent substrates directly, or indirectly, via consumption of the proton gradient. Direct measurements made use of the fluorescent properties of the AcrB substrate *N*-phenylnaphthylamine (NPN). NPN, added to membranes in aqueous solution readily inserts into these membranes and exhibits strong fluorescence. In cells, AcrB removes NPN from the membrane and expels it to the outside of the cell, where NPN's fluorescence is strongly decreased due to the lack of the hydrophobic environment. Consequently, the transport of NPN can be traced via fluorescence measurements [77]. However, in these experiments AcrB substrate transport could neither be detected directly (by NPN fluorescence) nor indirectly (by measuring proton consumption via ACMA fluorescence).

Reconstitution experiments

In *E. coli*, beside AcrB, there are other multidrug efflux pumps that have an overlapping substrate specificity. The reconstitution of AcrB into liposomes provides some considerable advantage over inverted vesicles experiments: a controlled liposome system with AcrB as the only protein present.

Purified wt AcrB and a non-functional AcrB variant (AcrB_D407N/D408N (AcrB nf), negative control) were reconstituted into Triton X-100 destabilized liposomes. As additional negative control, destabilized liposomes were supplemented with AcrB sample buffer. The integration of AcrB was checked with a 2100 Bioanalyzer (Agilent Technologies Inc.) using the Agilent Protein 230 chip (Figure 4.5). Data from the protein chip indicated that AcrB is associated with the liposomes after the reconstitution process. In the systemic negative control no signal of protein is observed. However, detailed information about the orientation or whether insertion resembles the situation in the bacterial membrane, cannot be drawn from these experiments.

The integrity of the membranes of the proteoliposomes was tested using the fluorescent dye 3,3'-diethyloxacarbocyanine iodide ($DiOC_2(3)$) [148]. The fluorescence signal of this dye shifts in the presence of a membrane potential. Proteoliposomes, loaded with potas-

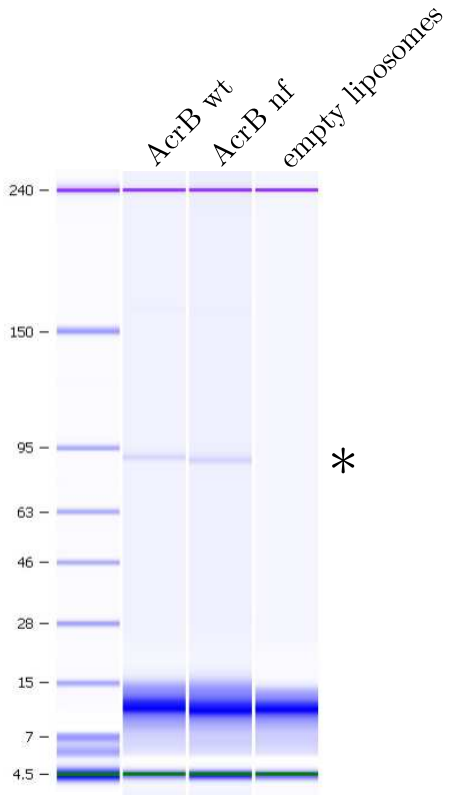

Figure 4.5: SDS-PAGE gel like representation (Agilent protein 230 chip, Agilent Bioanalyzer 2100) of liposomes with reconstituted protein. Lanes: 1. protein size ladder, 2. liposomes with AcrB wt, 3. liposomes with non-functional (nf) AcrB and 4. empty liposomes (reconstitution process with AcrB sample buffer). (*) indicates the electrophoretic mobility of the AcrB protein band at about 90 kDa. The signals between 7 and 15 kDa derive from the lipids and are not observed in liposome free samples (not shown). Signals between 4.5 and 7 kDa and at 240 kDa correspond to system signals and do not represent protein.

sium phosphate buffer, were resuspended in *N*-Methyl-D-glucamine (NMDG)-HEPES buffer and a potassium diffusion membrane potential was generated by addition of valinomycin (1 µM). The fluorescence emission of $DiOC_2(3)$ increased as the membrane potential established and a stable plateau was achieved. The addition of KCl diminished the potassium diffusion potential and the fluorescence signal decreased to the initial value (Figure 4.6). This data provides evidence that the membranes of the AcrB proteoliposomes were capable of maintaining a stable membrane potential.

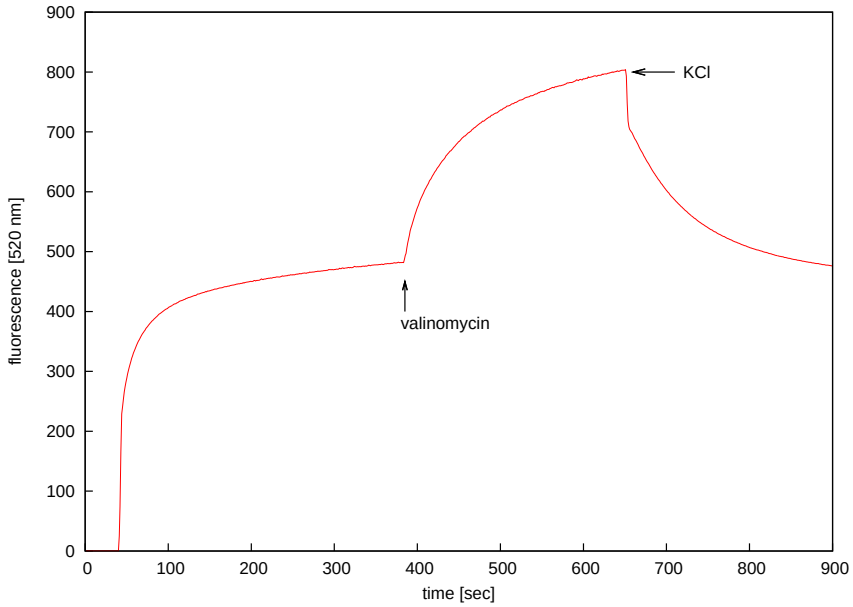

Figure 4.6: Fluorescence trace of a $DIOC_2(3)$ experiment with proteoliposomes with reconstituted wildtype AcrB to test the capability of the liposome membranes to retain a membrane potential (leak-tight proteoliposomes). Proteoliposomes loaded with potassium phosphate buffer were resuspended in *N*-Methyl-D-glucamine (NMDG)-HEPES buffer. The fluorescent agent $DIOC_2(3)$ was added to the resuspended liposomes. The addition of valinomycin generated a potassium diffusion membrane potential that increased the fluorescence of the membrane potential sensitive $DIOC_2(3)$. Addition of KCl diminished the membrane potential and resulted in a decrease of the fluorescence to the initial value.

Transport experiments with the H^+/substrate antiporter AcrB require a proton gradient over the membranes of liposomes with reconstituted protein. A ΔpH and a $\Delta pH/\Delta\Psi$ combined were generated in the experimental setups. The fluorescent substrates Hoechst 33342 and *N*-phenylnaphthylamine (NPN) were used to follow transport activity in the reconstituted setup. Both dyes are lipophilic molecules that immediately associate with phospholipid membranes. The ability of these substances to exhibit high fluorescence in hydrophobic environments and significantly lower fluorescence in aqueous environment

makes them valuable for studying AcrB drug transport. The rationale is that the dyes integrate into the membranes of the proteoliposomes, where they show strong fluorescence. When these molecules are transported from the membrane to the lumen or the outside of the liposomes, their fluorescence signals are quenched. Despite considerable efforts, transport of Hoechst 33342 and NPN by AcrB could not be observed.

Hoechst 33342 has been used in many occasions to measure secondary multidrug transport e. g. [149]. Yu *et al.* employed the dye for transport experiments in inverted vesicles and liposomes enriched with NorA, a H^+/substrate antiporter of the major facilitator superfamily (MFS). In their work, they were able to demonstrate quenching of Hoechst 33342 fluorescence in proteoliposomes by NorA transport upon the generation of a proton gradient.

The inability to trace Hoechst 33342 or NPN fluorescence quenching by AcrB transport may be due to several reasons. On the one hand, the activity of AcrB may be non-existent or too slow in a reconstitute system described above. *In vivo*, it has been reported that the AcrA/AcrB/TolC complex is inactive if any of the three proteins is non-functional [142]. In a reconstitute system, isolated AcrB may therefore be inactive too. On the other hand, Hoechst 33342 transport observed in NorA containing proteoliposomes [149] may significantly differ from that in AcrB proteoliposomes. NorA probably transports substrates from the lumen (or inner membrane leaflet) across the membrane to the outside of the liposomes, whereas AcrB hypothetically features transport from the outer leaflet to the outside. Redistribution of the expelled dye from the outside into the outer leaflet is a quick process and may exceed AcrB's transport capabilities resulting in a futile transport cycle, where no change in fluorescence is detectable. In a NorA reconstitute system, the dye would not only have to redistribute into the outer leaflet of the membrane but additionally relocate into the inner leaflet via slow flip-flop processes.

4.3 Materials and Methods

Protein expression and purification TolC_bl was generated using site directed mutagenesis based on the Quikchange protocol from Stratagene. Loop1 and 2 were removed

in two consecutive PCR reactions. The resulting product was verified by sequencing. Chemical competent *E. coli* BL21 (DE3) cells were transformed with the plasmid pET24_tolC_bl. Overexpression was performed in Terrific Broth medium and initiated by the addition of 0.5 mM IPTG at OD_{600}=1. After four hours at 18 °C, cells were harvested and resuspended in 20 mM Tris/Cl, pH 8 containing 500 mM NaCl, 2 mM $MgCl_2$, 0.2 mM diisopropylfluorophosphate and trace amount of DNaseI and passed three times through the EmulsiFlex®-C5 (Avestin Inc.) at 10-15 kpsi. Cell debris was separated by centrifugation at 9,000×g for 10 minutes. Supernatant was applied to a Ni^{2+}-NTA column (Ni-NTA Agarose Qiagen) pre-equilibrated in buffer1 (20 mM Tris/Cl, pH 7.5, 150 mM NaCl, 10 mM imidazole, pH 7.5, 10 % glycerol). The column was washed with 35 ml buffer1 and subsequently washed with 30 ml buffer2 (20 mM Tris/Cl, pH 7.5, 150 mM NaCl, 50 mM imidazole, pH 7.5, 10 % glycerol). TolC_bl was eluted in 6 ml buffer3 (20 mM Tris/Cl, pH 7.5, 150 mM NaCl, 200 mM imidazole, pH 7.5, 10 % glycerol) and concentrated 8.5 fold. 4 µl of non-concentrated whole cell lysates, centrifugation pellet, supernatant and elution fraction were loaded on an Agilent protein 230 chip (Agilent Bioanalyzer 2100) for qualitative evaluation.

Size-exclusion chromatography Concentrated protein sample (0.9 $mg \cdot ml^{-1}$; 0.7 ml) was subjected to size exclusion chromatography (running buffer: 20 mM Tris/Cl, pH 7.5, 150 mM NaCl) using a GE Superdex 200 10/300GL column coupled to a GE Äkta Prime FPLC. Size-exclusion chromatography was performed at a flow rate of 0.5 $ml \cdot min^{-1}$ and fractions of 0.5 ml were collected.

ACMA fluorescence measurements Bacterial membranes containing 200 µg total protein were suspended in 10 mM KP_i, pH 7.5, 10 mM $MgSO_4$ (2 ml) and constantly stirred during measurements. Fluorescence traces were recorded in a RF-5301 PC spectrofluorophotometer (Shimadzu) at excitation and emission wave lengths of 430 nm and 474 nm, respectively, using 5 nm slit width in both, excitation and emission. 9-amino-2-chloro-6-methoxy acridine (ACMA, 0.25 µM), 1 mM ATP, 5 µM carbonylcyanide-m-chlorophenylhydrazon (CCCP) and 10 mM NH_4Cl (final concentrations) were added when indicated.

Protein expression and purification AcrB was expressed and purified from *E. coli* C43 (DE3) cells as described previously [74, 125]. After purification via Ni^{2+}-NTA affinity chromatography, AcrB was reconstituted into liposomes.

Generation of inverted vesicles from *E. coli* pET24 vectors carrying the wildtype and non-functional variant of AcrB were transformed into *E. coli* BW25113Δ*acrB* (DE3) and AcrB protein was overexpressed in these cells in LB medium with 0.5 mM IPTG. After four hours at 27 °C, cells were harvested and resuspended in 20 mM Tris/Cl, pH 8 containing 500 mM NaCl, 2 mM $MgCl_2$, 0.2 mM diisopropylfluorophosphate and trace amount of DNaseI and passed three times through the French pressure cell at 1200 psi gage pressure which corresponds to 18,000 psi cell pressure when using a 1 ” piston. Cell debris was separated by centrifugation at 9,000×g for 10 minutes. Inverted membrane vesicles were collected at 150,000×g for 60 minutes at 4 °C, resuspended in 50 mM KP_i, pH 7.5 and stored at -80 °C.

Reconstitution of AcrB Preparation and reconstitution was carried out according to the protocol of Geertsma *et al.* [150] with adaptations. Bio-Beads SM-2 Adsorbent (5 g, Bio-Rad) were consecutively washed with 100 ml methanol, 100 ml ethanol and degassed in 100 ml water (bidest). Then the bead slurry was washed 10 times in 100 ml water (bidest). Prepared beads were stored at 4 °C submersed in water. Lipids that were used in these experiments were L-α-Phosphatidylcholine from soy bean (P5638, Sigma), *E. coli* total lipid extract (100500C, Avanti Polar Lipids, Inc.) and a *E. coli* total lipid extract: L-α-phosphatidylcholine (Egg, Chicken, 840051C, Avanti Polar Lipids, Inc.) of 3:1 (w/w). Stock solutions of lipids in chloroform were mixed in desired ratios. Mixture was dried using a rotary evaporator, subsequently washed in diethyl ether and dried again. Dried lipid mixture was resuspended in buffer (for example 50 mM KP_i, pH 6.5) to a final concentration of 20 $mg \cdot ml^{-1}$ at room temperature using 45 ° bent 20-gauge needle. Lipid suspension was sonicated 6 times (15 s + 45 s pause) at a peak-to-peak intensity of 4 µm on ice. Samples were kept under a stream of nitrogen gas during sonification. Generated small unilamellar vesicles (SUVs) were flash-frozen and gently thawn 3 times at room temperature to obtain large multilamellar vesicles (LMVs). LMVs were flash-frozen in 0.5 ml aliquots and stored in liquid nitrogen.

For reconstitution, LMVs (20 mg·ml^{-1}) are thawn and extruded through a 400 nm filter 11 times to generate large unilamellar vesicles (LUVs) which were subsequently diluted to 4 mg·ml^{-1} with the buffer used for resuspension of the lipids. LUVs were titrated to R_{sat} with 10 µl aliquots of 10 % (wt/vol) Triton X-100. Another 5 aliquots of Triton X-100 were added (R_{work}) to destabilize the liposomes (Figure 4.7). For a

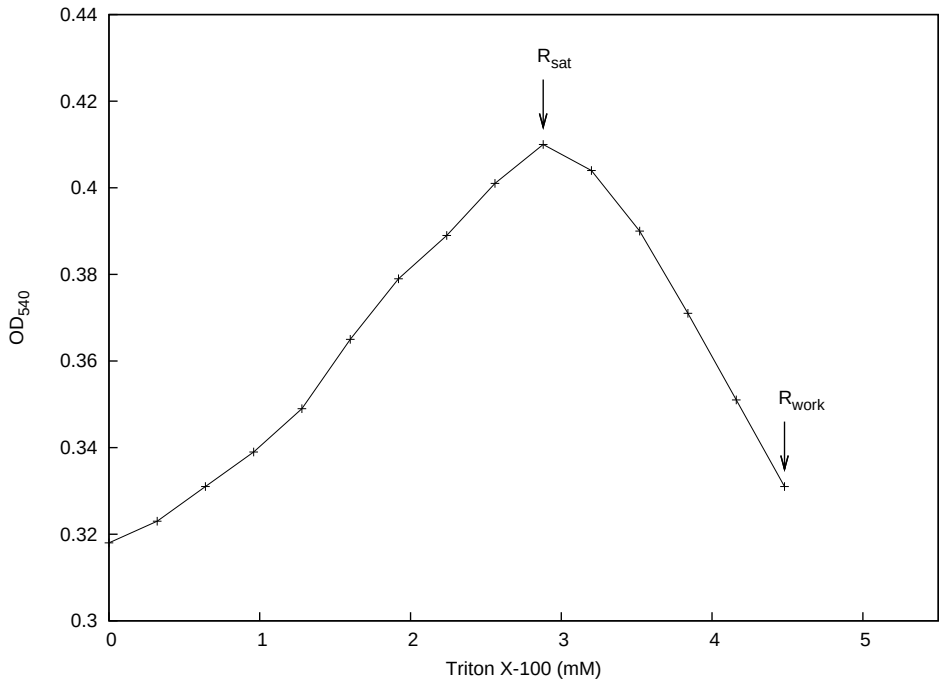

Figure 4.7: Light scattering of large unilamellar vesicles at OD_{540} at increasing Triton X-100 concentrations. R_{sat} and working concentration (R_{work}) for reconstitution were obtained at about 3 and 4.5 mM Triton X-100, respectively.

1:100 (wt/wt) protein to lipid ratio, 0.2 ml of purified AcrB (1 mg·ml^{-1} in 50 mM KP_i, pH 7.8, 20 % glycerol, 200 mM NaCl, 500 mM imidazole, pH 7.5, 0.03 % DDM) were added to 5 ml detergent destabilized liposomes and incubated on a blood wheel gently agitating for 15 minutes at RT. Bio-Beads (200 mg wet weight) were added to the protein-liposome suspension and the mixture was incubated 30 minutes at RT . In additional two steps, 200 mg Bio-Beads were added each and incubated at 4 °C for 60 minutes and overnight, respectively. After overnight incubation, another 200 mg Bio-Beads were added to the sample, followed by incubation for 120 minutes at 4 °C. Incubation steps were performed on a bloodwheel, gently agitating. The suspension was filtered from the beads using a gravity flow column equipped with one frit (sintered glass). Beads were washed with 45 ml 50 mM KP_i, 2 mM $MgSO_4$, pH 6.5, and the

flowthrough was used to dilute the proteoliposome suspension to lower the glycerol concentration. Proteoliposomes were collected by centrifugation in a TFT65.38 Sorvall rotor at 50,000 rpm (175,000-200,000×g) and 4 °C for 60 minutes and subsequently resuspended in 1 ml 50 mM KP_i, 2 mM $MgSO_4$, pH 6.5, to a lipid concentration of 20 mg·ml^{-1}. These proteoliposomes were frozen in 0.5 ml aliquots and stored in liquid nitrogen. For use in transport experiments, proteoliposomes were 5 times froze-thawn in liquid nitrogen and extruded 11 times through a 200 nm filter. Extruded proteoliposomes were collected by centrifugation (TFT65.38 rotor, 140,000×g, 4 °C, 30 minutes), resuspended in 50 mM KP_i, 2 mM $MgSO_4$, pH 6.5, to a lipid concentration of 80 mg·ml^{-1}, stored on ice and used within 24 hours.

Testing membrane integrity of liposomes The fluorophotospectrometer (Shimadzu RF-5301) was set to excitation wavelength 482 nm and emission wavelength 520 nm using 1.5 and 3 nm slit width, respectively. Prepared liposomes (15 µl), loaded with 100 mM KP_i, 2 mM $MgSO_4$, pH 6.5, were resuspended in 2 ml 100 mM *N*-Methyl-D-glucamine(NMDG)-HEPES, 2 mM $MgSO_4$, pH 7, and constantly stirred in a 2 ml quartz cuvette. After start of recording the emission, 3,3'-diethyloxacarbocyanine iodide ($DiOC_2(3)$) was added to a concentration of 5 µM. When a stable fluorescent signal was obtained, valinomycin was added to a final concentration of 1 µM. The increase of $DIOC_2(3)$ was traced until a plateau was reached and KCl was added to a final concentration of 200 mM.

Transport experiments with reconstituted AcrB using fluorescent substrates For the fluorescent AcrB substrates *N*-phenylnaphthylamine (NPN) and Hoechst 33342 settings at the fluorophotospectrometer (Shimadzu RF-5301) were set to excitation wavelength 355 nm, emission wavelength 420 nm and 355 nm, 457 nm, respectively. Slit width for excitation and emission was set to 5 nm. Prepared liposomes (15–50 µl) were resuspended in KP_i buffers of lower pH to establish a ΔpH and in NaP_i buffers of lower pH to generate ΔpH and $\Delta\Psi$ after the addition of valinomycin. The sample was constantly stirred in a quartz cuvette during measurements. The AcrB substrates NPN and Hoechst 33342 were added to concentrations of 0.25–1 µM and 0.05–0.25 µM, respectively.

5 Discussion

5.1 Allostery and cooperativity in multimeric assemblies

Allosteric regulation is a mechanism to control the activity of a catalytic protein (e. g. enzyme, carrier or pump) without altering this protein's availability. The concept of allostery envisions binding of "effector" molecules to the allosteric site (which is a site other than the primary binding site) of the catalytic protein in order to modulate its activity by structural conversions. These modulations may be positive or negative, in- or decreasing the activity, respectively. Typically, allosteric regulated proteins share certain attributes. They often consist of two (or more) identical subunits and the holoenzyme exhibits a symmetric architecture. Furthermore, these proteins commonly adopt two conformations, referred to as the T (tense) and the R (relaxed) state, where substrate affinity generally is higher in the R state. Stimulatory and inhibitory allosteric effectors stabilize the R and T state, respectively, modulating the rate of the reaction. Cooperativity is a self-regulatory effect emerging from two or multiple substrate binding sites in which binding of a ligand to one of the binding sites alters the affinity of the ligands to the other binding sites by structural changes. Cooperativity can again have stimulatory or inhibitory effects and is typically observed in multimeric assemblies.

The MWC (Monod/Wyman/Changeux) or symmetry model describes allosteric changes in homomultimeric proteins to adapt substrate affinity [151]. The best known implementation of this model is the description of cooperative binding of oxygen to hemoglobin. Hemoglobin is a pseudosymmetric tetramer, composed of 2 α and 2 β subunits, each harboring a heme prosthetic group involved in the binding of one molecule of oxygen. Each of the four subunits can adopt two different conformations: the T (tight) state (conformation of deoxyhemoglobin) and the R (relaxed) state (conformation of oxyhemoglobin). In the symmetry model, binding of oxygen to one of the protomers in T conformation enhances the subsequent T to R transition of all four subunits and as a result, increases oxygen affinity of the ligand-free monomers. The cooperativity mode is explained by the tight packing of the subunits and the spontaneous leveraging of conformational changes to the adjacent subunits. The MWC model suggests symmetric distribution of the conformational states in a way that all subunits adopt either the T

or R conformation, independent of the oxygenated state of the subunits. An alternative model to the MWC model was presented by Koshland/Némethy/Filmer [152], also known as the sequential or KNF model. This model anticipates a sequential conformational conversion of single subunits upon substrate binding and features cooperative interactions of adjacent subunits, resulting in a change of substrate affinity. Applied to oxygen binding of hemoglobin, this model starts with deoxyhemoglobin in which all four subunits are present in the T state. Binding of oxygen to one of the subunits causes transition to the R conformation of the oxygen binding subunit and simultaneous increase of oxygen affinity of the adjacent subunit. Binding of oxygen continues until all four subunits adopted the R conformation and the hemoglobin is fully oxygenated. The featured cooperativity can be positive (as observed in hemoglobin) as well as negative.

Concerning trimeric RND efflux pumps, both models are still up for sale. Whereas the proposed functional rotation model for AcrB is much along what would be described by the KNF model, the MWC model may be possibly used to describe the mechanism of CusA, a copper and silver ion RND transporter in *Escherichia coli*. Latest crystal structure data indicate the presence of two different conformations, depending on the presence of its substrate, for example copper ions [45]. In contrast to the asymmetric crystal structures of AcrB [73–75] the structures of CusA reveal symmetric trimers, where one conformation is observed in the absence and one conformation in the presence of copper ions. Experimental support for the KNF model type of allostery in the case of AcrB was provided by whole cell efflux kinetics. The group of Nikaido developed *in vivo* assays to determine efflux kinetics in *E. coli* cell mediated by AcrAB-TolC. Investigated substrates were cephalosporins [153] and penicillins [154]. These studies showed that efflux kinetics of most tested substrates revealed a sigmoidal rather than a Michaelis-Menten type saturation curve. The observation of sigmoidal curves is a strong indication for a positive cooperative binding to AcrB, since it describes an increase of substrate affinity with increasing substrate concentration. Calculated Hill coefficients (varying between 1.9 and 4.7) provide indication for rather strong cooperative kinetics due to more than one binding site for substrates within the AcrB trimer.

Molecular basis of allostery and cooperativity and putative determinants for AcrB

In hemoglobin, the molecular mechanism of cooperativity is well studied. Human hemoglobin is comprised of two identical α-chains (α1 and α2) and two identical β-chains (β1 and β2). Association of molecular oxygen to the heme iron causes a structural change and configurational shift (undoming) of the porphyrinring. These rather subtle structural alterations are leveraged via a covalently attached histidine side chain (His F8) to an adjacent helix (helix F) which is coupled to changes at the α1 - β2 and α2 - β1 interfaces where disruption of hydrogen bonds and formation of new ones occurs. As a consequence, the subunits have a different set of hydrogen bonding pattern at the interface region in the T or R state. Since the R-state has a higher affinity for oxygen, the allosteric conformational change caused by the binding of oxygen to the neighbouring monomer results in the observed cooperative binding kinetics [155].

Another case of enzymatic allostery is displayed by the aspartate transcarbamoylase (ATCase) of *E. coli*, which catalyzes the generation of *N*-carbamoyl aspartate from carbamoyl phosphate and aspartate. This multimeric enzyme complex exhibits cooperative kinetics due to the binding of both of it substrates and furthermore is allosterically regulated e. g. stimulatory by ATP and inhibitory by the downstream product cytidine triphosphate (CTP). The latter feedback mechanism tightly regulates the production of CTP in the bacterial cell. The ACTase is comprised of six catalytic subunits and six regulatory subunits. The catalytic subunits are arranged in two trimers that congruently face each other. Three dimers of the regulatory subunits bind to the catalytic assembly in a threefold symmetry. The transition from T to R state features a conformation in which the two catalytic trimers move together and rotate to form the catalytic active form of the ATCase. Similar to the situation in hemoglobin, quaternary alterations are crucial for the allosteric regulation [155].

Yet another example of allostery is reported for the glycogen phosphorylase, which catalyzes the degradation of glycogen. It is a homodimeric enzyme and the active site is occluded in the T and accessible in the R state. The conformational shift from T to R is promoted by phosphorylase kinase which results in changes in the tertiary and ultimately quarternary structure of the enzyme. Crucial for the quarternary alterations

is the tilting of the "tower helices" that connect the two monomers. The tower helices, one from each subunit, are oriented antiparallel at the interface of the monomers. In the transition from the T to R conformation, they move relatively to each other. Like observed in the hemoglobin, this results in a change of interaction profile (hydrogen bonds, ionic interactions) of the side chains located on the helices. The glycogen phosphorylase is allosterically inhibited by downstream products of glycogen breakdown (glucose, adenosine triphosphate, glucose-6-phosphate) stabilizing the T state [156].

As the examples described above demonstrate, cooperativity may be mediated by hydrogen bonds or ionic interactions at the interfaces of monomers. Changes in the tertiary structure (conformation) of the monomers may shift, break or establish single or a series of hydrogen bonds or salt bridges that transmit conformational information to the adjacent monomer. On the basis of the asymmetric model of AcrB (pdb ID: 2GIF) by Seeger *et al.* [74] hydrogen bonding and salt bridges at the interfaces of the three monomers were analyzed using the web based tool PISA (Protein interfaces, surfaces and assemblies service PISA at European Bioinformatics Institute (http://www.ebi.ac.uk/msd-srv/prot_int/pistart.html), authored by E. Krissinel and K. Henrick [157]). Numerous hydrogen bonds and a few salt bridges were found to be established at the interfaces of the AcrB monomers (Tables 5.1, 5.2 and 5.3).

Table 5.1: Hydrogen bonds observed at the interfaces between L, T and O of the asymmetric AcrB based on the high resolution model (pdb ID: 2GIF). Only dynamic bonds that are present in one or two of the three interfaces are specified. Residue names and numbers, distances and involved atom (e. g. [OD2]) are indicated.

Residue 1	Distance (Å)	Residue 2	Interface	Residue 1	Distance (Å)	Residue 2	Interface
PHE 11 [N]	3.80, 3.19	GLU 893 [OE1]	OL, OT	ASN 109 [OD1]	3.27	VAL 129 [N]	OL
PHE 11 [N]	3.68	GLU 893 [OE2]	OL	LYS 110 [NZ]	2.82	VAL 129 [O]	TL
TYR 49 [OH]	2.67	ARG 239 [NH2]	OT	LYS 110 [NZ]	2.94	ASP 174 [OD1]	OT
GLY 51 [O]	3.56, 3.31	ALA 216 [N]	TL, OL	ASN 161 [ND2]	3.71	GLN 687 [O]	TL
GLY 51 [O]	2.98, 2.81	GLY 217 [N]	TL, OL	ARG 168 [NH1]	3.21	ASN 820 [O]	OL
THR 56 [OG1]	2.96, 2.77	GLN 213 [NE2]	TL, OL	ARG 168 [NH2]	2.69	ASN 820 [O]	TL
ASP 59 [O]	3.39, 2.53	ARG 239 [NH1]	TL, OL	ARG 168 [NH2]	3.84	GLY 821 [O]	OT
ASP 59 [O]	3.81	VAL 768 [N]	OT	ALA 209 [O]	3.21	GLN 733[NE2]	OL
THR 60 [OG1]	3.84	ARG 239 [NH2]	TL	GLN 218 [NE2]	3.82	GLN 622 [OE1]	OL
GLN 63 [OE1]	2.78, 3.05	VAL 768 [N]	TL, OL	THR 222 [N]	3.24, 3.72	GLN 622 [OE1]	OL, OT
GLU 66 [O]	3.06	ARG 168 [NH2]	OL	THR 222 [OG1]	2.60	TYR 275[O]	TL
GLN 67 [OE1]	3.13	ARG 767 [NH2]	OT	THR 222 [OG1]	3.64	GLN 584 [OE1]	TL
MET 69 [O]	2.75	ARG 168 [NE]	OL	THR 222 [OG1]	3.32	ASP 276 [N]	OL
ASN 70 [OD1]	3.73	VAL 175 [N]	OT	THR 222 [OG1]	2.58	ASP 276 [OD1]	OT
GLY 71 [N]	3.25, 3.36	SER 167 [O]	TL, OL	GLN 228 [N]	3.85	GLU 585 [OE1]	OT
ASP 73 [OD2]	2.76, 2.65	LYS 131 [NZ]	TL, OL	GLN 228 [O]	3.25	THR 583 [OG1]	OT
ASN 74 [N]	2.67	SER 170 [OG]	TL	LEU 230 [N]	3.81	THR 583 [OG1]	TL
ASN 74 [OD1]	3.75	SER 170 [OG]	TL	ASN 231 [ND2]	3.07	GLN 622 [OE1]	OL
ASP 101 [O]	3.41	ASN 109[ND2]	OT	GLN 237 [NE2]	3.77	ASN 747 [OD1]	OL
ASP 101 [OD1]	3.30	GLN 106 [NE2]	TL	GLN 237 [OE1]	3.78	ASN 747 [ND2]	TL
ASP 101 [OD2]	2.77	GLN 106 [NE2]	OT	THR 238 [OG1]	3.86, 3.44	LYS 728 [NZ]	OL, OT
GLN 108 [NE2]	3.65	ASN 109 [OD1]	OT	LEU 250 [O]	3.65	GLN 737 [NE2]	TL
GLN 108 [NE2]	3.13	ASN 109 [O]	OT	ARG 259 [NE]	2.99	GLU 734 [OE2]	OL
GLN 108 [OE1]	3.87	GLN 112 [NE2]	TL	ARG 259 [NH1]	2.78	GLU 734 [OE2]	TL
GLN 108 [OE1]	3.89	LEU 113 [N]	OT				

A total number of 49 dynamic hydrogen bonds were found at the investigated interfaces. These interactions, only present in one or two of the three surfaces, may be the structural basis for a potential cooperative mechanism. Eleven hydrogen bonds were found to be specific for the OL interface and 14 bonds for the OT and TL interface, each. The number of hydrogen bonds found in two out of three interfaces was significantly smaller: three and seven for OL, OT and TL, OL, respectively. Interestingly, there are no common hydrogen interactions observed in the TL, OT interfaces. Out of the 63 reported hydrogen bonds, 14 were found in all three interfaces. These static interactions are shown in Table 5.2. Remarkably, the majority (12) of these static hydrogen bond interactions involve the intermonomeric loop (Loop) and the DC subdomain of the TolC docking domain or the PC1 subdomain. The occurrence of the static hydrogen bonds in all three interfaces makes them rather unlikely candidates for participation in cooperativity mechanisms; on the other hand the observed interactions may emphasize the loop structure as a determining structure for the trimeric assembly of AcrB. The trimer might be stabilized by these static intermonomer interactions (Chapter 2).

Additionally to the static hydrogen bonds associated with the Loop, there is an interaction involving the PN1 and the TolC docking domain and one observed in the transmembrane domain (TM1-TM8).

In addition to the hydrogen interactions in the three intermonomeric interfaces, also ionic interactions were analyzed. A total number of 10 individual ionic interactions (salt bridges) could be observed in five pairs of residues (Arg 8 - Glu 893, Asp 73 - Lys 131, Lys 110 - Glu 130, Lys 110 - Asp 174, Arg 259 - Glu 734) (Table 5.3).

Ionic interactions could be observed in all three interfaces and five, two and one interactions were found to be specific for the OL, TL and OT interface, respectively. Interestingly, the ionic interaction pairs Asp 73 - Lys 131 and Arg 259 - Glu 734 were observed at the interfaces of TL (T monomer and L monomer) and OL (O monomer and L monomer), whereas these interaction were not found in the OT interface. These specific salt bridges are established between the PN1 subdomains (Asp 73 - Lys 131) and between the DN subdomain and the neighboring DC subdomain (Arg 259 - Glu 734), respectively. Lysine 131 was found to interact with aspartate 73 at the TL (2

Table 5.2: Static hydrogen bonds of the interfaces of the L, T and O monomer of AcrB (based on the high resolution structure pdb ID: 2GIF) and involved domains. TM: transmembrane helix, docking domain: TolC docking domain, Loop: intermonomeric loop of AcrB.

Residue 1	Distance (Å)	Residue 2	Domains
ILE 10 [N]	3.06	GLU 893 [OE1]	TM1-TM8
GLN 63 [NE2]	3.52	GLY 766 [O]	PN1-docking domain
GLN 218 [N]	3.56	TRP 754 [O]	Loop-DC
GLY 220 [N]	3.51	ARG 780 [O]	Loop-DC
GLY 220 [N]	3.08	MET 781 [O]	Loop-DC
GLY 221 [O]	3.00	ARG 780 [NH1]	Loop-DC
PRO 223 [O]	2.59	ARG 780 [NH2]	Loop-DC
GLY 227 [N]	2.62	GLU 585 [OE1]	Loop-PC1
GLN 228 [NE2]	3.41	MET 781 [O]	Loop-DC
ASN 231 [N]	3.25	GLY 581 [O]	Loop-PC1
SER 233 [O]	2.87	PHE 727 [N]	Loop-DC
ILE 235 [O]	2.71	ILE 729 [N]	Loop-DC
ILE 235 [N]	2.76	PHE 727 [O]	Loop-DC
ALA 236 [O]	2.68	LYS 728 [NZ]	Loop-DC

interactions) and OL (1 interaction) interface whereas at the OT interface this specific interaction was absent (Figure 5.1).

Notably, no ionic interactions are observed which are present in all three interfaces and only one interaction is present at the interface OT (Table 5.3).

The characterized dynamic hydrogen bonds as well as the salt bridges, may be involved in a cooperative mechanism of the AcrB trimer. Mutagenesis studies to disrupt specific interactions may reveal their influence on the activity of AcrB.

Cooperative effect of other known membrane transporters

Cooperative substrate binding effects in membrane transporters is a well described phenomenon. In the monomeric eukayotic multidrug exporter P-glycoprotein (P-gp or MDR1) it was found that two substrate binding sites exhibit positive cooperativity

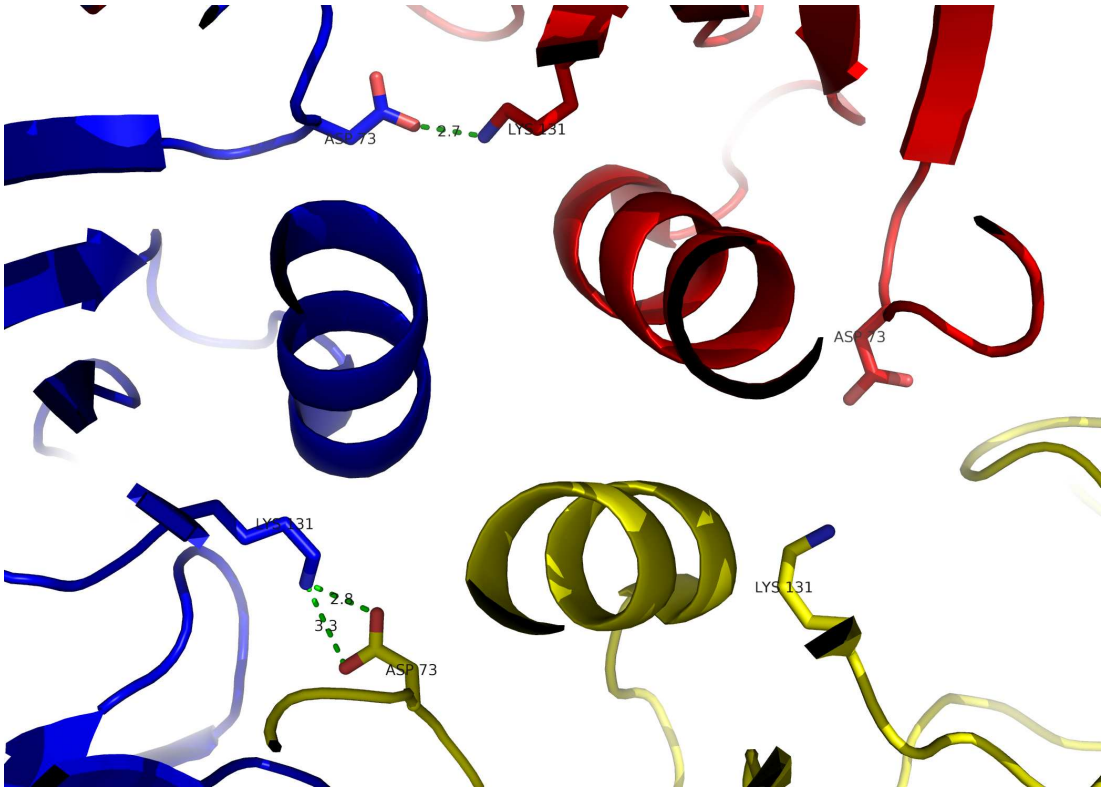

Figure 5.1: Top view on the PN1 subdomains of the loose (L, blue), tight (T, yellow) and open (O, red) monomers of AcrB (pdb ID: 2GIF) in cartoon representation. In the center, the three "pore helices" of the PN1 subdomains are visible. Aspartate 73 and lysine 131 that are involved in salt bridging are shown as sticks and the salt bridges (with the distances in Å) are indicated by green dotted lines. The salt bridge at the interface of TL (lower left) and OL (top) is not present at the OT interface (lower right).

Table 5.3: Salt bridges of the interfaces between L, T and O of the asymmetric AcrB based on the high resolution model (pdb ID: 2GIF). Residue names and numbers, distances, involved atom (e. g. [NH1]) and interfaces are indicated.

Residue 1	Distance (Å)	Residue 2	Interface
ARG 8 [NH1]	3.96	GLU 893 [OE2]	OL
ASP 73 [OD1]	3.35	LYS 131 [NZ]	TL
ASP 73 [OD2]	2.76, 2.65	LYS 131 [NZ]	TL, OL
LYS 110 [NZ]	2.88	GLU 130 [OE1]	OL
LYS 110 [NZ]	3.43	GLU 130 [OE2]	OL
LYS 110 [NZ]	2.94	ASP 174 [OD1]	OT
ARG 259 [NE]	3.93, 2.99	GLU 734 [OE2]	TL, OL
ARG 259 [NH1]	2.78	GLU 734 [OE2]	TL
ARG 259 [NE]	3.31	GLU 734 [OE1]	OL
ARG 259 [NH2]	3.22	GLU 734 [OE2]	OL

[158]. In the bacterial LeuT leucine transporter, cooperativity between leucine binding and sodium ion binding has been observed in all-atom free-energy perturbation (FEP)/molecular dynamics (MD) simulations using a high resolution (1.65 Å) model [159]. The sodium dependent LeuT harbors a leucine binding site as well as two distinct sodium binding sites. FEP/MD simulations revealed a strong cooperativity between leucine binding and sodium coordination in the adjacent sodium binding site (NA1) whereas binding of sodium to the second binding site (NA2) seems non-cooperative. The structural basis for this interaction arises from the fact that the carboxyl group of the bound leucine is involved in the coordination of the sodium in NA1 [160].

Also in the sodium dependent citrate transporter CitS of *Klebsiella pneumonia* cooperativity of binding of the two sodium ions was demonstrated [161, 162]. However, the structural basis for this mechanism remains occluded due to the lack of a crystal structure for CitS.

Recently, the structural basis for cooperativity in the sodium-independent carnitine/butyrobetaine antiporter CaiT from *Proteus mirabilis* was revealed using high resolution structures. Binding experiments exhibited a Hill coefficient greater than one, thus

suggesting cooperativity in substrate binding. It could be shown that binding of butyrobetaine causes structural rearrangements that open the second binding site [163].

A different mechanism of cooperativity is observed for the trimeric glycine betaine (*N,N,N*-trimethylglycine) symporter BetP from *Corynebacterium glutamicum* that imports the osmolyte betaine from the environment to escape osmotic stress. In a reconstituted system the C-terminal domain was shown to be crucial for the regulation via sensing of high cytosolic K^+ concentrations in the case of osmotic stress [164]. BetP was shown to be a trimer in membranes by 2D crystallography and electron cryomicroscopy [165]. Recent high resolution data revealed the presence of a trimer with non-crystallographic symmetry (NCS) [166]. The crystal structure further indicates the role of the C-terminal helix as an intermonomeric activator that exhibits "protein-protein interactions" [167] between the C-terminal domain and residues of the neighboring monomer. At the interface of the B and the C monomer, a salt bridge between arginine 565 on the C-terminal domain of the C monomer and aspartate 131 on the loop structure "loop 2" from the B monomer is observed (Figure 5.2). Glutamate 132 on loop 2, on its part, is also involved in a salt bridge interaction with arginine 390 located on loop 8. This interaction network may establish a link between the C-terminal helix and loop 8, which is gating the substrate pathway, via loop 2. Changes of orientation in the regulatory C-terminal helix upon stimulatory osmotic alterations are postulated to induce conformational changes that would unblock the pathway [167]. Via this mechanism the C-terminal domain of BetP is supposed to activate and deactivate the adjacent monomer by pushing and pulling the gating loop 8 by way of this salt bridge network. Activation of BetP, therefore, seems to be dependent on its trimeric state. In contrast, transport experiments [168] clearly indicated that transport itself is non-cooperative, suggesting independent action of each monomer in the trimeric assembly.

5.2 AcrB: Cooperativity and the binding change mechanism

The functional assembly of the AcrAB-TolC drug efflux pump in *E. coli* appears to be controlled by the concentration of the three components itself in the cell. Specifically, it appears that AcrA concentration inside the periplasm is key to modulating the activity

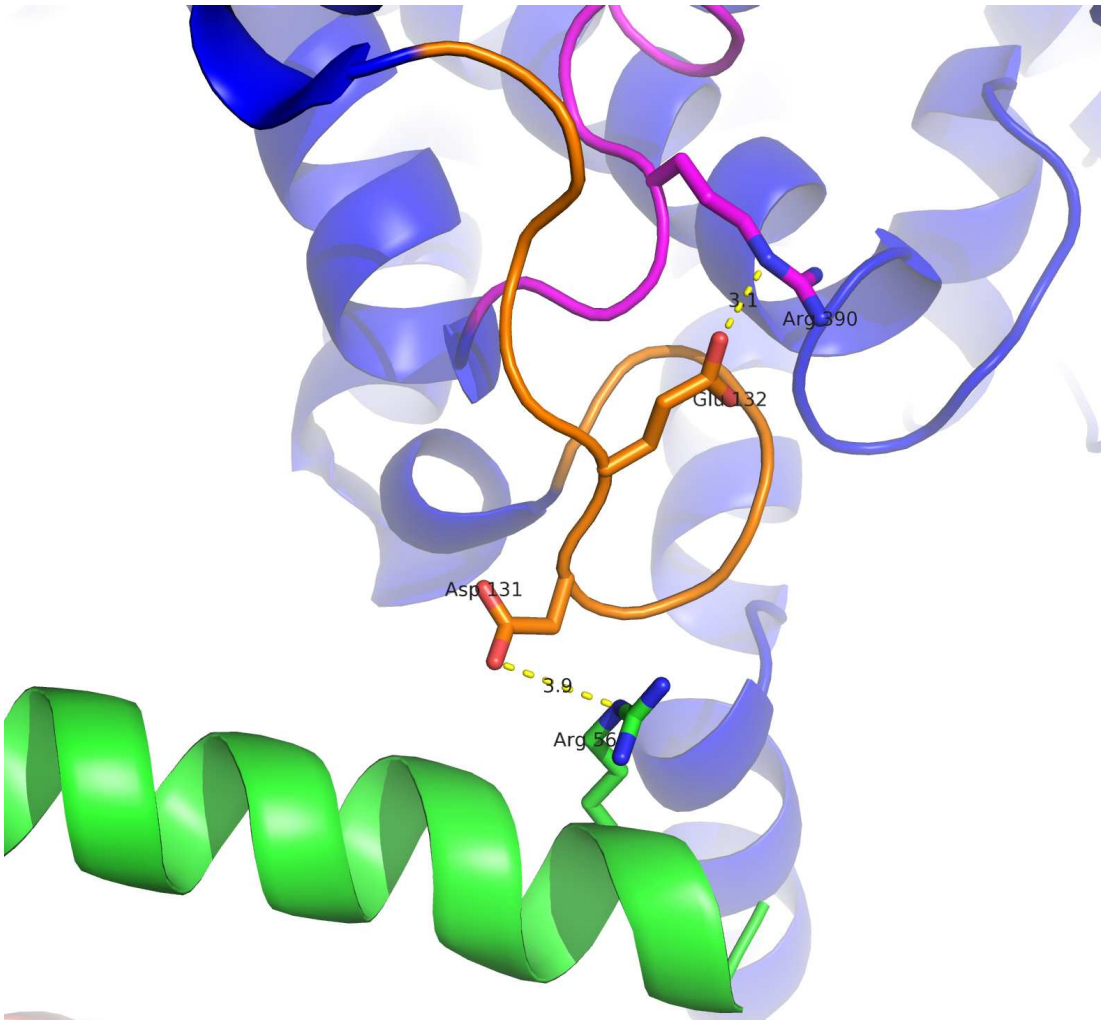

Figure 5.2: Close up view of the salt bridge network of the glycine betaine transporter BetP from *Corynebacterium glutamicum* (pdb ID: 2WIT). The loop structures "loop 2" and "loop 8" of the B monomer (blue) are shown in orange and magenta, respectively. The ionic interactions of the arginine 565 at the C-terminal domain of the C monomer (green helix) and the aspartate 131 (loop 2) and glutamate 132 (loop 2) and arginine 390 (loop 8) are shown in yellow (distance in Å). These salt bridge interactions may leverage changes in the orientation of the C-terminal helix to the substrate pathway via loop 2 and loop 8. These changes are suggested to happen upon alteration in the osmolarity of the cell and promote transport activity in the B monomer.

of this specific RND system by its ability to recruit TolC (and AcrB) [169]. Drug transport by the AcrB trimer has been shown to be a highly cooperative process [153, 154]. The basis for this cooperativity lies in the functional rotation mechanism with the much emphasized analogy to the binding change mechanism as originally proposed by Boyer for the enzyme ATP synthase [83, 170, 171].Trimeric AcrB has been directly observed in a symmetric (closely resembling a LLL configuration) state in initial [70, 72, 125] and in LTO configuration in recent crystal structures [73–75]. Whereas the LTO state of the trimer is strongly suggested to represent a physiological state of AcrB, the LLL state is believed to display an inactive form i. e. in the absence of substrates [86, 172]. This postulate was recently substantiated by molecular dynamics (MD) simulations of the porter domains of the AcrB trimer by Yao *et al.* [173]. Interpretation of the simulation data suggests that the binding of substrate to the T monomer stabilizes the LTO state, whereas dissociation of the substrate may sustain a LLL state. The simulations were conducted with one AcrB substrate present, whereas in the physiological situation, more than one drug molecules might be binding to AcrB. The understanding of the possible conformations of the AcrB trimer led to a schematic representation of the functional rotation mechanism that illustrates a conformational cycling and integrates possible intermediate steps found in crystal structures and derived from crosslinking data (Figure 5.3) [86].

Additionally, a TTT configuration has been observed in the crystal structures of two individual binding pocket variants of AcrB (Eicher *et al.* , unpublished; Cha *et al.* , unpublished). Furthermore, low resolution crystallographic data of one of the crosslink variants (Chapter 3) indicates a TTT configuration. In contrast to the binding pocket variants, this variant did not show altered substrate specificity and MIC data suggest its transport activity resembles that of the wildtype. So, theoretically, a TTT trimer may also be a possible intermediate step in the wildtype AcrB. In contrast to that assumption, a TTT state could not be observed in the MD simulations [173]. This, however, may be attributed to the fact that single substrate simulations were performed. Nevertheless, recent crystallographic studies on the AcrB homolog CusA, a metal ion transporter of *E. coli*, revealed two different conformations, one of which with copper ions bound to all three monomers of CusA [45]. The conformations of the apo and

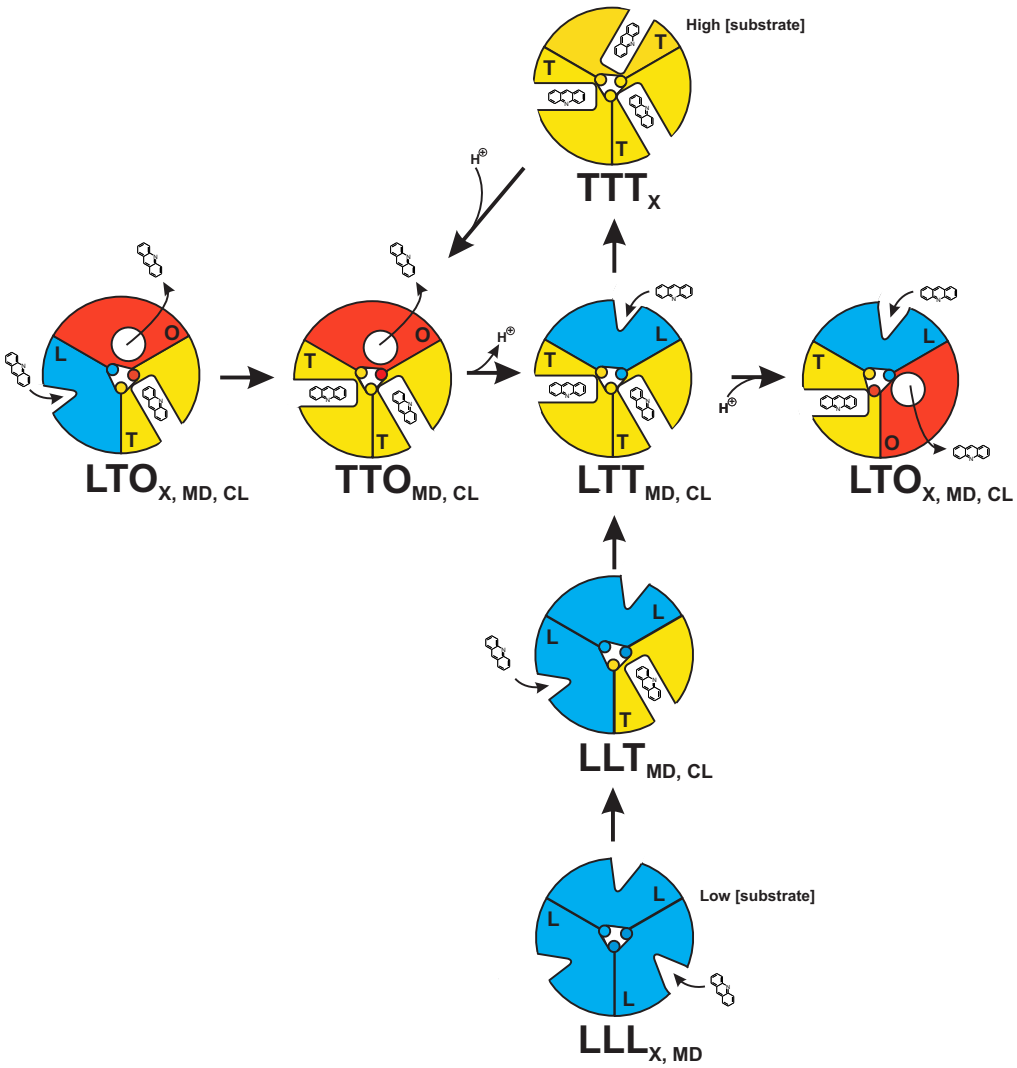

Figure 5.3: Schematic representation of the functional rotation of the homotrimeric multidrug efflux pump AcrB. Monomers adopting the conformations, loose (L), tight (T) and open (O) are colored blue, yellow and red, respectively. The horizontal succession may represent the transport cycle in AcrB, whereas the states TTT and LLL (and LLT) may represent states of high and low substrate concentrations, respectively. Evidence for the existence of individual states by crystallographic (X), molecular dynamics (MD) and cross-link (CL) experiments are indicated. Adapted from Pos [86] with permission.

copper bound CusA closely resemble OOO and TTT states of AcrB, respectively. In the T state, substrates (e. g. 9-bromo-minocyclin, doxorubicin or minocyclin) were shown to bind to the binding pocket of AcrB ([73] and Pos *et al.* , unpublished).

Crosslink studies with AcrB double cysteine variants also revealed evidence for the existence of trimer configurations, other than LLL, LTO and TTT. Due to crosslink quantification in the cysteine variants, it has been shown that more than one monomer may adopt the L or T conformation [77]. This would allow the trimer to (hypothetically) form LLT, TTO and TTL. These trimer states have not been observed in crystal structures of AcrB so far. It might be possible that they represent temporary trimer states that are part of the actual rotation mechanism. In contrast to the LLL, TTT or LTO trimers, these may be utmost transient transitional geometries. Some indication for the occurrence of these transitional states was provided by thermodynamic analysis of the AcrB trimer porter domains by Yao *et al.* [173]. Using calculated inter-protomer interactions of the AcrB trimer, probabilities for different states of the trimer were obtained by equilibrium thermodynamic simulations. Whereas the probability of TTL and LLT were found to be modest in simulations with bound substrate, evidence for TTL could only be detected in the simulations optimized for the asymmetric state. Interestingly, an additional state of LLO could be observed in these simulations without bound substrate.

In the postulated transport cycle (Figure 5.3), the LLO configuration has not been considered so far. However, dynamic simulations indicated that drug transport in only one monomer may be completed without the necessity of the other monomers to undergo full functional rotation. Consequently, the transport scheme may theoretically be extended in a way that describes only one monomer to undergo conformational cycling in the sense of an LLL - LLT - LLO transition. However, this consideration is based on single substrate simulations and contradicts the "bi-site activation" postulated for AcrB [86] on basis of the analogy to this effect observed in the F_1F_O-ATPase. Nevertheless, Yao *et al.* state that "... the complete conformational changes in the trimer are necessary for the next cycle" [173]. In theory this fact may suggest another model for the transport cycle where the monomers not necessary follow concerted change of conformation. In contrast to the proposed model, the monomers may independently

cycle through the conformations L, T and O to a certain extent. The results from the dynamic simulations clearly indicate successful drug export via the exit leading to the TolC docking domain although only one or two monomers changed their conformation. This idea envisages a big variety of different trimer states that come along with the partially independent rotation of the monomers. All possible combinations of the three conformations may be possible with the exception of two neighboring O conformers. These O conformers would result in a steric clash of porter subdomains [174]. However, the suggestion of largely independent conformational cycling of the monomers appears to be in contrast to the findings of Takatsuka *et al.* [80], where it was shown that the inactivation of one of the monomers leads to an inactivation of the entire trimer.

Additionally, one may think of an equilibrium between the L and T conformation since these conformers are relatively similar to each other. In fact single monomer simulations suggest that transition frequencies between L and T conformations are significantly higher than to and from the O conformation [173]. This mechanism may allow substances allow entering and binding, in case they are substrates, or being released from AcrB when they do not bind to the binding pocket. Bound substrate, however, may stabilize the T state and subsequently allow protonation and transition to the O monomer. This speculative alternative model sustains the explanation of LLL trimers due to low substrate concentrations, but cannot explain the extraordinary stability of the LTO state, as demonstrated by numerous crystal structures of AcrB representing LTO. However, it explains the existence of other observed asymmetric configurations other than LTO (Figure 5.3).

Crystal structures from the covalently linked AcrB, carrying one non-functional monomer (D407N) from Takatsuka *et al.* [80] are highly anticipated and may reveal new insights on the conformational rotation of AcrB. According to the proposed mechanism, the change from T to O is energy dependent. In the structure of the covalent AcrB, the non-functional monomer is expected to adopt the L or T conformation, however not the O conformation. It can only be speculated which conformations the neighboring monomers adopt or what the conformational state of a covalently linked trimer carrying two non-functional monomers might be.

As a synthesis of the findings discussed above, the transport mechanism of AcrB may

alternatively be described as a quasi two state model. According to the alternate access model of Jardetzky, the mechanism may be explained by an inside facing and an outside facing conformation. The open (O) conformation would constitute the outside facing conformation and the loose (L) and tight (T) conformations display two variations of inward accessible conformation in equilibrium.

6 Conclusions and outlook

AcrB is the most intensively studied RND protein and probably one of the best characterized bacterial multidrug efflux pumps in *Escherichia coli*, both structural and functional. Especially structural information about AcrB is abundant. At the present time there are 26 crystal structure deposits in the Protein Data Bank (www.pdb.org). Some of the structures were co-crystallized with ligands, e. g. substrates, DARPin binders, ions and peptides and most structures represent AcrB as a symmetric trimer, whereas the more recent structures reveal an asymmetric configuration of the trimer. The few kinetic data on AcrB are limited to observations from *in vivo* experiments. The lack of *in vitro* transport and substrate binding data is attributed to the lack of a suitable and successful transport assay of membrane vesicles containing AcrB or liposomes harboring reconstituted AcrB.

Crystallization of crosslink variants of AcrB

The presented structures from AcrB crosslink variants (Chapter 3) revealed insights into the conformational cycling of AcrB. It could be shown that the PC2 subdomain may move independently from the PN1 subdomain during conformational cycling and interestingly the intermediate conformation of PC2 still allows DARPin binding. Furthermore, there is indication of an all tight (TTT) configuration of one of the crosslink variants in low resolution data. This TTT state of AcrB could only be observed in binding pocket variants so far. Improvement of these putative TTT crystals and the up to now non-diffracting loop-PC1 crystals may lead to additional insights into the functional rotation process. Crystal microseeding and co-crystallization with different substrates may lead to better crystals and higher resolution. Furthermore, the crystallization of the non-functional mutants, carrying deteriorating amino acid substitution in the proton translocation pathway, may display novel or additional conformational states and provide deeper understanding of the functional rotation of AcrB. Especially, the crystallization of the covalently linked trimer containing one or two non-functional monomers of AcrB constructed by Takatsuka *et al.* [80] would be of great interest in view of the conformational cycling.

Reconstitution of AcrB into proteoliposomes

The functional reconstitution of AcrB is imperative to establish a suitable method to investigate substrate binding and transport parameters of AcrB. Measurements done in bacteria and membrane vesicles from bacterial cells, theoretically, may be falsified by the presence of other endogenous multidrug efflux systems with overlapping substrate specificities. Kinetic parameters have already been obtained from intact cells expressing AcrB by indirect measurements [153, 154]. These studies provide a good approximation of the transport kinetics of β-lactams but measurements in a reconstituted system would provide access to data for other substrate classes as well. Initial experiments of reconstituting AcrB were performed in this thesis (Chapter 4). Although incorporation of AcrB into liposomes after the reconstitution process has been shown, experiments with electrochemical proton gradients and different AcrB substrates did not succeed demonstrating substrate transport across the membrane via fluorescence tracing. These findings may confirm *in vivo* experiments [142] showing that only the holo complex (AcrAB-TolC) acts as a functional drug export machinery. Despite the fact that AcrB is the energy conversion module and the substrate determining factor within the tripartite complex, in a reconstitute system it may require structural assists of docked AcrA and TolC to perform drug transport. To circumvent this problem, one could envisage a reconstituted system, addition of AcrA and soluble TolC may promote the formation of the tripartite system *in vitro* and give rise to AcrB activity. Furthermore, the present experimental setup may be inapplicable for transport studies with lipophilic AcrB substrates. These substrates were thought to be relocated from the liposome membranes to the aqueous outside medium and indicated by changes in fluorescence. It is imaginable that these compounds readily reinsert again into the membrane after being expelled. Especially when the partitioning kinetics outperforms AcrB's transport rate, the detection of transport would be futile. On the contrary, transport could be detected in equal experiments with primary (LmrA [175]) and also secondary transporters (NorA [149]). It is imaginable, that these transporters exhibit higher transport rates than AcrB and thus exceed repartitioning of the substrate into the membranes which resulted in a measureable net export of the substrate. One potential approach to avoid this situation is the use of different populations of vesicles/liposomes,

similar to the experiments performed by Zgurskaya *et al.* [142]. One may use two different liposome species each containing reconstituted AcrB or TolC in orientations so that they may, in the presence of soluble AcrA, spontaneously form a complex resembling that in bacterial cells. Using such an experimental setup, preloaded substrates may be transported from AcrB containing liposomes into TolC liposomes. Target (TolC) liposomes needed to be separated to measure substrate transport.

Small amounts of soluble monomeric β-barrel less TolC protein could be purified. In order to use this TolC variant in transport experiments it is crucial to express and purify it as stable trimeric assemblies. Revised construction in accordance to the work of Kim *et al.* [145] may result in a soluble trimeric TolC variant lacking the β-barrel domain. This variant may be useful in transport experiments in a reconstituted system with AcrB and AcrA. Furthermore, complex formation with purified, solubilized AcrB, AcrA and the TolC variant may be studied *in vitro*. The ultimate goal will be the co-crystallization of the individually purified compounds AcrA, AcrB and the TolC variant to understand the complex function of this tripartite efflux machinery (Figure 6.1).

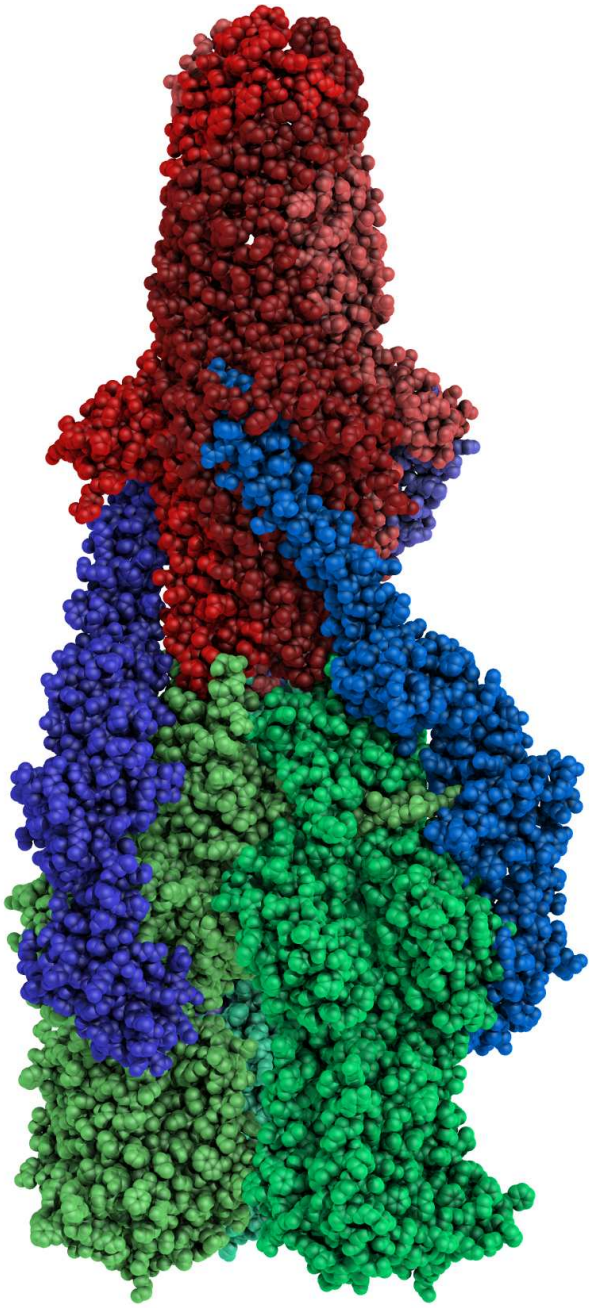

Figure 6.1: Schematic side view of the AcrAB-TolC assembly of *E. coli*. The inner membrane pump AcrB (green) is inserted in the inner membrane and the outer membrane protein TolC (red) is embedded in the outer membrane. In the periplasm the complex is stabilized by the membrane fusion protein AcrA (blue). This model based on crosslink experiments shows a 1:1:1 stoichiometry of the three components [94]. The model coordinate file is a courtesy of Martyn Symmons.

References

[1] Livermore, DM (2004) *Clinical Microbiology and Infection: The Official Publication of the European Society of Clinical Microbiology and Infectious Diseases* **10**, 1–9

[2] Hawkey, PM (1998) *BMJ : British Medical Journal* **317**, 657–660

[3] Hooper, DC (1999) *Drug Resistance Updates* **2**, 38–55

[4] Michel, M and Gutmann, L (1997) *The Lancet* **349**, 1901–1906

[5] Kohler, T, Michea-Hamzehpour, M, Epp, SF, and Pechere, J (1999) *Antimicrob Agents Chemother* **43**, 424–427

[6] Borges-Walmsley, MI, McKeegan, KS, and Walmsley, AR (2003) *The Biochemical Journal* **376**, 313–338

[7] Paulsen, IT, Brown, MH, and Skurray, RA (1996) *Microbiological Reviews* **60**, 575–608

[8] Saier, J and Paulsen, IT (2001) *Seminars in Cell & Developmental Biology* **12**, 205–213

[9] TCDB: transport classification database. http://www.tcdb.org/

[10] Piddock, LJV (2006) *Nat Rev Micro* **4**, 629–636

[11] Dawson, RJP and Locher, KP (2007) *FEBS Letters* **581**, 935–938

[12] Szakacs, G, Paterson, JK, Ludwig, JA, Booth-Genthe, C, and Gottesman, MM (2006) *Nat Rev Drug Discov* **5**, 219–234

[13] Higgins, CF (2007) *Nature* **446**, 749–757

[14] Hollenstein, K, Dawson, RJP, and Locher, KP (2007) *Current Opinion in Structural Biology* **17**, 412–418

[15] Bolhuis, H, Molenaar, D, Poelarends, G, van Veen, HW, Poolman, B, Driessen, AJ, and Konings, WN (1994) *J Bacteriol* **176**, 6957–6964

[16] Seeger, MA and van Veen, HW (2009) *Biochimica et Biophysica Acta* **1794**, 725–737

[17] Dawson, RJP and Locher, KP (2006) *Nature* **443**, 180–185

[18] Aller, SG, Yu, J, Ward, A, Weng, Y, Chittaboina, S, Zhuo, R, Harrell, PM, Trinh, YT, Zhang, Q, Urbatsch, IL, and Chang, G (2009) *Science (New York, NY)* **323**, 1718–1722

[19] Guan, L, Mirza, O, Verner, G, Iwata, S, and Kaback, HR (2007) *Proceedings of the National Academy of Sciences of the United States of America* **104**, 15294–15298

[20] Abramson, J, Smirnova, I, Kasho, V, Verner, G, Kaback, HR, and Iwata, S (2003) *Science* **301**, 610–615

[21] Huang, Y, Lemieux, MJ, Song, J, Auer, M, and Wang, D (2003) *Science* **301**, 616–620

[22] Sobczak, I and Lolkema, JS (2005) *Current Opinion in Microbiology* **8**, 161–167

[23] Fluman, N and Bibi, E (2009) *Biochimica et Biophysica Acta (BBA) - Proteins & Proteomics* **1794**, 738–747

[24] Chen, Y, Pornillos, O, Lieu, S, Ma, C, Chen, AP, and Chang, G (2007) *Proceedings of the National Academy of Sciences of the United States of America* **104**, 18999–19004

[25] Jack, DL, Yang, NM, and Saier, MH (2001) *European Journal of Biochemistry* **268**, 3620–3639

[26] Bay, DC, Rommens, KL, and Turner, RJ (2008) *Biochimica et Biophysica Acta (BBA) - Biomembranes* **1778**, 1814–1838

[27] Steiner-Mordoch, S, Soskine, M, Solomon, D, Rotem, D, Gold, A, Yechieli, M, Adam, Y, and Schuldiner, S (2008) *EMBO J* **27**, 17–26

[28] Schuldiner, S (2009) *Biochimica et Biophysica Acta (BBA) - Proteins & Proteomics* **1794**, 748–762

[29] Soskine, M, Steiner-Mordoch, S, and Schuldiner, S (2002) *Proceedings of the National Academy of Sciences of the United States of America* **99**, 12043–12048

[30] Ninio, S, Elbaz, Y, and Schuldiner, S (2004) *FEBS Letters* **562**, 193–196

[31] Rapp, M, Granseth, E, Seppala, S, and von Heijne, G (2006) *Nat Struct Mol Biol* **13**, 112–116

[32] Rapp, M, Seppala, S, Granseth, E, and von Heijne, G (2007) *Science* **315**, 1282–1284

[33] He, X, Szewczyk, P, Karyakin, A, Evin, M, Hong, W, Zhang, Q, and Chang, G (2010) *Nature* **467**, 991–994

[34] Hvorup, RN, Winnen, B, Chang, AB, Jiang, Y, Zhou, X, and Saier, MH (2003) *European Journal of Biochemistry* **270**, 799–813

[35] Morita, Y, Kataoka, A, Shiota, S, Mizushima, T, and Tsuchiya, T (2000) *J Bacteriol* **182**, 6694–6697

[36] Kuroda, T and Tsuchiya, T (2009) *Biochimica et Biophysica Acta (BBA) - Proteins & Proteomics* **1794**, 763–768

[37] Chen, J, Morita, Y, Huda, MN, Kuroda, T, Mizushima, T, and Tsuchiya, T (2002) *Journal of Bacteriology* **184**, 572–576

[38] Huda, MN, Morita, Y, Kuroda, T, Mizushima, T, and Tsuchiya, T (2001) *FEMS Microbiology Letters* **203**, 235–239

[39] Nishino, K and Yamaguchi, A (2001) *J Bacteriol* **183**, 5803–5812

[40] Long, F, Rouquette-Loughlin, C, Shafer, WM, and Yu, EW (2008) *Antimicrob Agents Chemother* **52**, 3052–3060

[41] He, G, Kuroda, T, Mima, T, Morita, Y, Mizushima, T, and Tsuchiya, T (2004) *J Bacteriol* **186**, 262–265

[42] Su, X, Chen, J, Mizushima, T, Kuroda, T, and Tsuchiya, T (2005) *Antimicrob Agents Chemother* **49**, 4362–4364

[43] Sennhauser, G, Bukowska, MA, Briand, C, and Grütter, MG (2009) *Journal of Molecular Biology* **389**, 134–145

[44] Goldberg, M, Pribyl, T, Juhnke, S, and Nies, DH (1999) *The Journal of Biological Chemistry* **274**, 26065–26070

[45] Long, F, Su, C, Zimmermann, MT, Boyken, SE, Rajashankar, KR, Jernigan, RL, and Yu, EW (2010) *Nature* **467**, 484–488

[46] Nikaido, H and Takatsuka, Y (2009) *Biochimica et Biophysica Acta* **1794**, 769–781

[47] Pinto, FGS, Chueire, LMO, Vasconcelos, ATR, Nicolás, MF, Almeida, LGP, Souza, RC, Menna, P, Barcellos, FG, Megías, M, and Hungria, M (2009) *Functional & Integrative Genomics* **9**, 263–270

[48] de Keyzer, J, van der Does, C, and Driessen, A (2003) *Cellular and Molecular Life Sciences* **60**, 2034–2052

[49] Pasca, MR, Guglierame, P, Rossi, ED, Zara, F, and Riccardi, G (2005) *Antimicrob Agents Chemother* **49**, 4775–4777

[50] Tsuge, K, Ohata, Y, and Shoda, M (2001) *Antimicrobial Agents and Chemotherapy* **45**, 3566–3573

[51] Scott, C and Ioannou, YA (2004) *Biochimica et Biophysica Acta* **1685**, 8–13

[52] Vanier, MT, Pentchev, P, Rodriguez-Lafrasse, C, and Rousson, R (1991) *Journal of Inherited Metabolic Disease* **14**, 580–595

[53] Goel, AK, Rajagopal, L, Nagesh, N, and Sonti, RV (2002) *Journal of Bacteriology* **184**, 3539–3548

[54] Ma, Y, Erkner, A, Gong, R, Yao, S, Taipale, J, Basler, K, and Beachy, PA (2002) *Cell* **111**, 63–75

[55] Stone, DM, Hynes, M, Armanini, M, Swanson, TA, Gu, Q, Johnson, RL, Scott, MP, Pennica, D, Goddard, A, Phillips, H, Noll, M, Hooper, JE, de Sauvage, F, and Rosenthal, A (1996) *Nature* **384**, 129–134

[56] Porter, JA, Young, KE, and Beachy, PA (1996) *Science (New York, NY)* **274**, 255–259

[57] Kuwabara, PE and Labouesse, M (2002) *Trends in Genetics* **18**, 193–201

[58] van den Heuvel, M and Ingham, PW (1996) *Nature* **382**, 547–551

[59] Chen, Y and Struhl, G (1996) *Cell* **87**, 553–563

[60] Nikaido, H (1989) *Antimicrobial Agents and Chemotherapy* **33**, 1831–1836

[61] Lin, J, Michel, LO, and Zhang, Q (2002) *Antimicrobial Agents and Chemotherapy* **46**, 2124–2131

[62] Magnet, S, Courvalin, P, and Lambert, T (2001) *Antimicrob Agents Chemother* **45**, 3375–3380

[63] Kobayashi, N, Nishino, K, and Yamaguchi, A (2001) *J Bacteriol* **183**, 5639–5644

[64] Lomovskaya, O and Lewis, K (1992) *Proceedings of the National Academy of Sciences of the United States of America* **89**, 8938–8942

[65] Lewis, K (2000) *Current Biology* **10**, R678–R681

[66] Poole, K (2004) *Clinical Microbiology and Infection: The Official Publication of the European Society of Clinical Microbiology and Infectious Diseases* **10**, 12–26

[67] Ma, D, Cook, DN, Alberti, M, Pon, NG, Nikaido, H, and Hearst, JE (1993) *Journal of Bacteriology* **175**, 6299–6313

[68] Fralick, JA (1996) *Journal of Bacteriology* **178**, 5803–5805

[69] Thanassi, DG, Cheng, LW, and Nikaido, H (1997) *Journal of Bacteriology* **179**, 2512–2518

[70] Murakami, S, Nakashima, R, Yamashita, E, and Yamaguchi, A (2002) *Nature* **419**, 587–593

[71] Yu, EW, McDermott, G, Zgurskaya, HI, Nikaido, H, and Koshland, DE (2003) *Science (New York, NY)* **300**, 976–980

[72] Pos, KM, Schiefner, A, Seeger, MA, and Diederichs, K (2004) *FEBS Letters* **564**, 333–339

[73] Murakami, S, Nakashima, R, Yamashita, E, Matsumoto, T, and Yamaguchi, A (2006) *Nature* **443**, 173–179

[74] Seeger, MA, Schiefner, A, Eicher, T, Verrey, F, Diederichs, K, and Pos, KM (2006) *Science (New York, NY)* **313**, 1295–1298

[75] Sennhauser, G, Amstutz, P, Briand, C, Storchenegger, O, and Grütter, MG (2007) *PLoS Biology* **5**, e7

[76] Guan, L and Nakae, T (2001) *Journal of Bacteriology* **183**, 1734–1739

[77] Seeger, MA, von Ballmoos, C, Eicher, T, Brandstätter, L, Verrey, F, Diederichs, K, and Pos, KM (2008) *Nature Structural & Molecular Biology* **15**, 199–205

[78] Bohnert, JA, Schuster, S, Seeger, MA, Fähnrich, E, Pos, KM, and Kern, WV (2008) *Journal of Bacteriology* **190**, 8225–8229

[79] Seeger, MA, von Ballmoos, C, Verrey, F, and Pos, KM (2009) *Biochemistry* **48**, 5801–5812

[80] Takatsuka, Y and Nikaido, H (2009) *Journal of Bacteriology* **191**, 1729–1737

[81] Nakamura, H, Hachiya, N, and Tojo, T (1978) *Journal of Bacteriology* **134**, 1184–1187

[82] Okusu, H, Ma, D, and Nikaido, H (1996) *Journal of Bacteriology* **178**, 306–308

[83] Boyer, PD (1997) *Annual Review of Biochemistry* **66**, 717–749

[84] Takatsuka, Y and Nikaido, H (2010) *Methods in Molecular Biology (Clifton, NJ)* **634**, 343–354

[85] Murakami, S and Yamaguchi, A (2003) *Current Opinion in Structural Biology* **13**, 443–452

[86] Pos, KM (2009) *Biochimica et Biophysica Acta (BBA) - Proteins & Proteomics* **1794**, 782–793

[87] Dinh, T, Paulsen, IT, and Saier, MH (1994) *Journal of Bacteriology* **176**, 3825–3831

[88] Aires, JR and Nikaido, H (2005) *Journal of Bacteriology* **187**, 1923–1929

[89] Tikhonova, EB and Zgurskaya, HI (2004) *The Journal of Biological Chemistry* **279**, 32116–32124

[90] Mikolosko, J, Bobyk, K, Zgurskaya, HI, and Ghosh, P (2006) *Structure* **14**, 577–587

[91] Akama, H, Matsuura, T, Kashiwagi, S, Yoneyama, H, ichiro Narita, S, Tsukihara, T, Nakagawa, A, and Nakae, T (2004) *Journal of Biological Chemistry* **279**, 25939–25942

[92] Higgins, MK, Bokma, E, Koronakis, E, Hughes, C, and Koronakis, V (2004) *Proceedings of the National Academy of Sciences of the United States of America* **101**, 9994–9999

[93] Zgurskaya, HI and Nikaido, H (1999) *Journal of Molecular Biology* **285**, 409–420

[94] Symmons, MF, Bokma, E, Koronakis, E, Hughes, C, and Koronakis, V (2009) *Proceedings of the National Academy of Sciences of the United States of America* **106**, 7173–7178

[95] Elkins, CA and Nikaido, H (2003) *J Bacteriol* **185**, 5349–5356

[96] Touze, T, Eswaran, J, Bokma, E, Koronakis, E, Hughes, C, and Koronakis, V (2004) *Molecular Microbiology* **53**, 697–706

[97] Tikhonova, EB, Wang, Q, and Zgurskaya, HI (2002) *Journal of Bacteriology* **184**, 6499–6507

[98] Koronakis, V, Sharff, A, Koronakis, E, Luisi, B, and Hughes, C (2000) *Nature* **405**, 914–919

[99] Bavro, VN, Pietras, Z, Furnham, N, Pérez-Cano, L, Fernández-Recio, J, Pei, XY, Misra, R, and Luisi, B (2008) *Molecular Cell* **30**, 114–121

[100] Lobedanz, S, Bokma, E, Symmons, MF, Koronakis, E, Hughes, C, and Koronakis, V (2007) *Proceedings of the National Academy of Sciences of the United States of America* **104**, 4612–4617

[101] Nikaido, H and Saier, M (1992) *Science (New York, NY)* **258**, 936–942

[102] Stroebel, D, Sendra, V, Cannella, D, Helbig, K, Nies, DH, and Covès, J (2007) *Biochimica et Biophysica Acta (BBA) - Biomembranes* **1768**, 1567–1573

[103] Kim, H, Nagore, D, and Nikaido, H (2009) *Journal of Bacteriology*

[104] Saier, MH, Tam, R, Reizer, A, and Reizer, J (1994) *Molecular Microbiology* **11**, 841–847

[105] Franke, S, Grass, G, Rensing, C, and Nies, DH (2003) *J Bacteriol* **185**, 3804–3812

[106] Baranova, N and Nikaido, H (2002) *Journal of Bacteriology* **184**, 4168–4176

[107] Nagakubo, S, Nishino, K, Hirata, T, and Yamaguchi, A (2002) *Journal of Bacteriology* **184**, 4161–4167

[108] Mokhonov, VV, Mokhonova, EI, Akama, H, and Nakae, T (2004) *Biochemical and Biophysical Research Communications* **322**, 483–489

[109] Zgurskaya, HI and Nikaido, H (2000) *Journal of Bacteriology* **182**, 4264–4267

[110] Tamura, N, Murakami, S, Oyama, Y, Ishiguro, M, and Yamaguchi, A (2005) *Biochemistry* **44**, 11115–11121

[111] Fernandez-Recio, J, Walas, F, Federici, L, Pratap, JV, Bavro, VN, Miguel, RN, Mizuguchi, K, and Luisi, B (2004) *FEBS Letters* **578**, 5–9

[112] Pos, KM (2009) *Proceedings of the National Academy of Sciences of the United States of America* **106**, 6893–6894

[113] Takatsuka, Y and Nikaido, H (2007) *Journal of Bacteriology* **189**, 8677–8684

[114] Nikaido, H (2009) *Annual Review of Biochemistry* **78**, 119–146

[115] Zgurskaya, HI, Yamada, Y, Tikhonova, EB, Ge, Q, and Krishnamoorthy, G (2009) *Biochimica et Biophysica Acta* **1794**, 794–807

[116] Binz, HK, Amstutz, P, Kohl, A, Stumpp, MT, Briand, C, Forrer, P, Grütter, MG, and Plückthun, A (2004) *Nature Biotechnology* **22**, 575–582

[117] Mosavi, LK, Cammett, TJ, Desrosiers, DC, and yu Peng, Z (2004) *Protein Science* **13**, 1435–1448

[118] Hanes, J and Plückthun, A (1997) *Proceedings of the National Academy of Sciences of the United States of America* **94**, 4937 –4942

[119] Smith, GP (1985) *Science (New York, NY)* **228**, 1315–1317

[120] Sennhauser, G and Grütter, MG (2008) *Structure* **16**, 1443–1453

[121] Morgner, N, Kleinschroth, T, Barth, H, Ludwig, B, and Brutschy, B (2007) *Journal of the American Society for Mass Spectrometry* **18**, 1429–1438

[122] Morgner, N, Zickermann, V, Kerscher, S, Wittig, I, Abdrakhmanova, A, Barth, H, Brutschy, B, and Brandt, U (2008) *Biochimica et Biophysica Acta* **1777**, 1384–1391

[123] Hoffmann, J, Sokolova, L, Preiss, L, Hicks, DB, Krulwich, TA, Morgner, N, Wittig, I, Schägger, H, Meier, T, and Brutschy, B (2010) *Physical Chemistry Chemical Physics: PCCP* **12**, 13375–13382

[124] Hoffmann, J, Aslimovska, L, Bamann, C, Glaubitz, C, Bamberg, E, and Brutschy, B (2010) *Physical Chemistry Chemical Physics: PCCP* **12**, 3480–3485

[125] Pos, KM and Diederichs, K (2002) *Acta Crystallographica Section D, Biological Crystallography* **58**, 1865–1867

[126] Morgner, N, Barth, H, and Brutschy, B (2006) *Aust J Chem* **59**, 109–114

[127] Schuck, P (2000) *Biophysical Journal* **78**, 1606–1619

[128] Lipfert, J, Columbus, L, Chu, VB, Lesley, SA, and Doniach, S (2007) *The Journal of Physical Chemistry B* **111**, 12427–12438

[129] Valiyaveetil, FI, Zhou, Y, and MacKinnon, R (2002) *Biochemistry* **41**, 10771–10777

[130] Guan, L, Smirnova, IN, Verner, G, Nagamori, S, Nagamoni, S, and Kaback, HR (2006) *Proceedings of the National Academy of Sciences of the United States of America* **103**, 1723–1726

[131] Nikaido, H (1998) *Drug Resistance Updates* **1**, 93–98

[132] (1994) *Acta Crystallographica Section D, Biological Crystallography* **50**, 760–763

[133] Woodcock, DM, Crowther, PJ, Doherty, J, Jefferson, S, DeCruz, E, Noyer-Weidner, M, Smith, SS, Michael, MZ, and Graham, MW (1989) *Nucleic Acids Research* **17**, 3469–3478

[134] Maniatis, T, Sambrook, J, Fritsch, EFEF, and Laboratory, CSH (1982) *Molecular cloning : a laboratory manual / T. Maniatis, E.F. Fritsch, J. Sambrook.* Manual for genetic engineering. Cold Spring Harbor Laboratory, Cold Spring Harbor, N.Y. :

[135] Miroux, B and Walker, JE (1996) *Journal of Molecular Biology* **260**, 289–298

[136] Binz, HK, Stumpp, MT, Forrer, P, Amstutz, P, and Plückthun, A (2003) *Journal of Molecular Biology* **332**, 489–503

[137] Kabsch, W (1993) *Journal of Applied Crystallography* **26**, 795–800

[138] Vagin, A and Teplyakov, A (2010) *Acta Crystallographica Section D, Biological Crystallography* **66**, 22–25

[139] Adams, PD, Afonine, PV, Bunkóczi, G, Chen, VB, Davis, IW, Echols, N, Headd, JJ, Hung, L, Kapral, GJ, Grosse-Kunstleve, RW, McCoy, AJ, Moriarty, NW, Oeffner, R, Read, RJ, Richardson, DC, Richardson, JS, Terwilliger, TC, and Zwart, PH (2010) *Acta Crystallographica Section D, Biological Crystallography* **66**, 213–221

[140] Murshudov, GN, Vagin, AA, and Dodson, EJ (1997) *Acta Crystallographica Section D, Biological Crystallography* **53**, 240–255

[141] Emsley, P and Cowtan, K (2004) *Acta Crystallographica Section D, Biological Crystallography* **60**, 2126–2132

[142] Zgurskaya, HI and Nikaido, H (1999) *Proceedings of the National Academy of Sciences of the United States of America* **96**, 7190–7195

[143] Iwakura, M and Nakamura, T (1998) *Protein Engineering* **11**, 707–713

[144] Fumia, S (2003). Diploma thesis: Characterisierung der periplasmatischen Domäne des Antibiotika Efflux Transporters AcrB aus *Escherichia coli*.

[145] Kim, S, Yum, S, Jo, W, Lee, BL, Jeong, M, and Ha, N (2008) *Journal of Microbiology and Biotechnology* **18**, 845–851

[146] Blasi, U, Fraisl, P, Chang, C, Zhang, N, and Young, R (1999) *J Bacteriol* **181**, 2922–2929

[147] Nieuwenhuis, FJ, Kanner, BI, Gutnick, DL, Postma, PW, and van Dam, K (1973) *Biochimica et Biophysica Acta* **325**, 62–71

[148] Novo, D, Perlmutter, NG, Hunt, RH, and Shapiro, HM (1999) *Cytometry* **35**, 55–63

[149] Yu, J, Grinius, L, and Hooper, DC (2002) *Journal of Bacteriology* **184**, 1370–1377

[150] Geertsma, ER, Mahmood, NABN, Schuurman-Wolters, GK, and Poolman, B (2008) *Nature Protocols* **3**, 256–266

[151] Monod, J, Wyman, J, and Changeux, JP (1965) *Journal of Molecular Biology* **12**, 88–118

[152] Koshland, DE, Némethy, G, and Filmer, D (1966) *Biochemistry* **5**, 365–385

[153] Nagano, K and Nikaido, H (2009) *Proceedings of the National Academy of Sciences of the United States of America* **106**, 5854–5858

[154] Lim, SP and Nikaido, H (2010) *Antimicrobial Agents and Chemotherapy* **54**, 1800–1806

[155] Voet, D, Voet, JG, and Pratt, CW (2006) *Fundamentals of Biochemistry: Life at the Molecular Level.* Wiley, 2 edition

[156] Johnson, LN (1992) *The FASEB Journal: Official Publication of the Federation of American Societies for Experimental Biology* **6**, 2274–2282

[157] Krissinel, E and Henrick, K (2007) *Journal of Molecular Biology* **372**, 774–797

[158] Shapiro, AB and Ling, V (1997) *European Journal of Biochemistry / FEBS* **250**, 130–137

[159] Yamashita, A, Singh, SK, Kawate, T, Jin, Y, and Gouaux, E (2005) *Nature* **437**, 215–223

[160] Noskov, SY and Roux, B (2008) *Journal of Molecular Biology* **377**, 804–818

[161] Lolkema, JS, Enequist, H, and van der Rest, ME (1994) *European Journal of Biochemistry / FEBS* **220**, 469–475

[162] Kästner, CN, Dimroth, P, and Pos, KM (2000) *Archives of Microbiology* **174**, 67–73

[163] Schulze, S, Koster, S, Geldmacher, U, van Scheltinga, ACT, and Kühlbrandt, W (2010) *Nature* **467**, 233–236

[164] Schiller, D, Rübenhagen, R, Krämer, R, and Morbach, S (2004) *Biochemistry* **43**, 5583–5591

[165] Ziegler, C, Morbach, S, Schiller, D, Krämer, R, Tziatzios, C, Schubert, D, and Kühlbrandt, W (2004) *Journal of Molecular Biology* **337**, 1137–1147

[166] Ressl, S, van Scheltinga, ACT, Vonrhein, C, Ott, V, and Ziegler, C (2009) *Nature* **458**, 47–52

[167] Krämer, R and Ziegler, C (2009) *Biological Chemistry* **390**, 685–691

[168] Peter, H, Burkovski, A, and Krämer, R (1998) *Journal of Biological Chemistry* **273**, 2567 –2574

[169] Tikhonova, EB, Dastidar, V, Rybenkov, VV, and Zgurskaya, HI (2009) *Proceedings of the National Academy of Sciences of the United States of America* **106**, 16416–16421

[170] Hackney, DD, Rosen, G, and Boyer, PD (1979) *Proceedings of the National Academy of Sciences of the United States of America* **76**, 3646 –3650

[171] Hutton, RL and Boyer, PD (1979) *The Journal of Biological Chemistry* **254**, 9990–9993

[172] Su, C, Li, M, Gu, R, Takatsuka, Y, McDermott, G, Nikaido, H, and Yu, EW (2006) *Journal of Bacteriology* **188**, 7290–7296

[173] Yao, X, Kenzaki, H, Murakami, S, and Takada, S (2010) *Nature Communications* **1**, 117

[174] Seeger, MA, Diederichs, K, Eicher, T, Brandstätter, L, Schiefner, A, Verrey, F, and Pos, KM (2008) *Current Drug Targets* **9**, 729–749

[175] Venter, H, Velamakanni, S, Balakrishnan, L, and van Veen, HW (2008) *Biochemical Pharmacology* **75**, 866–874

List of Figures

List of Tables

Curriculum vitae

Name	BRANDSTÄTTER Lorenz
Date of Birth	March 18th, 1981 in Klagenfurt, Austria
Nationality	Austrian
Email	lorenz.brandstaetter@gmx.at

Education

11/2006–1/2011	**Doctoral thesis** in the group of Prof. Dr. François Verrey at the Institute of Physiology, Universität Zürich, Switzerland. Supervisor: Prof. Dr. Klaas M. Pos. Title: *Structure - Function Relationship of the Multidrug Efflux Protein AcrB, a Bacterial Homolog of the Human Niemann-Pick C1 Transporter.*
8/2008–8/2010	Forschungskredit der Universität Zürich
4/2006	Final certification: **Diploma study Microbiology**, Karl-Franzens Universität Graz, Austria
9/2004–10/2005	**Diploma Thesis** in the group of Prof. Bergler at the Institute of Microbiology, Karl-Franzens Universität Graz, Austria. Title: *Characterisation of the Nop4 pre-ribosomal Particle.*
9/1999–4/2006	**Diploma study**: Microbiology at the Karl-Franzens Universität Graz, Austria
6/1999	**Matura** "with excellence" (Gymnasium), Peraugymnasium Villach, Austria
9/1991–6/1999	**Gymnasium**, Peraugymnasium Villach, Austria

Publications

Thomas Eicher, **Lorenz Brandstätter** and Klaas M Pos (2009) Structural and functional aspects of the multidrug efflux pump AcrB. *Biological Chemistry* 390(8):693-9

Markus A Seeger, Kay Diederichs, Thomas Eicher, **Lorenz Brandstätter**, Andre Schiefner, François Verrey and Klaas M Pos (2008) The AcrB efflux pump: conformational cycling and peristalsis lead to multidrug resistance. *Current Drug Targets*, 9(9):729-49

Markus A Seeger, Christoph von Ballmoos, Thomas Eicher, **Lorenz Brandstätter**, François Verrey, Kay Diederichs and Klaas M Pos (2008) Engineered disulfide bonds support the functional rotation mechanism of multidrug efflux pump AcrB. *Nature Structural & Molecular Biology*, 15(2):199-205

Acknowledgments

This is a tribute to all the people who have helped me during my doctoral studies and/or created an enjoyable atmosphere in the lab and in the office.

First of all, I'd like to thank Martin, who supervised and scientifically guided me in the last four years. He always had an open ear for questions, suggestions and comments and I always enjoyed discussing with him (even topics not directly related to science). I especially appreciate his engagement in supporting me staying in Zürich, after he has moved to Frankfurt.

I like to thank François, my doctoral father, for his continuous support and giving me the opportunity to stay in his group and finish my work.

Thomas, my irreplaceable fellow: I missed his sarcastic comments and amusing encouragements in the last one and a half years. With pleasure I think back to our night- and day-shifts at the synchrotron and profound debates (often with Döner Kebap and Efes) over size-exclusion chromatograms are unforgettable.

Thanks to Markus for the pleasant overlapping time (first month), the introduction to the topic, the discussions and his lasting interest in my project. I still remember our first common (extremely toxic) experiment.

Thanks to the rest of the Verrey crew, especially Brigitte for her help, Simone for the background noise and my office colleagues: Tina, Nicola, Beni and Josua for the entertaining and enjoyable chats, the lunch and coffee breaks. I not only learned a lot about Ussing chamber and Bärn Düütsch, organ chamber, animal experiments and dietary effects of single amino acids.

Ich danke meiner Mutter, meiner Schwester Hemma und Klaus für die Aufmunterungen und Unterstützung.

Der grösste Dank gilt meiner Freundin Anna, die immer für mich da war und mir immer mit Ermutigung zur Seite stand.